INVESTIGATION OF STAINS EXISTING ON FOSSIL SAMPLES FROM THE STERKFONFEIN ARCHEAOLOGICAL SITES

By

SICEBISO RICHMAN HLATSHWAYO

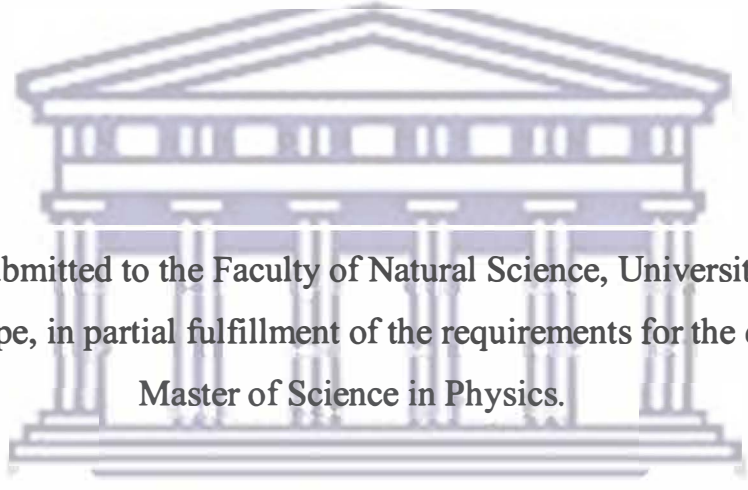

A thesis submitted to the Faculty of Natural Science, University of the Western Cape, in partial fulfillment of the requirements for the degree of Master of Science in Physics.

Supervisor: Dr. A. M. Venter (NECSA)
Co-supervisor: Prof. D. Adams (UWC)

December 2006

INVESTIGATION OF STAINS EXISTING ON FOSSIL SAMPLES FROM THE STERKFONTEIN ARCHAEOLOGICAL SITES

Sicebiso Richman Hlatshwayo

KEYWORDS

Investigation

Manganese

Stains

Fossils

Sterkfontein

Archaeological

Sites

SEM

XRF

XRD

INVESTIGATION OF STAINS EXISTING ON FOSSIL SAMPLES FROM THE STERKFONTEIN ARCHAEOLOGICAL SITES

Sicebiso Richman Hlatshwayo

Abstract

It is known that fossilised bone samples excavated from the Sterkfontein archaeological sites have prominent brown stains on their surfaces. Their existence has been postulated by researchers from Transvaal museum to be reminiscent of Mn deposits from lichen growth in the Mn rich geological environment of the area [Tha2005]. To investigate the chemical nature of the stains, we report results from experimental studies on fossilised antelope bone samples as well as rocks from the archaeological sites. The fossil samples cover the age period 1 to 2.5 million years ago. A chert rock sample is of specific interest to this study as it contains both live lichen growth (green residue) and brown stains (believed to be the residue of dead lichen).

The techniques used in this study include scanning electron microscope (SEM/EDX), x-ray fluorescence (XRF) and x-ray diffraction (XRD) existing on the NECSA site. These techniques were chosen as they enable analysis of the near surface regions, i.e. specifically the surface deposits and stains, due to the limited penetration depths of electron and x-ray beams.

The chert rock is confirmed to be a silicate (SiO_2) and dolomite to be calcium magnesium carbonate ($CaMg(CO_3)_2$). XRF analysis of the live lichen indicates a weak Mn signal, whereas the brown stains show prominent Mn content from both XRF and SEM analysis. The weak Mn signal in the lichen is related to the presence of biological material within which the Mn is distributed (diluted). Due to the absence of biological material in the brown stains the Mn is a more concentrated form.

This study confirms the elemental content of the fossilised bone material to comprise of Ca and P reminiscent of hydroxylapatite ($Ca_5(PO_4)_3OH$). XRF and SEM analysis on the visually visible stains on the bone samples, do not all show the stains to contain Mn. It is concluded that Mn is only seen with XRF and SEM when the stains are sufficiently thick such as when it fills crevices and grooves on the uneven surface. XRD analysis of all the bone samples indicate that the hexagonal crystallites of the hydroxylapatite structure do not have random orientations, but that the c-axis of the hexagonal structure has a preferential alignment along the dendrite directions of the bone material. This phenomenon is referred as preferred orientation of the crystallite dendrites.

It is concluded that the stains are substantially less than 6.5μm in thickness, based on the observation that XRD measurements do not give any indication of Mn, whereas XRF and SEM do show minor presence of Mn (within limits of detection) in some of the samples. This study does not show correlation between the Mn presence and the age of the fossils, or their pantalaeogical origin.

[Tha2005] Thackeray J.F, Sénégas F. and Laden G., "Manganese dioxide staining on hominid crania from Sterkfontein and Swartkrans: possible associations with lichen" South African Journal of Science **101**, January/February 2005.

Declaration

I declare that *Investigation of stains existing on fossil samples from the Sterkfontein archaeological sites*, that it has not been submitted for any degree or examination in any other university, and that all the sources I have used have been indicated and acknowledged by complete references.

Full Name:..... Date:.....

Signed:.....

Acknowledgements

First and for most I would like to thank our mighty father God for guiding me through difficult and nice times during this study.

I will like to thank my family for being supportive to my career, especially my parents Mr. M.O and Mrs. N.G Hlatshwayo, my brothers Mlungisi, Thushu and Ntoko, my sister Thulisile.

My thanks also go to UWC physics department, UniZul physics and Engineering department and iThemba Labs for the opportunity to do a MSc. I must also thank Mrs B Kibirige for her guidance during undergraduate studies.

I would also like to thank NECSA for allowing me to do research with their resources. My first acknowledgement goes to my supervisor Dr A.M Venter for his guidance and I would also like to thank the following NECSA personnel:

- Mr. H Coetzee from Pelindaba Analytical Lab for helping with XRF measurements.
- Miss P. Segonyane for the assistance with SEM and PIXE measurements.
- Mrs B. Mhlungu and Miss F.D Maphai for their advice and supportive ideas.
- Mr. D. Nthite for his assistance with XRD measurements.
- Dr C.B. Franklyn and Mrs.V.C. Msutwana Qupe for their guidance and support.

I would also like to extend my acknowledgements to Transvaal Museum especially Dr F.C. Thackeray and Ms. S. Potse for coming up with a project and for the samples.

I must also thank NRF through iThemba Labs for financial assistance, without your help it was not going to happen.

To 2005 Matsci/Manus class especially Sdumo, Jay, Tshwala, Senzo, Shuan, Chris, Manyosi, Gugu, Gebhu Nja Ndini, Mhlathi and Mkhwamubi thanks a lot for everything you have done for me I will always miss year2005 because of you.

"Akukho okwendlula ukuzimisela nokuzikhandla noma engaba kunzima kanjani"

Table of Contents

Chapter 1

Introduction and literature review

1.1 Introduction and background

Investigation of fossils from Sterkfontein archaeological sites plays an important role in the study of the evolution of humankind. Fossils also give information on what kinds of animals were living in these sites millions of years ago. Samples of this study were taken from the Sterkfontein archaeological sites. The Cradle of Humankind World Heritage archaeological sites include the caves Sterkfontein, Swartkrans and Kromdraai. Sterkfontein archaeological sites are situated 9 kilometers (km) north north west of Krugersdorp in the Gauteng province as indicated in Fig 1.1

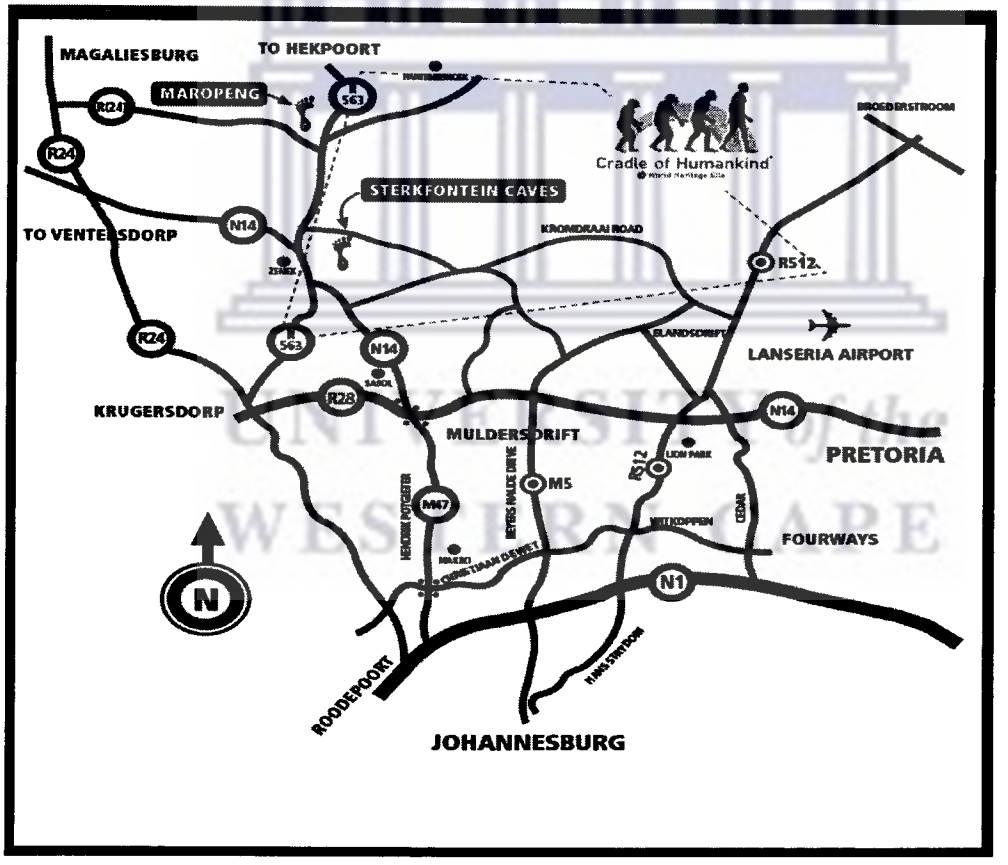

Figure 1.1 Map showing directions to Sterkfontein Archaeological sites [www01].

Many fossil discoveries have been made in these sites that have contributed, significantly towards the study of the evolution of humankind. Famous research topics emanating from the study of fossils from these sites include Mrs. Ples [Bro1947] and Little Foot [Cla1998]. Mrs. Ples is the name given to the female skull that was discovered in 1947 at Sterkfontein caves by Dr Robert Broom with his assistant John Robinson from the Transvaal Museum. Many scientists believed that this skull represented a distant human relative who lived on the South African highveld between 2 to 2.5 million years ago. The skull was formerly known as Plesianthropus that means almost humankind [Pra2001]. The recent research shows that the skull is actually representing a male species. The image of Mrs. Ples is shown in Fig 1.2.

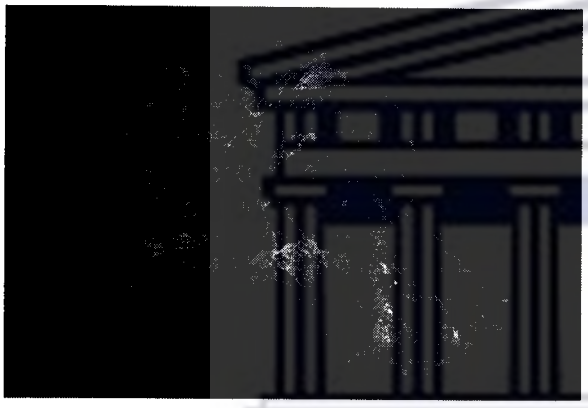

Figure 1.2 Photo of the Mrs. Ples skull [www02].

Little Foot is a name given to a fossil foot bone that was discovered in 1994 at Sterkfontein Archaeological sites by Dr Ron Clarke from Wits University. Little Foot is also believed to be a vital link in the research on the evolution of humankind [Cla1998]. The excavation of little foot is yet to be done.

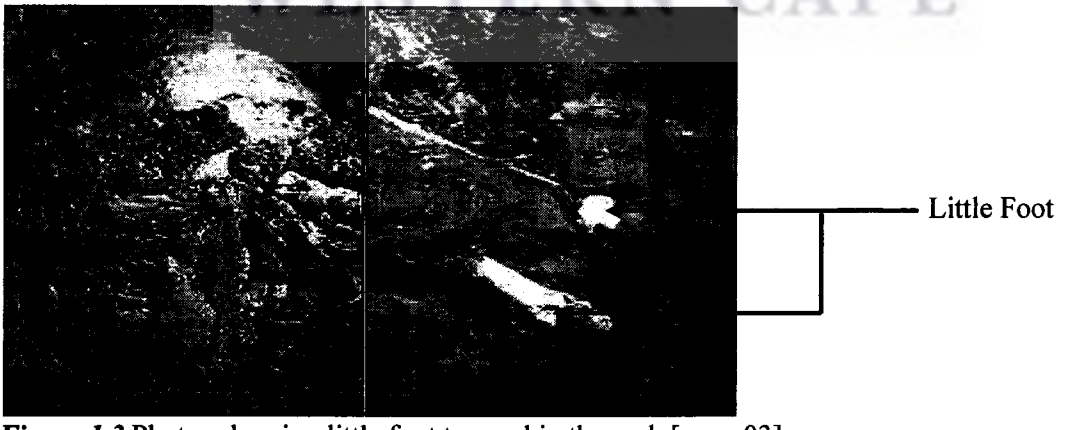

Figure 1.3 Photos showing little foot trapped in the rock [www03].

Most of the fossilised bones found at the Sterkfontein archaeological sites contain prominent dark stains on their surfaces [Tha2005]. These stains were found to be mainly manganese dioxide (MnO_2) and small amounts of iron oxide compound (Fe_2O_3) [Cuk2005]. Individual stains are generally less than 5mm in diameter [Tha2005]. Larger stains are thought to result from the nerging of smaller stains. It is postulated that the stains are caused by lichen growth [Tha2005]. The cave entrances provide favourable conditions for the growth of lichens. Lichens are known to absorb elements during their growth. It is hypothesised that the lichens absorbed elements during their growth phase above the cave ceiling that after cave in ended up inside the caves where the conditions are unfavourable for lichen growth where they died and ended up depositing their elemental contents to their points of attachment. The deposited elements in the Sterkfontein region dominantly Mn oxidises to MnO_2.

As a continuation of the studies by Thackeray, we report results of investigations on fossilised antelope bone samples representing different age periods in the formation of the Sterkfontein archaeological sites. The study includes the investigation of a sample of chert rock that contains both lichen and brown stains on its surface. The chert rock was taken from the entrance of the Sterkfontein cave.

1.2 Literature review

1.2.1 Literature review boundaries

Literature review includes defining lichen, suitable environmental conditions for lichen growth, and literature review on the cave formation to describe how the samples ended up in the caves.

1.2.2 Lichens

Lichens are symbiotic associations of fungi and algae [Ara2004, www04]. Symbiotic association means that lichen is created mutually between the fungus and alga [www05]. If fungus and green alga are compatible they form a thallus also generally referred to as

the lichen body. Only certain algae and fungi can get together to form lichens. The fungus is a manganese rich organism. Thallus helps in assigning names and making lichen identification, for example foliose lichens and crustose lichens [www04]. The alga uses sunlight to produce sugar and food that feeds the fungus and alga. Lichens produce food through photosynthesis under suitable environmental conditions where there is moisture and the light is not too limited [Tha2005]. Photosynthesis is a biological process where carbohydrates, oxygen and lipids are produced by plant matter through sunlight. A photograph of lichen growing on a tree stem is shown in Fig 1.4.

Figure 1.4 Photograph of lichen on a tree stem [Ara2004].

1.2.2.1 Properties of lichens

Lichens contain amorphous and crystalline material in the thallus with a ratio of 70%: 30% [Ara2004]. Crystalline material comes from lipids, which are produced, by fungal cells. Lichens take a long time to dry and their photosynthesis and other physiological parameters do recover after dehydration [Lás2002]. To check this we sealed some lichen samples in a glass desiccator and put it in a dark cupboard. After a period of 8 months no visible change in the appearance of the lichen samples was seen. Lichens have no vascular tissues, xylem, phloem or roots and as a result they attach themselves to

substrates such as rock or tree bark using rhizines. Rhizines are roots or fungal structures found in the lower cortex of the lichens. Vascular tissues are supportive and conductive tissues in plants, consisting of xylem and phloem [www06]. Xylem refers to a supporting and water conducting tissue of vascular plants, primarily consisting of woody tissue [www07]. Phloem is a tissue that conducts synthesized food substances to parts where needed [www08]. Lichens are entirely dependent on the water and nutrients present on the host surface or in the atmosphere [www09].

1.2.2.2 Lichen growth

Lichens are slow growing organisms that maintain a uniform morphology with time [Berg2004]. Their growth is fractions of millimeters over a year [www05]. Under the right conditions lichens absorb elements that are available in that particular atmospheric environment, i.e. if there is high concentration of manganese, lichen will contain more Mn than other elements [Cla1999, Baf2002]. They are known to absorb elements such as manganese (Mn), lead (Pb), titanium (Ti), strontium (Sr), and zinc (Zn). Some lichen species absorb more manganese than others; the species that absorb primarily manganese are cynobacteria whereas the species that absorb less manganese are chlorolichens [Mar2005]. Lichens also absorb air pollutants like sulfur and as a result can be used for monitoring air pollution [Cla1999]. If lichens absorbed too high concentration of elements such as Mn or toxic elements they may die [Mar2005]. Lichens may also die when covered with sediment that inhibits photosynthesis. Subsequently they may deposit the elements absorbed during their growth to their host [Nie1978].

1.2.3 Dolomite and chert

Dolomite and chert are two types of rocks found in the caves of the Sterkfontein archaeological sites. Figure 1.5 shows photographs of the chert rock and dolomite samples investigated in this study. The chert sample has prominent lichen growth as well as brown stains on its surface. Chemically dolomite contains calcium magnesium carbonate ($CaMg(CO_3)_2$) as identified from the XRD pattern in Fig 1.6. Dolomite was

named after the French mineralogist Deodat de Dolomieu [www10] and plays a big role in cave formation due to the chemical reaction of calcium magnesium carbonate with rainwater. Chert comprises mostly chalcedony-cryptocrystalline silica, or quartz (SiO_2) as inferred from the XRD pattern in Fig 1.7.

Figure 1.5 Photographs of chert (a) and dolomite (b) rock from the Sterkfontein area. Areas of lichen growth on the chert rock are shown within the □ and the brown stains by ○.

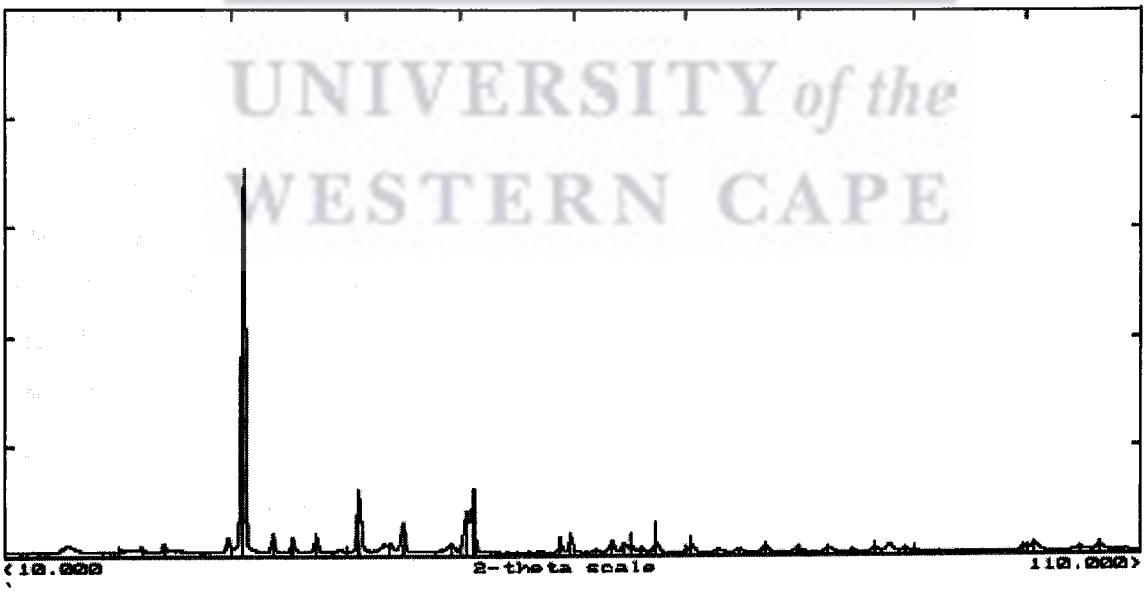

Figure 1.6 XRD pattern showing results of powdered dolomite sample. The pattern is identified to be calcium magnesium carbonate. The vertical lines indicate the intensities and positions of the ICDD standard for dolomite.

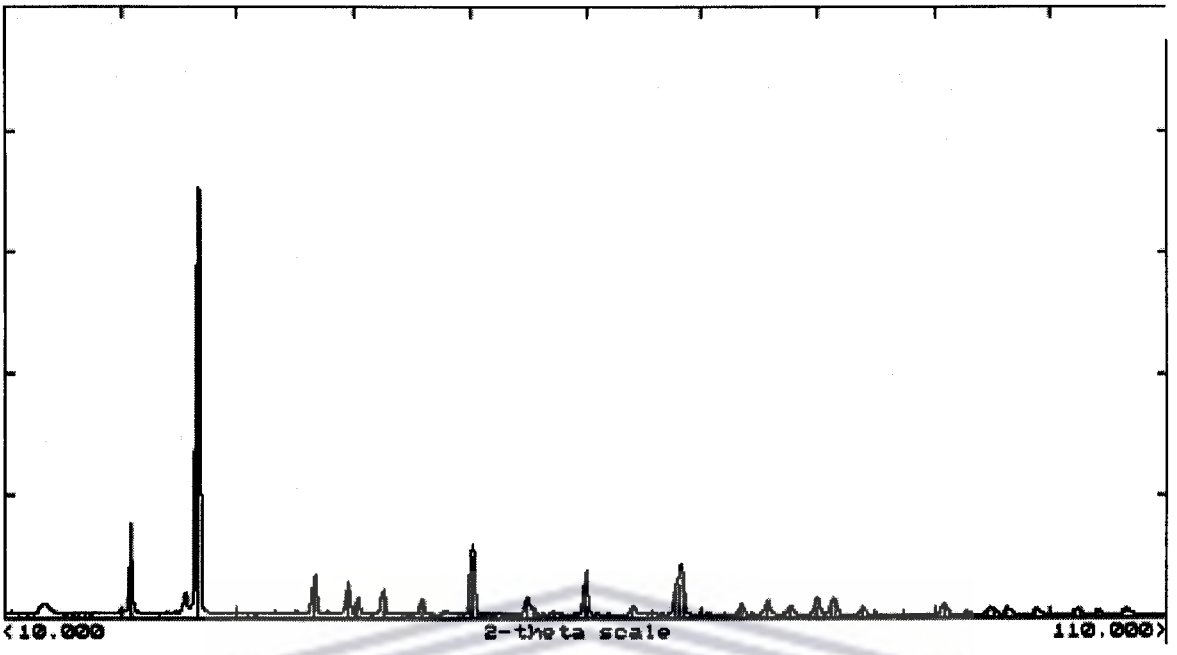

Figure 1.7 XRD pattern of chert powder. The pattern is identified to be silicon dioxide (SiO_2).

1.2.4 Formation of caves

In general caves are formed in all sorts of rocks i.e. igneous, sedimentary or metamorphic by processes such as volcanic, tectonic, or physical erosion by water and chemical solution [www11]. Igneous rock is formed by solidification of molten magma during volcanic eruptions. Metamorphic refers to the rock altered by pressure and heat. The Sterkfontein caves were formed through water and chemical solution of the sedimentary dolomite rocks [Bra1981]. Caves are formed by processes inside and outside the earth [www11]. The rain picks up dissolved carbon dioxide gas from the atmosphere and decaying plant matter in the soil. This leads to the formation of weak carbonic acid solution following the chemical reaction.

$$H_2O + CO_2 \rightarrow H_2CO_3 \qquad (1.1)$$

This carbonic acid will dissolve calcium carbonate in limestone and dolomite forming calcium bicarbonate in water.

$$CaCO_3 + H_2O + CO_2 \rightarrow Ca(HCO_3)_2 \quad (1.2)$$

This process dissolves the dolomite rock over thousands of millions of years forming cave passages. At this stage the cave is water filled without an opening. While the underground passage is growing larger, the surface above continues to erode thus lowering the water table and allowing air into the cave. The cave becomes partially air filled. When this happens, some of dissolved carbon dioxide escapes and changes the acidity of the water. The calcium carbonate comes out of solution and is deposited as crystallized calcite following the chemical reaction.

$$Ca(HCO_3)_2 \rightarrow CaCO_3 + H_2O + CO_2 \quad (1.3)$$

Erosion continues until surface streams cut the valleys at the joints intersecting the surface. After some years this causes thinning of the roof until it collapses and falls in thus exposing the cave. Whatever is on the roof surface ends up inside the cave. From this, fossils on top of the ground end up inside the cave [www11]. With time this layer is coated with ground falling from the surface. In many cases trees surround the cavities. Predators stow and eat their prey such as antelope in the trees with the bones subsequently falling into the cavity. Thus systematically a prismatic deposit forms on the cave floor. The term Members refer to fossils found in sequential ground layers. Erosion continues to remove much of the roof and in many cases expose the cave and thus exposing its content such as fossils. The caves at Sterkfontein archaeological sites are at this stage [Brain 1981].

1.2 Aim

The aim of this research is to determine possible correlations between the chemical nature of stains existing on fossil bone samples and their age, using Scanning Electron microscope (SEM), X-Ray Fluorescence (XRF) and X-Ray Diffraction (XRD). Part of the aim is to explore the hypothesis of Thackeray and his team that the stains are related

to the lichen growth that was stiffened after the bones inside the caves were covered by sediment [Tha2005].

1.3 Thesis overview

The current chapter serves as introduction and literature review of the research. The rest of the thesis is on results obtained from investigation of the stains on the fossils with the experimental techniques.

Chapter 2 is about the samples and their preparation.

Chapter 3 discusses experimental techniques and procedures.

Chapter 4 reports results and discussions.

Chapter 5 gives conclusions and recommendations.

References are given at the end of the manuscript.

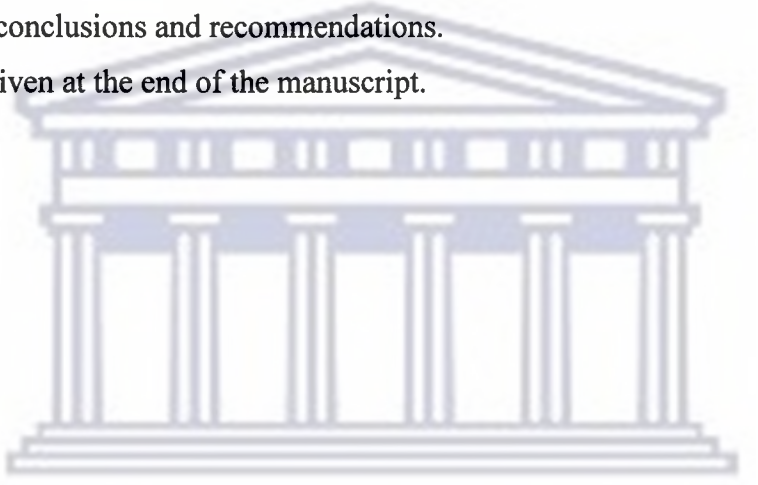

Chapter 2

Samples

This study reports the investigation of antelope fossil bone samples excavated from the Sterkfontein, Swartkrans and Kromdraai caves, chert rock that contains both live lichens and brown stains on its surface as well as dolomite rock. The bone samples represent different ages periods referred to in archaeological terms as members. The sample series encompasses seven members. The age periods relevant to different members are:

- Swartkrans Member 3 = 1 million years.
- Swartkrans Member 2 = 1.5 million years.
- Swartkrans Member 1 = 1.7 million years.
- Kromdraai A = 1.5 - 1.8 million years.
- Kromdraai B = 1.95 million years.
- Sterkfontein Member 5 = 1.8 million years.
- Sterkfontein Member 4 = 2.5 - 2.1 million years.

The piece of chert rock was taken from the Sterkfontein cave entrance and the dolomite from inside the Sterkfontein cave. Table 2.1 summarises all the samples of this study. Photographs of the samples are shown in Figs 2.1 to 2.5.

2.1 Photographic Images of Fossil Samples

Figure 2.1 shows photographs of the fossil samples taken by optical spectroscopy. These images were taken after preparation and cleaning. The images include samples from all caves. Samples from Swartkrans caves have more prominent stains compared to others from the other caves, followed by samples from Kromdraai caves.

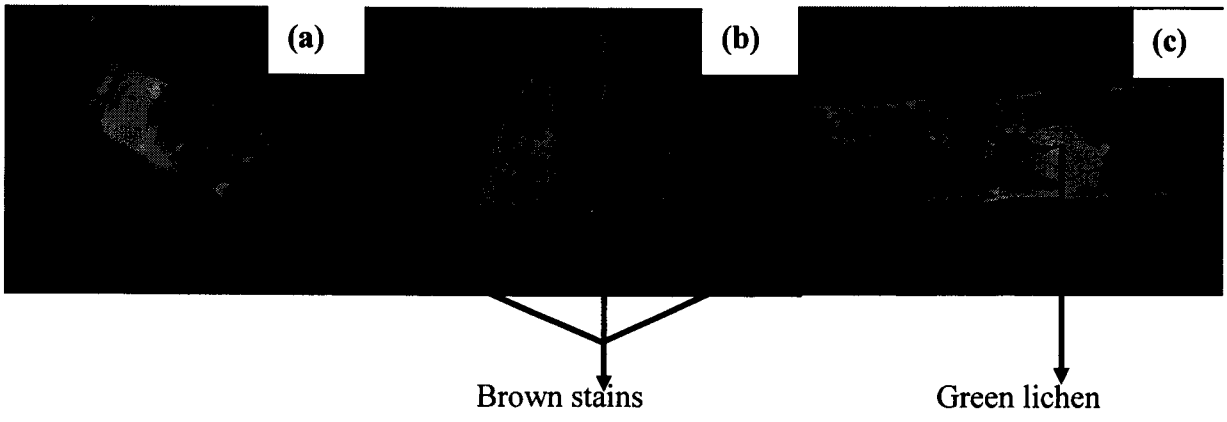

Figure 2.1 Optical spectroscopy photographs of (a) sample SK20217 from Swartkrans member 2, (b) SK10313 from Swartkrans member 1 and (c) a piece of chert rock with lichen and brown stains on its surface.

2.1.1 Samples selected for XRF and SEM

A selection of two samples per member were analysed as well as the chert rock. Two regions were investigated on each of the bone samples i.e. on and off the stains. Photographic images of the samples are shown in Figs 2.2 to 2.5. Three regions were investigated on the chert rock, which included lichen, brown stain, and the chert rock itself. The analysed regions are indicated by □ for the on-stains positions, ○ for the off-stains (substrates) positions and Δ for the live lichen on the chert rock.

Figure 2.2 Photos of samples selected from the Sterkfontein cave members, (a) sample SE50207, (b) SE50510, (c) ST40404 and (d) ST40202. The regions of interest are indicated by the symbols ○ for the off-stains and □ for the on-stains.

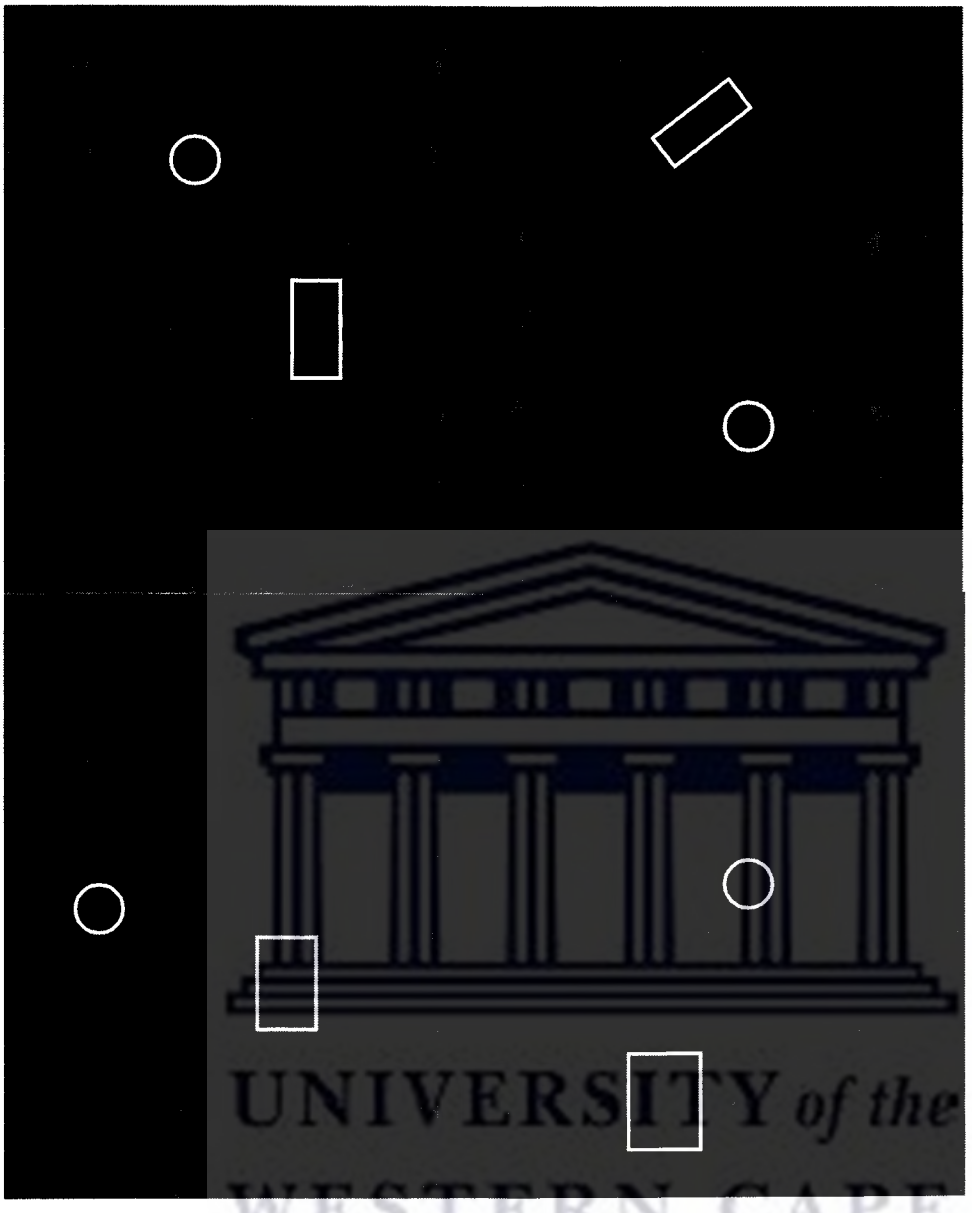

Figure 2.3 Photos of samples selected from the Kromdraai cave members, (a) sample KDA0530, (b) KDA0227, (c) KDB0131 and (d) KDB0434. The regions of interest are indicated by the symbols ○ for the off-stains and □ for the on-stains.

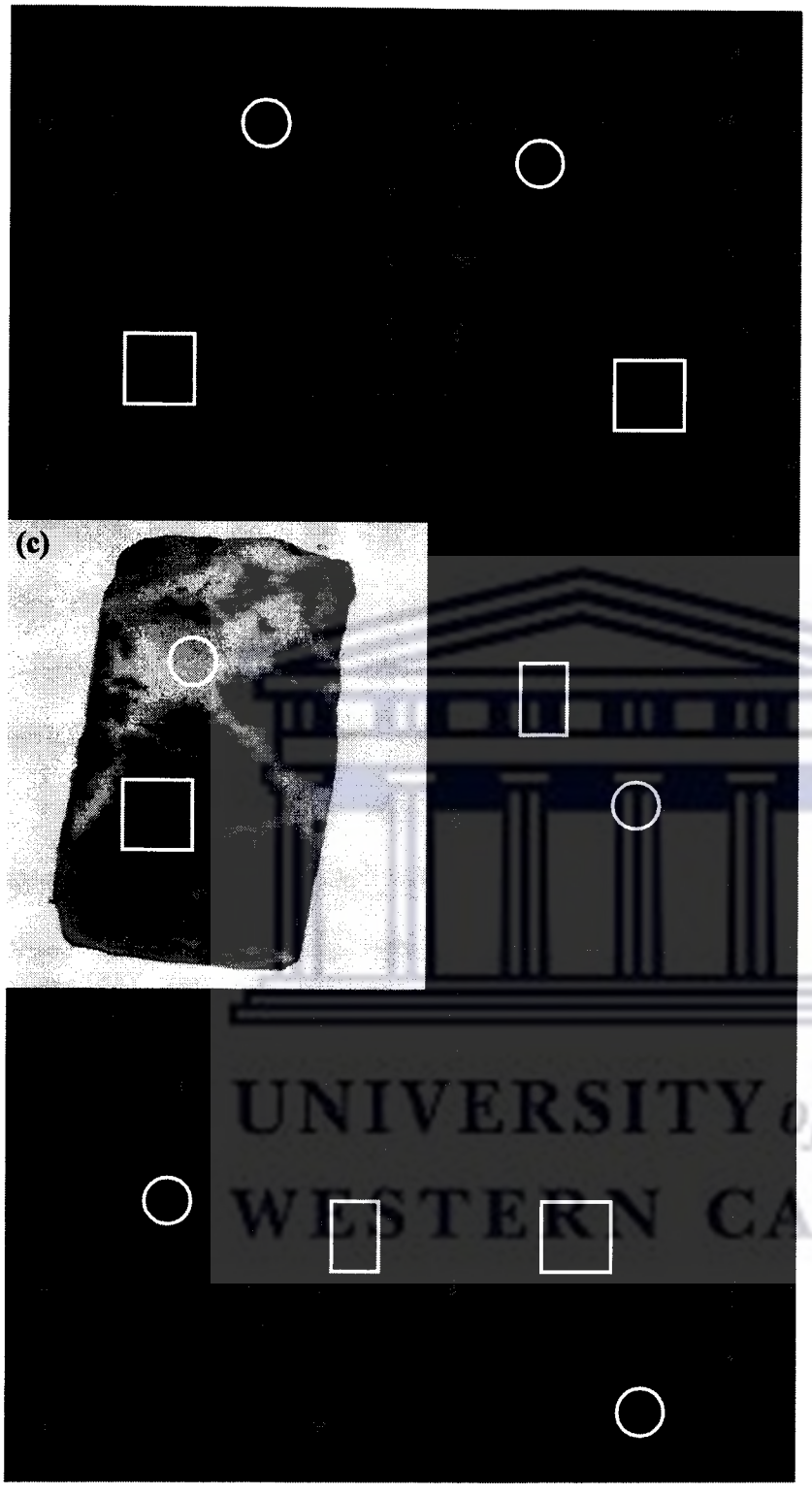

Figure 2.4 Photos of samples selected from the Swartkrans cave members, (a) sample SK10114, (b) SK10313, (c) SK20419, (d) SK20217 (e) SK30323 and (f) SK30121. The regions of interest are indicated by the symbols ○ for the off-stains and □ for the on-stains.

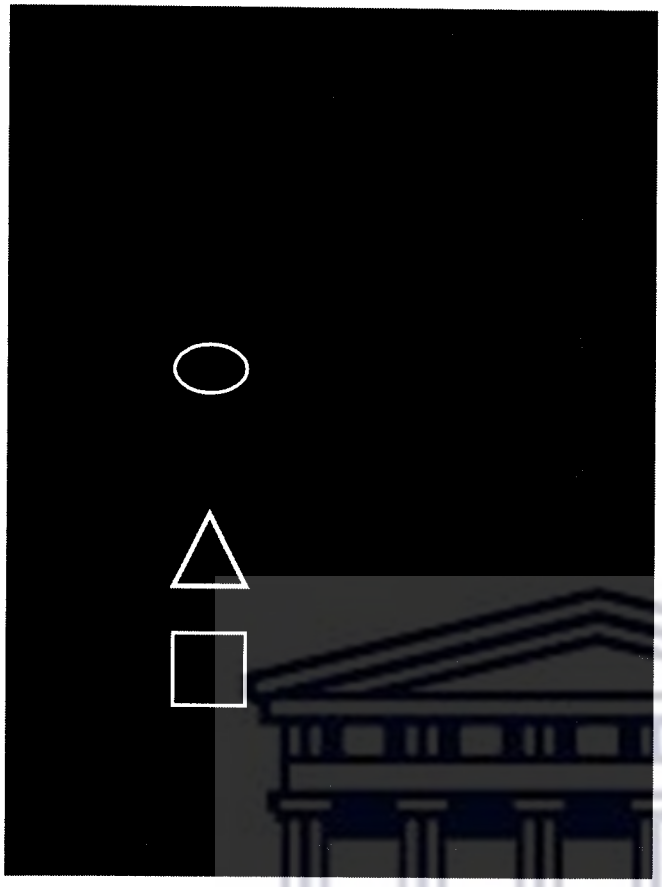

Figure 2.5. Photo of a small sample cut from the large chert rock originating from the Sterkfontein cave entrance. The regions of interest are indicated by the symbols ○ for the off-stains, □ for the on-stains and Δ for the green lichen.

2.2 Preparation of samples

2.2.1 Identification of the regions of interest

Samples were selected according to the following criteria:

- Presenting as smooth and flat surfaces as possible to enable favourable conditions for experimental investigation with electrons and x-ray beams that are sensitive to the near surface regions only due to their limited penetration depths (μm).
- Presence of a number of stains per sample.
- Visibility of bone material (hydroxylapatite) on the fossil samples for comparative investigations.

2.2.2 Cutting of samples

The samples were cut with a diamond saw using water as lubricant and coolant to sections approximately 2x2x3cm^3(the size of a human thumb) to fit into the sample holder stages of the instruments. It took approximately two minutes per cut. The regions of interest with the investigations were taken to be almost at the center of the samples.

2.2.3 Cleaning of samples

The samples were ultrasonically cleaned twice with distilled water for 15 minutes and handled with no longer skin contact. Distilled water was used to limit additional contamination of samples.

2.2.4 Referencing of samples

Referencing of fossil samples is divided into the palaeontological sample reference and the laboratory reference. Laboratory reference is the sample identification used during experimental measurements; this referencing includes the origin of the sample, sample number within a particular member and the sample number from all the samples of this study. For example the x-ray diffraction and x-ray fluorescence lab reference KDA 01 26, KDA implies that the sample originates from Kromdraai caves member A, 01 refers to the sample number 1 within batch of samples from Kromdraai member A and 26 indicates the sequence 26 out 35 samples, but for this study only 16 samples were analysed and are identified in Table 2.1. The sample referencing is that used by palaeontologists who take into consideration the origin of the sample, for instance SK1 17307, which is the sample from Swartkrans, caves member 1 with 17307 being the sequence number. Table 2.1 summarises references. The L and S referencing refers to different orientations of the samples, this will be explained in details under XRD results.

Sample Description	Sample Ref	Sample Age	Lab Ref
Sterkfontein Type Site Member 4 (STS,ST4)	STS 1321	2.1-2.5 million years	ST4 0101
	STS 1227		ST4 0202
	STS 1876		ST4 0404
Sterkfontein Extention Member 5 (SE, SE5)	SE 1363		SE5 0207
	SE 2308		
	SE 888		SE5 0510
Swartkrans Member 1 (SK1)	SK1 39843	1.7 million years	SK1 0313
	SK1 38406		SK1 0414
Swartkrans Member 2 (SK2)	SK2 3829	1.5 million years	SK2 0217
	SK2 3546		SK2 0419
Swartkrans Member 3 (SK3)	SK3 35925	1 million years	SK3 0121
	SK3 30530		SK3 0323
Kromdraai Member A (KA, KDA)	KA 2210	1.5-1.8 million years	KDA 0227
	KA 2242		KDA 0530
Kromdraai Member B (KB, KDB)	KB 527	1.95 million years	KDB 0131
	KB 351		KDB 0434
Sterkfontein Caves	Chert rock		Chert rock
	Dolomite		Dolomite

Table 2.1 Summary of samples used in this study. The laboratory references for the SEM, XRF and XRD are indicated.

Chapter 3

Experimental techniques and procedures

The three materials characterization techniques scanning electron microscopy (SEM), x-ray fluorescence (XRF) and x-ray diffraction (XRD) were used in this study. The XRF and XRD instruments are available at NECSA, with the SEM utilised at the CSIR Pretoria. Each technique will be discussed in detail on its relevant section of this chapter. The fundamentals of the radiation types and their interaction with matter are discussed.

3.1 Electrons

Electrons are fundamental subatomic particles that carry an electric charge. George Johnstone Stoney coined the word electron in 1891. J.J Thomson made the discovery that an electron was a subatomic particle in 1897. They are found in the atomic shells around the nuclei of atoms. Electrons have a negative electrical charge of -1.6022×10^{-19} coulombs, and a mass of 9.11×10^{-31} kg (approximately $1/1836$ of that of a proton). The electron symbol that is widely used in the world is e^-. Electrons exist in many configurations in matter.

Electrons are widely used in different kinds of analytical techniques used in material science studies. They are either used directly as the probe or in the production of secondary particles such as x-rays. Penetration depth of electrons is directly proportional to their accelerating voltage.

3.2 X-rays

A German physicist Willem Roentgen accidentally discovered x-rays in 1895 when he was doing experiments with an electron beam in a gas discharge tube. The exact nature of x-rays was determined in 1912 as well as the phenomenon of diffraction by crystals. Diffraction can reveal details of a periodic structure in the order of 0.1 nanometer (nm) in size (1nm = 10^{-9}m=10Å) [Cul1978].

X-rays are a form of electromagnetic radiation similar in nature to light, but have much shorter wavelengths. X-rays used in diffraction analysis have wavelengths lying approximately in the range 0.5 – 2.5Å whereas light has wavelengths in the order of 6000Å. On the electromagnetic spectrum, x-rays occupy the region between gamma and ultraviolet rays as shown in Fig 3.1[Cul1978, Gui1963].

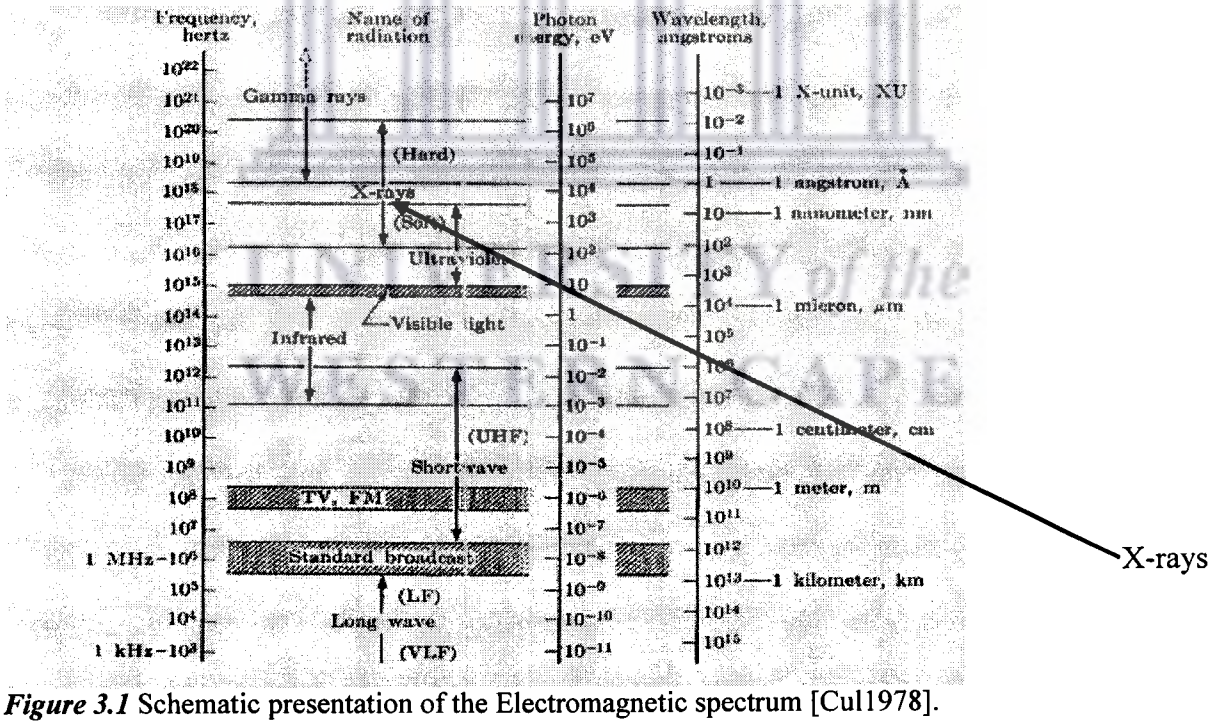

Figure 3.1 Schematic presentation of the Electromagnetic spectrum [Cul1978].

X-rays are produced when any electrically charged particles, usually electrons, are accelerated at a very high voltage and subsequent high kinetic energy from the source

(cathode) to collide with a metal target (anode). The XRD instrument at NECSA uses a copper (Cu) target that gives a range of x-rays, only monochromatic wavelength 1.5418Å is used. All the processes take place inside the x-ray tube at the point of impact and radiates in all directions. The kinetic energy at the impact point is given by:

$$E_k = eV = \frac{1}{2}mv^2 \tag{3.1}$$

Where V is the accelerating voltage across the electrodes, m is the mass of an electron, v is the velocity before the impact point and e is the electron charge. Less than 1% of the kinetic energy is transformed to radiation with the rest converted to heat.

Two processes happen when x-rays encounter matter i.e. they are either partly transmitted or partly absorbed. The fractional decrease in the intensity of the x-ray beam passing through any homogenous substance is proportional to the distance x traversed and this relationship is given by:

$$\frac{dI}{I} = -\mu dx \tag{3.2}$$

where μ is linear absorption coefficient measured per centimeter(cm^{-1}) and depends on the substance present, and I refers to the incident intensity. The linear absorption coefficient is proportional through the density (ρ) as μ/ρ (to the mass) is a constant of the material and is independent of its physical state of matter (solid, gas, liquid). Equation 3.2 can thus also be expressed as:

$$I(x) = I_0 e^{\left(-\mu/\rho\right)/\rho x} \tag{3.3}$$

I_0 is an intensity of the incident beam, and $I(x)$ the intensity of the transmitted beam after passing through a thickness x of material. For compounds with more than one chemical element (independent of its physical state of matter), the mass absorption coefficient is given by [Cul1978] [Gui1963]:

$$\mu/\rho = \sum_{I=1}^{N} \left(\frac{\mu}{\rho}\right)_I w_I \qquad (3.4)$$

w_I is the weight fraction of element I. The penetration depth of keV x-rays depends on the atomic mass and it is very small for heavy elements. The fundamentals of the analytical methods of SEM, XRF and XRD are discussed in the subsequent paragraphs.

3.3 Scanning Electron Microscope (SEM)

This instrument was developed during the early 1950's, and has since become a standard instrument employed by researchers to examine surface characteristics of samples. This microscope uses an electron beam to form images. The scanning electron microscope has many advantages over traditional microscopes owing to it large depth of field and having much higher resolution to enable magnification of small characteristics in the order of nm [www12] [Ege2005]. The penetration depth of the electron beam in to matter is given by the Kanaya Okayama depth penetration formula [Kan1972]:

$$R = \frac{0.0276AE^{1.67}}{(Z^{0.89}\rho)}\,\mu m \qquad (3.5)$$

R = Penetration depth of incident beam in to the material in μm.

A = Atomic weight (g/mole) of the material.

E = Beam energy (kV) of the incident beam.

Z = Atomic number of the material.

ρ = Density $(g/cm)^3$ of the material.

In the study of the fossil samples the SEM technique enables elemental analysis.

3.3.1 Operational principles of the SEM

Electrons that interact with a sample surface can undergo a number of possible interactions.

- Undeflected (i.e. transmitted without interaction with any atom in very thin samples).

- Deflected but looses no energy (i.e. elastically scattered).
- It loses a significant amount of energy and is probably deflected (i.e. inelastically scattered).

The latter interaction results in the emission of x-rays. In a SEM, a beam of electrons is produced from the electron gun and focused through an anode hole to the sample below the electron gun. The beam is focused vertically on the sample by electromagnetic fields and lenses. When the beam hits the sample surface inelastic interactions cause electrons and x-rays to be ejected from the sample as shown in Fig 3.2 [Cha1986, Joh1976].

All these x-rays and electrons are detected by detectors specifically positioned at optimum positions around the sample from where their signals are electronically converted to be viewed on a screen. [www12, Ege2005].

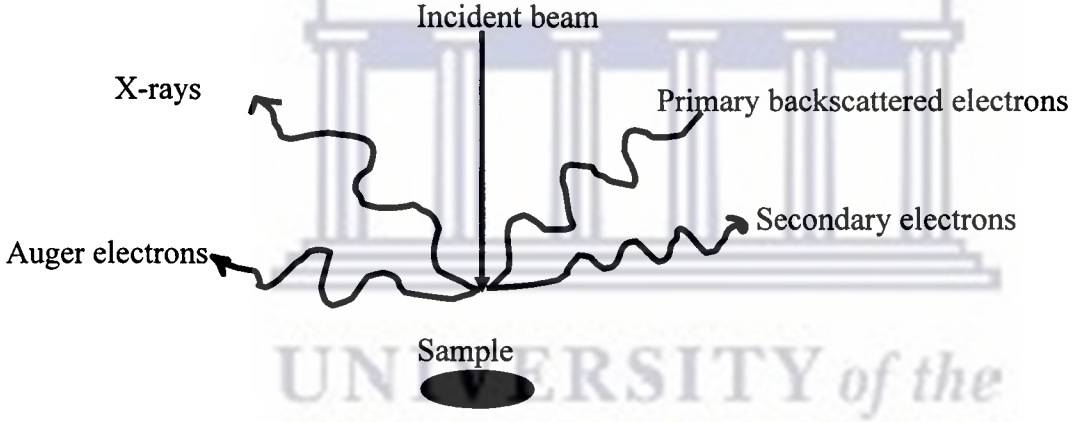

Figure 3.2. Schematic representation of radiation produced by high energy electron beam in a SEM instrument.

Backscattered electrons undergo single or multiple scattering events and escape back through the sample surface with energies greater than 50 eV. The signals from these electrons are used for atomic number contrast and topographical contrast. Backscattered electrons can also be used to form an electron backscatter diffraction (EBSD) image that can be used to determine the crystallographic texture of the sample [www13, Cha1986, Joh1976].

Secondary electrons refer to electrons that were knocked out from atoms by the incident primary electrons. These electrons have energies less than 50 eV. The signals from these electrons are used to study surface topography as they only penetrate a few nano meters into the surface and gives resolution of around 2 nm [www13, Cha1986, Joh1976].

3.3.2 Information produced by SEM

The examination of objects using SEM analysis enables information on[www14, Cha1986, Joh1976]:

- Topography, which gives features of the surface of an object or sample, this is obtained from the secondary electrons.
- Elemental composition, what the sample is composed of and the relative amounts of each, which is obtained from characteristic x-rays.
- Phase differentiation within the sample, which is obtained from the backscattered electrons.

3.3.3 Sample preparation for Scanning Electron Microscope

The fact that SEM utilises vacuum conditions and uses electrons to form an image, requires special preparations that must be done to the sample. Preparations include the following:

- Samples must be dry to prevent vaporisation in the vacuum.
- All electrically non-conducting samples must be coated with a thin layer of a conducting material.
- Samples must be cleaned with alcohol, distilled water and acetone that don't leave any residues.

Bulk samples can be examined in the SEM, but the sample size needs to have dimensions that will allow it to fit in the sample stage [www13].

3.3.4 SEM instrument at CSIR

The instrument enables energy dispersive x-ray microanalysis (EDX), which has a higher detector efficiency than wavelength dispersive x-ray microanalysis (WDX). The instrument is capable of detecting secondary electrons, backscattered electrons and characteristic x-rays. It is also capable of imaging from low magnifications (20x) up to high magnification (400 000x) and EDX spectroscopy enables analysis of elements from carbon to higher atomic numbers. The detection limit of the EDX spectroscopy is in order of 1wt% depending on the sample but it may go as low as 0.1wt%. In the EDX spectrum each detected x-ray produces a charge pulse with a small current in the detector (Si-Li detector). The current is converted to a voltage pulse then into a digital signal reflecting the energy of the original x-ray. The digital signal in turn, adds a single count to the appropriate energy channel of a multi channel analyzer (MCA). The process continues until there are multiple counts, which results in broad peaks. This is also illustrated in Fig 3.4. The photograph of the instrument is shown in Fig 3.5.

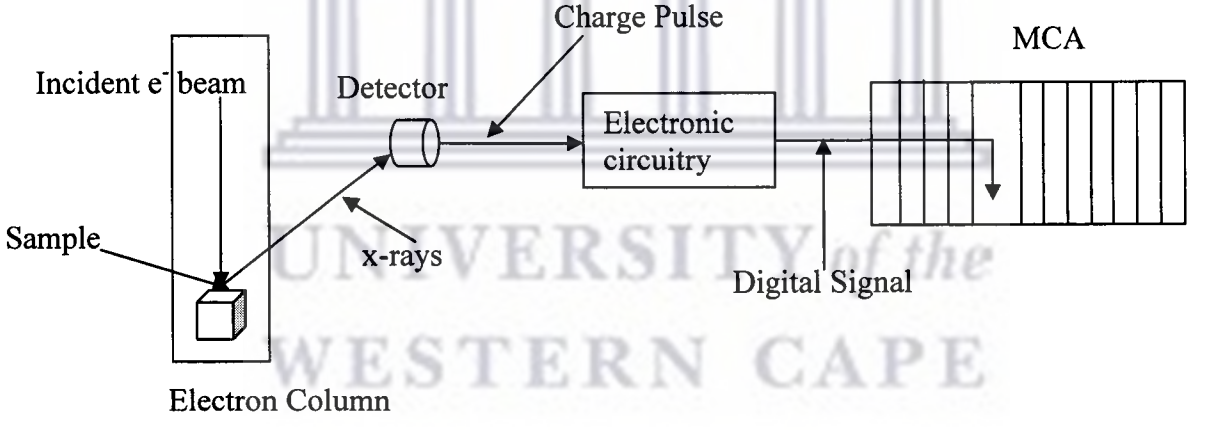

Figure 3.4 Schematic diagram of how an EDS processes the x-ray signals.

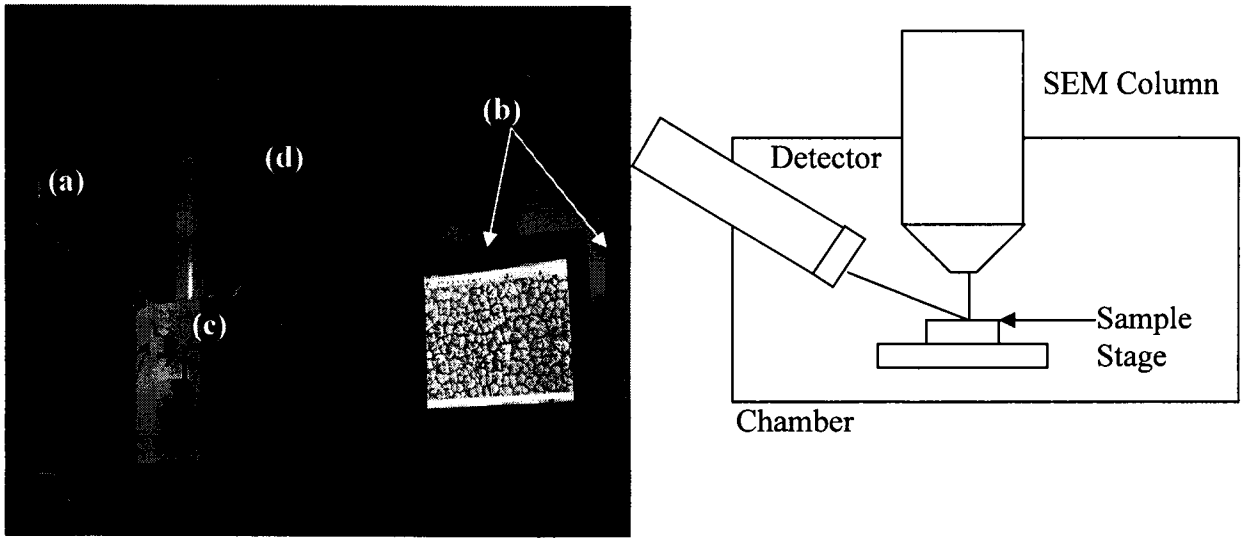

Figure 3.5 Photograph of the Leo Gemini 1525 FE-SEM instrument at CSIR, (a) EDX detector, (b) computers for viewing images and results, (c) is the sample chamber which is schematically illustrated on the right of the photograph and (d) is an electron column.

3.4 X-Ray Fluorescence (XRF)

XRF is a non-destructive technique used for elemental analysis of solids and liquids using x-rays as a probe. The sample is irradiated by an intense x-ray beam, which results in the generation of x-rays that are detected by either energy dispersive or wavelength dispersive detectors. Incident x-rays are more energetic than emitted x-rays from the sample. Energy dispersive detectors detect energies of the emitted x-rays at fixed angles whereas wavelength dispersive detectors resolve wavelengths of the emitted x-rays. The instruments are referred to as the Energy Dispersive Spectrometer or Wavelength Dispersive Spectrometer. The concentration of elements in the material being analysed are determined by the intensities of the emitted x-rays. This technique can analyse samples to depths that range from less than 1 millimeter (mm) depending on the energy of the emitted x-rays and sample composition. Elements that are routinely detectable range from sodium (Na) to uranium (U), but lighter elements from boron (B) to fluorine (F) may also be detected if they are in high concentrations [www15]. In this study a wavelength dispersive Spectrometer (Axios model) was used.

Aim of the x-ray fluorescence

The aim was to determine the elemental composition of the stains on the fossil samples.

3.4.1 Scientific method of XRF

X-rays are produced in the x-ray tube by accelerating electrons through a potential difference of 32 to 60 kV from the source (cathode (-)) to the metal target (anode (+)), that emits x-rays due to the collision interaction. These x-rays form an incident x-ray beam directed at the sample being analysed. The interaction between the x-ray incident beam and the electrons in the atom produce x-rays that are characteristic of the elements inside the sample [www15]. Each element has unique x-ray energies related to the binding energies of the element that are furthermore different depending on the electronic shell it falls from. This discrimination is possible since the difference in emitted x-ray energies between neighbouring elements on the periodic table are large enough to differentiate between elements.

During the interactions the incident x-ray beam knocks electrons from the inner shells of the atoms(s and d shells), thus creating vacancies that are filled by electrons falling from the outer shells to the inner shells. In the process these electrons dispose of their excess energy in the form of x-rays or photons. This is illustrated in Figs 3.6 and 3.7. The energies or wavelengths of these x-rays are detected in the detector used and analyses the emitted radiation for elemental analysis, together with the corresponding concentrations of the elements identified [www15].

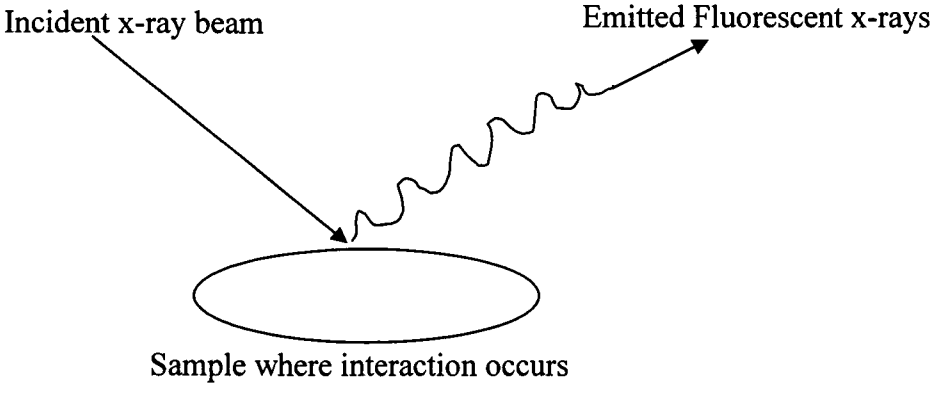

Figure 3.6 General XRF process.

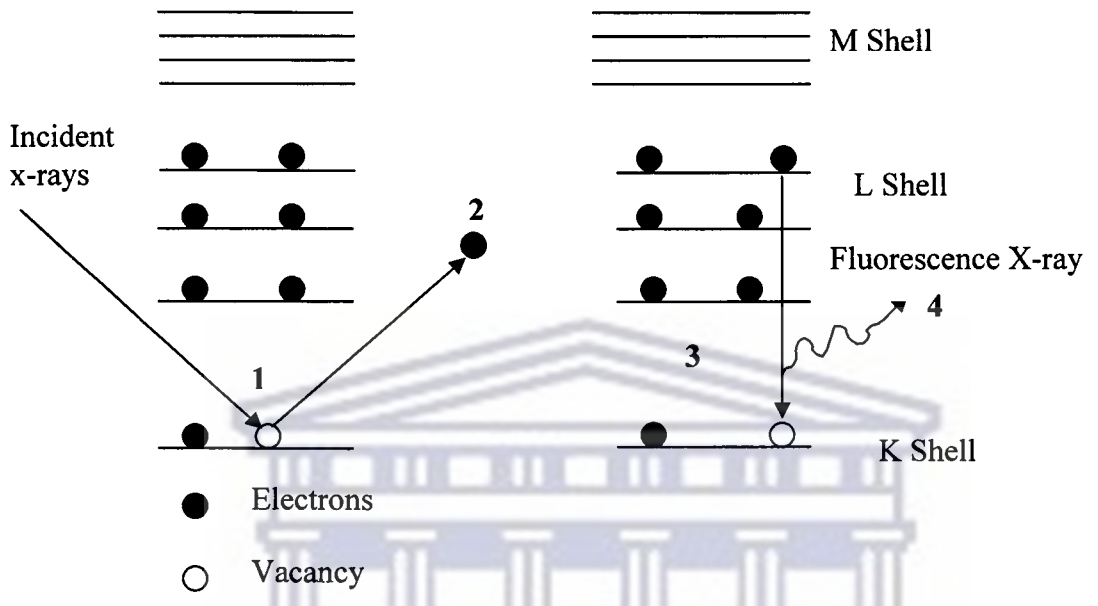

Figure 3.7 Schematic diagram of the XRF process. During stages 1 and 2 the incident x-ray beam knocks out an electron from a low level energy band (K shell), thus forming a vacancy. At stage 3 an electron from an outer energy shell (L shell) fills a vacancy in the inner shell (K shell) thus giving up excess energy in the form of x-ray or photon as shown in stage 4.

3.4.2 Wavelength dispersive spectrometer at NECSA

NECSA has recently procured a new wavelength dispersive XRF Pan Analytical Axios model and is shown in the Fig 3.8(a). The instrument uses wavelength scanning and is capable of qualitative and quantitative analysis depending on the sample conditions. The x-ray tube uses rhodium (Rh) as metal target (anode) for producing x-rays with a beryllium (Be) tube window. The instrument uses the iQ+ software package for measurement set-up and analysis. A data acquisition takes 3 to 15 minutes (iQ+ fast mode) to run. The sample holders are shown in Fig 3.6(b). The sample shape is not important as long as it is flat and has a size of approximately 30mm.

Measurement Procedure

A beam mask made of copper (Cu) was used to limit sample illumination to a smaller region of interest. The mask was put onto the sample with bostik to ensure that only the region of interest is exposed to the beam. The mask and sample were put into the sample cup holder as shown in Fig 3.8(b), with the latter put in the sample stage of the instrument.

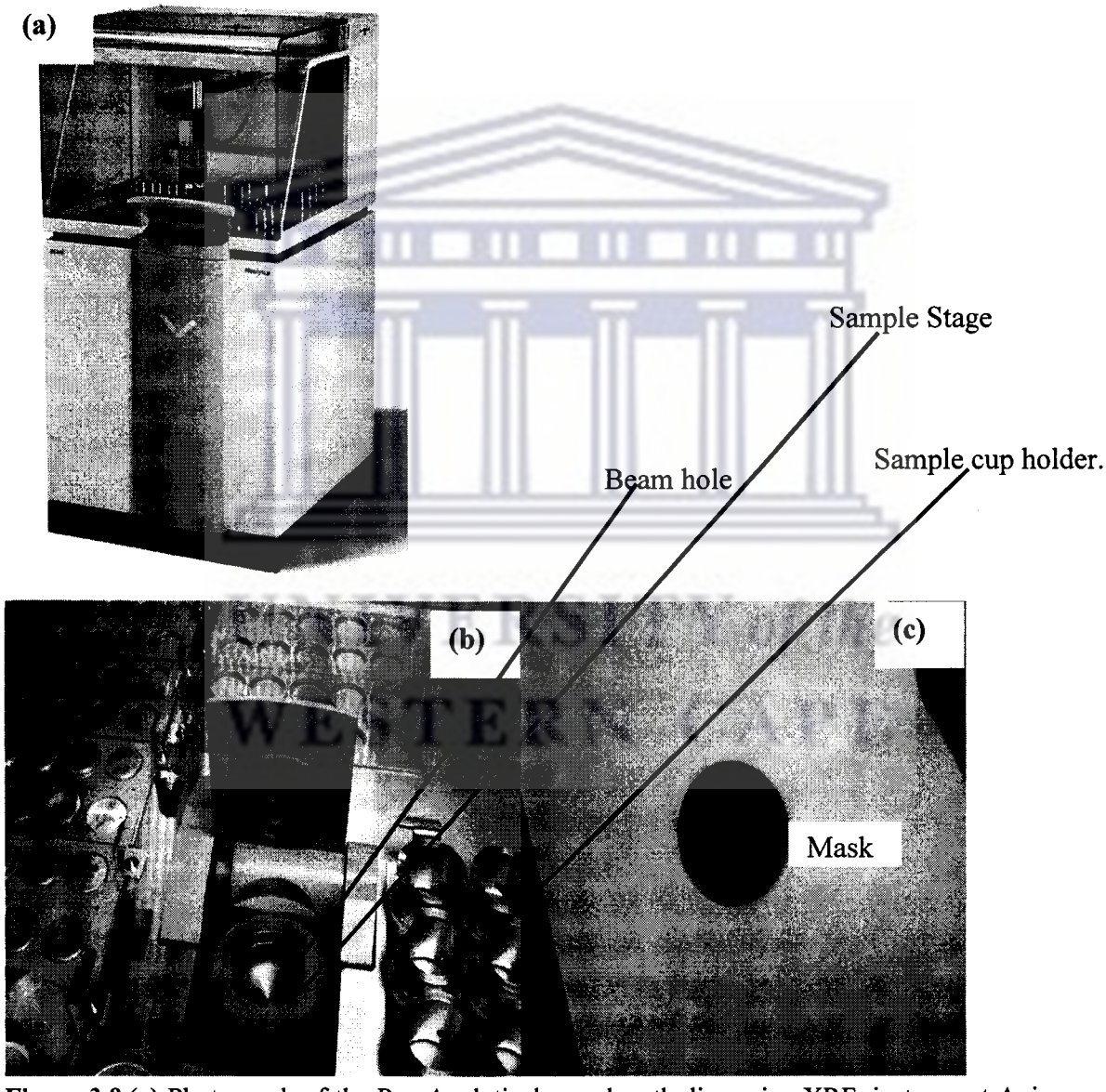

Figure 3.8 (a) Photograph of the Pan Analytical wavelength dispersive XRF, instrument Axios, model at NECSA; (b) shows the sample stage of the instrument where sample fits in cup holder, beam hole where beam comes through and sample cup holder; (c) shows the mask that is placed over the sample to expose a smaller part of the sample to the incident x-ray beam.

3.4.3 General derivation of results

Figure 3.9 shows the data acquisition, procedure from the incident x-rays to the spectrum. The x-ray tube emits a polychromatic x-ray beam. The incident beam is directed to the specimen where three spectral ranges having, short, intermediate and long wavelengths are separated via the analyser crystal [Eug1978].

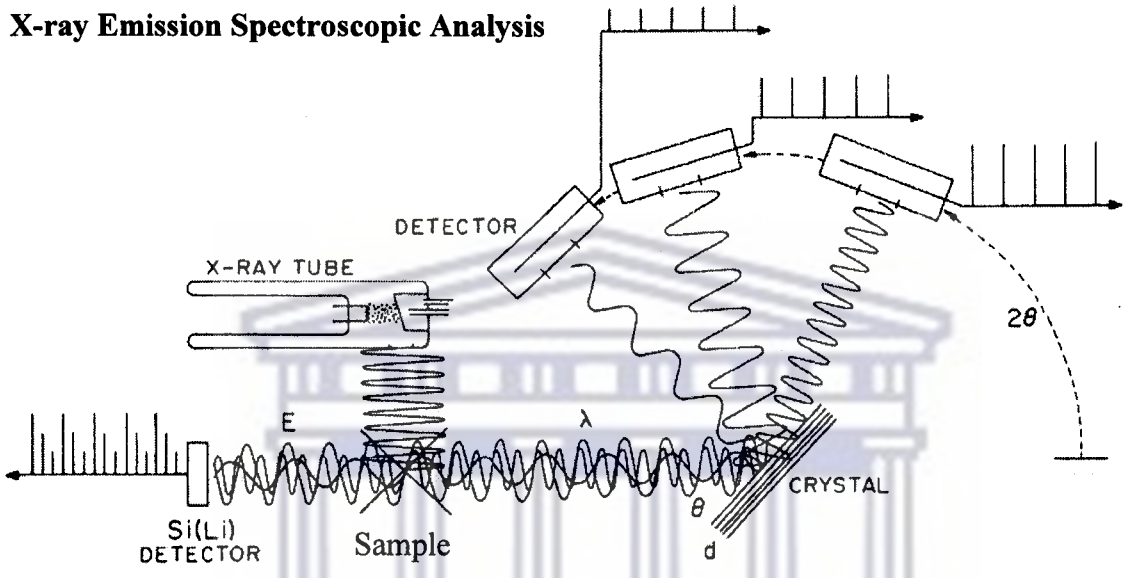

Figure 3.9 General Principle of WDS XRF Analysis [Eug1978].

E represents the energy dispersive spectrometer part of the instrument, λ refers to the wavelength dispersive spectrometer part of the instrument, and d is an interplanar spacing in the analyser crystal, θ is the crystal angle relative to the radiation emitted by the sample and 2θ is the detector angle relative to the radiation emitted by the sample.

Wavelength Dispersive Spectrometers

The principle of the WDS is shown in Fig 3.11. In this part of the instrument, the spectral lines from the three monochromatic wavelengths fall upon an analyser crystal that rotates synchronously through successive θ and 2θ angles with the detectors. As the crystal rotates, angle θ for its interplanar spacing d satisfies the Bragg law in accordance to

wavelength (λ), the detector receives the diffracted x-rays and converts the photons into a pulse of electric current having height proportional to the photon energy.

The Bragg Law is given by the following equation:

$$n\lambda = 2d\sin\theta \tag{3.6}$$

Where n is an integer giving the order of diffraction, λ is the monochromatic wavelength of the x-ray radiation, d is the interplanar spacing in the material and θ is the instrumental angle relative to incident radiation direction onto the sample. In the spectrometer d is fixed by the crystal used, θ is measured and nλ is calculated. For qualitative analysis, the spectrometer scans the 2θ range from 12^0 to 147^0. The output is a pattern of peaks on a scale of intensity versus 2θ angles. The elements present in the sample are identified from the 2θ angles at which diffraction peaks are observed on the pattern, whereas concentrations of elements present are determined by peak heights or intensities [Eug1978].

Figure 3.10

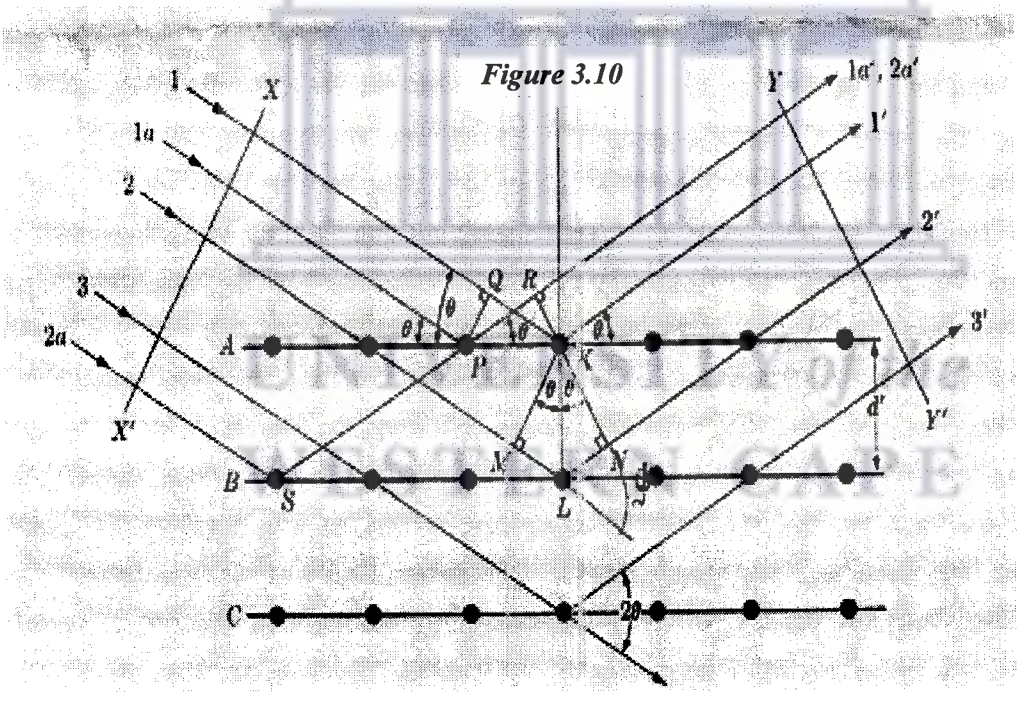

Figure 3.10 shows diffraction of x-rays by different atoms (K and L) on different planes (A, B and C). These planes are separated by the spacing d′. The difference in the path

length between rays 1 and 2 must be a multiple of the wavelength nλ, so that they can be in phase with rays $1^{/}$ and $2^{/}$ respectively.

$$ML + LN = n\lambda \tag{3.7}$$

The above equation is also the path difference of the x-rays scattered by S and P atoms, since there is no path difference between x-rays S and L or P and K.

By applying the sine rule in triangle KLN we get:

$$d^{/} \sin\theta = LN \tag{3.8}$$

The sine rule gives ML equal to NL, by substituting the values of ML and LN in equation 3.7 we get:

$$d^{/} \sin\theta + d^{/} \sin\theta = n\lambda$$

$$2d^{/} \sin\theta = n\lambda \tag{3.9}$$

Equation 3.9 was first derived by W.L Bragg and is known as the Bragg law and it states the specific condition that must be met in order for the diffraction to occur. Where n is an order of reflection $d^{'}$ is the interplanar spacing or space between the planes in the sample crystal; λ is the wavelength of incident beam and Θ is an angle on incidence of the x-ray radiation on the sample [Cul1978].

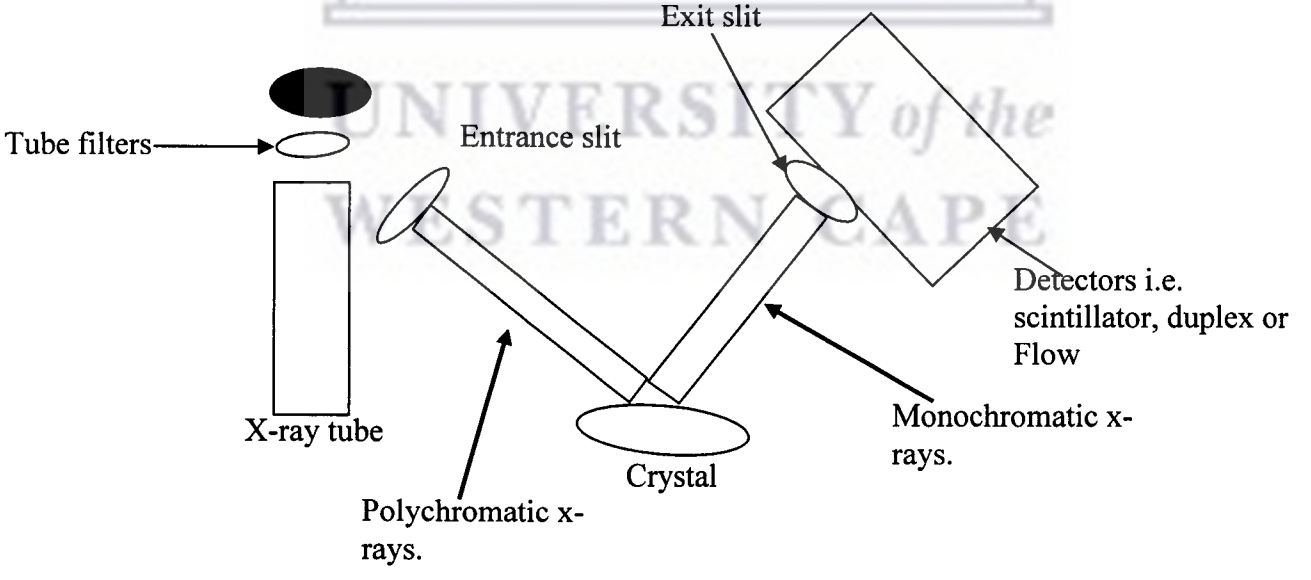

Figure 3.11 Schematic representation of the Pan Axios model XRF instrument. The x-rays are produced in the x-ray tube and directed to the sample; the sample emits x-rays that will be diffracted by the crystal via exit slit.

The instrument at NECSA gives ten simultaneously measured energy spectrums per measurement each captured by its own detector, each spectrum is sensitive to certain elements as illustrated in Table 3.1. Each spectrum has its own running time, start angle and end angle. This is also illustrated in Table 3.1. The penetration of x-rays ranges from 1 to 100 micron meters depending on the material.

No	KA range	LA range	Detector	Tube filter	Start angle(2θ)	End angle(2θ)	kV	mA
1	Te-Ce	-	Scintillator	Brass	14	18.6	60	66
2	Mo-I	-	Scintillator	Brass	12	21	60	66
3	Kr-Tc	Ra-Am	Scintillator	Al(750μm)	26.6	42	60	66
4	Zn-Rb	Re-U	Scintillator	Al(200μm)	37	62	60	66
5	V-Cu	Pr-W	Duplex	None	61	126	50	80
6	K-V	In-Ce	Flow	None	76	146	32	125
7	P-Cl	Zr-Ru	Flow	None	91	146	32	125
8	Si-Si	Rb-Sr	Flow	None	100	115	32	125
9	Al-Al	Br-Br	Flow	None	130	147.04	32	125
10	O-Mg	V-Se	Flow	None	20	60.05	32	125

Table 3.1 Summary of the parameters of each spectrum or scan. The parameters include the scan number, kinds of x-rays produced i.e. K alpha (KA) and L alpha (LA), detector used, beam energy, tube current, start angle and end angle, kV refers to tube energy and mA refers to tube current. KA and LA ranges indicate the elements for which the radiation energy is sensitive for detection.

3.5 X-ray diffraction (XRD)

Diffraction is the result of radiation being scattered by a regular array of scattering centers whose spacing is of the same magnitude as the wavelength of the radiation. A German physicist Von Laue first discovered this phenomenon in 1912. Two British physicists W.H Bragg and his son W.L Bragg later improved these concepts. [Cul1978]. XRD uses mostly monochromatic x-ray beams and is mostly applied to the investigation of crystalline material.

Aim

In this study, XRD was used to identify the chemical phase content and crystallographic texture (preferred orientation of crystallites from random). In addition, this technique was also used to check for differences between XRD patterns of samples from different origins and ages

Crystals

X-ray diffraction takes place only in crystalline materials and crystal materials contain different kinds of crystals. A crystal refers to the manner or pattern in which atoms are arranged in three dimensions. Atom arrangements can be in different systems such as cubic, tetragonal, orthorhombic, rhombohedral, hexagonal, monoclinic, and triclinic. The crystal systems are referred to as Bravais lattices. There 14 Bravais lattices [Cul1978, Jen1996].

Factors affecting the relative intensity of the diffraction intensity are:

- Structure factor.
- Multiplicity factor.
- Lorentz-polarization factor.
- Absorption factor.
- Temperature factor.
- Preferred orientation.
- Beam size.

Only the factors applicable to the phenomenon of this study are discussed.

Preferred orientation is of interest in this study. It refers to the way in which the crystallites making up the sample are oriented between the various grains. It is influenced by the crystal sizes and shapes [Cul1978] and the way in which crystals are rotated in the sample. Preferred orientation affects the physical properties of the material [Bun1982] as it introduces anisotropy, i.e. deviation from random. Preferred orientation of the crystal

grains are observed from variations between the observed intensities relative to that of random crystallite arrangements [Cul1978].

Preferred orientation determination is an elaborate process since it involves measurement of diffraction patterns, pole figure measurements from each hkl reflection and mathematical calculations of inverse pole figure and orientation distribution functions (ODF). In this study we are only considering diffraction patterns between different sample orientations. For this study the hexagonal structure shown in Fig 3.12 is relevant. The important crystal planes in a hexagonal structure are the prismatic and basal faces, when preferred orientation is being evaluated. The presence of preferred orientation of the crystallites can be identified from differences in the observed diffraction intensities compared to intensities from random crystallites orientations [Jen1996, Bun1982].

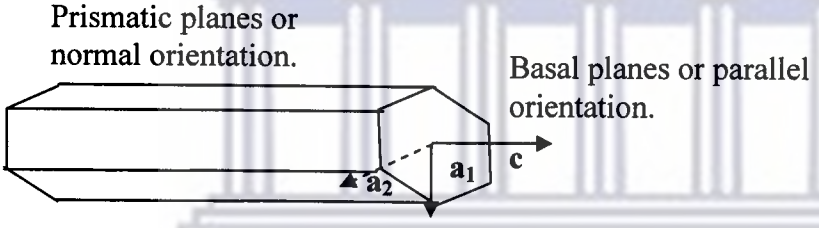

Figure 3.12 Schematic diagram of hexagonal crystal system structure showing the prismatic faces (a_1 and a_2) and basal face (c). Alphabets a_1, a_2 and c are axial direction defining the planes.

3.5.1 Operational principles of x-ray diffraction

Bragg diffraction of x-rays has been discussed in section 3.4.3. The production of x-ray occurs in the goniometer as discussed in section 3.2.

3.5.2 Penetration depth of x-rays in XRD

In XRD the x-rays penetrate only a few microns. Due to the measurement geometry the penetration depth is dependent on the diffraction angle. Since our start angle is 10^0 and the end angle is 110^0, we evaluate the penetration depth at the two extremes of the data acquisition procedure. Deeper penetration depth is expected at the end angle compared to

start angle. The chemical system of interest in this study is manganese dioxide (MnO_2). Manganese dioxide contains 3 atoms per unit cell with its mass absorption coefficient given by [JEN1996]:

$$\left(\frac{\mu}{\rho}\right)_{MnO_2} = \frac{1}{3}\left(\frac{\mu}{\rho}\right)_{Mn} + \frac{2}{3}\left(\frac{\mu}{\rho}\right)_{O} \tag{3.11}$$

By substituting values for the mass coefficients of each element we obtain [Cul1978]:

$$\left(\frac{\mu}{\rho}\right)_{MnO_2} = \left[\frac{1}{3}(272.5) + \frac{2}{3}(11.03)\right] cm^2 / g$$

$$= 98.19 cm^2 / g$$

The linear absorption coefficient is given by the following equation:

$$\mu_{MnO_2} = \left(\frac{\mu}{\rho}\right)_{MnO_2} X(\rho)_{MnO_2}$$

(3.12)

$\rho =$ is the density of the material which is $4.38 g / cm^3$. By substituting values in equation 3.12 we get the linear absorption coefficient of MnO_2. HA refers to hydroxylapatite.

$\mu_{MnO_2} = 98.19 cm^2 / g \times 4.38 g / cm^3 = 430.072 cm^{-1}$ (Manganese dioxide linear absorption coefficient). For the absorption of x-rays we use the following equation:

$$I_X = I_0 e^{-\mu X} \tag{3.13}$$

Equation 3.13 is further modified as follows:

$$\frac{I_X}{I_0} = e^{-\mu X}$$

$\ln\left(\frac{I_X}{I_0}\right) = -\mu X$ that can be written as:

$$X = \frac{\left(\ln\left(\frac{I_X}{I_0}\right)\right)}{-\mu_{MnO_2}} \tag{3.14}$$

for the diffraction process we assume a cut-off when $I_X = 50\% I_0$ i.e. $I_X = \frac{1}{2} I_0$. By substituting the value of I_X from equation 3.14 we get the following results.

$$X = \frac{\left(\ln\left(\frac{1}{2}\right)\right)}{-430.072}$$

$$= \frac{(\ln 1 - \ln 2)}{-430.072} = \frac{\ln 2}{430.072}(cm) = 0.0016cm = 16\mu m$$ as the largest pathlength possible that would enable a diffracted beam to emerge from the sample. For a pathlength through the material of 16 μm (50%) penetration depth of x-rays through the material the penetration depths are calculated at the two extremes of the diffraction measurement i.e. $2\theta = 10^0$ and $2\theta = 110^0$.

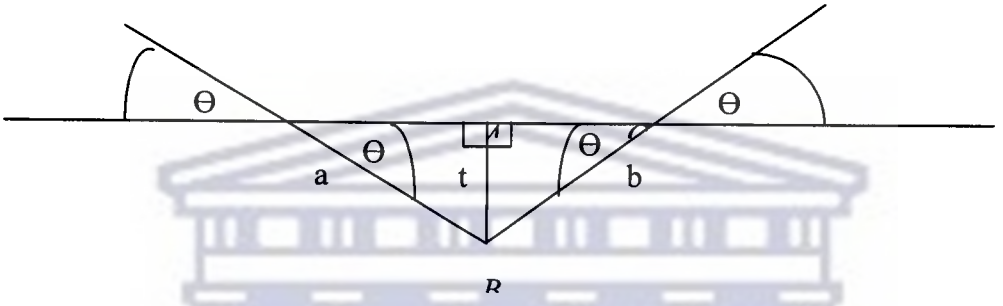

Figure 3.13 Schematic diagram of what happens when x-rays are directed to sample atoms during XRD measurements, t is the penetration depth, b + a is the path length and Θ is diffraction angle.

Taking into consideration angle ABC and $2\theta = 10^0$, this means that $\theta = 5^0$. if we use sine rule we get:

$Sin\theta = \frac{t}{b}$ By making d the subject of the formula we get $t = b\sin\theta$, but the value of b is 8 μm so:

$t = (8\sin 5^0)\mu m = 0.69\mu m$ This is the penetration depth for the starting angle of this study. Taking in consideration the same angle and the end angle of $2\theta = 110^0$, the penetration depth is given by:

$t = b\sin 55^0 = (8\sin 55^0)\mu m = 6.5\mu m$. Thus the maximum penetration depth into MnO_2 with monochromatic x-rays of wavelength 1.5418 Å is $6.5\mu m$.

3.5.3 The x-ray diffraction (XRD) instrument at NECSA

All the XRD analyses were done using a Siemens Theta-2Theta Diffractometer, producing monochromatic copper K alpha x-rays (λ = 1.5418Å). The instrument is shown in Fig 3.14. The processing of data from detection to analysis is shown schematically in Fig 3.15.

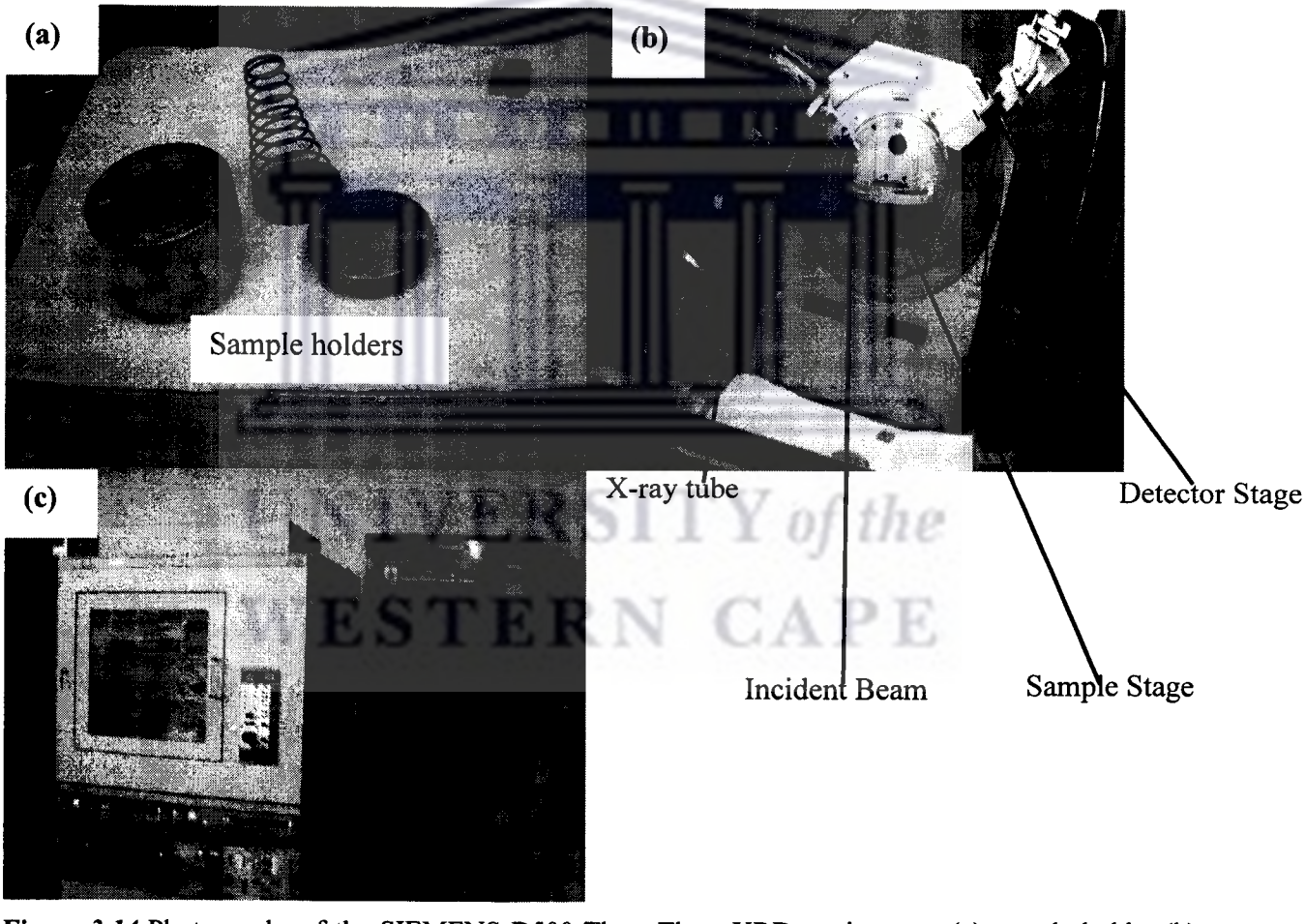

Figure 3.14 Photographs of the SIEMENS D500 Theta-Theta XRD goniometer; (a) sample holder (b) shows instrument layout of x-ray tube, incident beam, sample and detector stages. Figure (c) shows a photograph of the instrument.

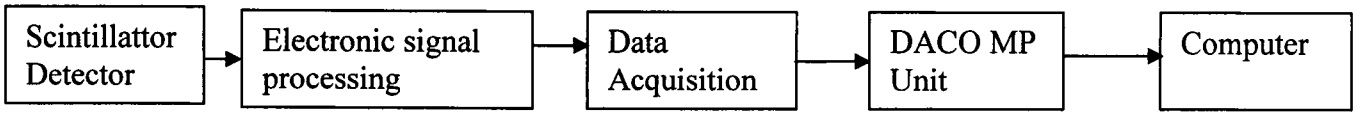

Figure 3.15.Block diagram of signal processing. The diffracted beam gets detected and stored in the DACO MP unit as the detector count at the various θ measurement positions. After completion the data is downloaded to the computer for analysis.

Conditions of XRD measurements

For this study the beam size is identified by four slits with divergences of 0.1^0, 0.3^0, 0.3^0 and 0.15^0 respectively from the source to the detector. The sample region illuminated by x-ray beam has a dependence on θ. At low θ the spot size is larger than at large θ values. The measurement conditions used were 2 hours 45 minutes for the entire measurement with 5 seconds per spot, scan ranges were 2θ from 10^0 to 110^0 and the step size was 0.05^0. Different orientations of the samples were investigated by placing the samples parallel and perpendicular to the incident beam direction to check for the presence of preferred orientation. This is illustrated by Fig 3.16. XRD measurements were also done on a manganese dioxide reference sample.

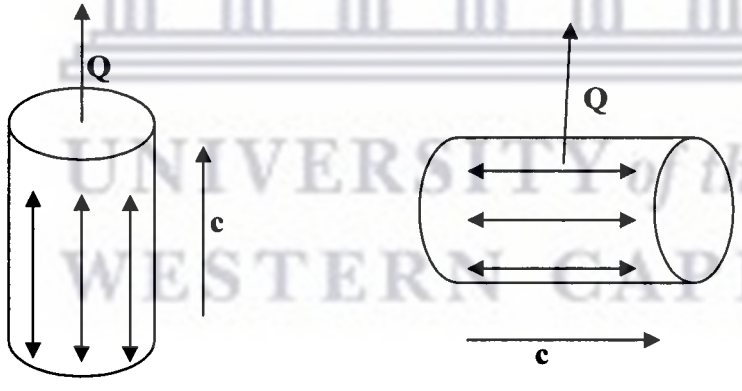

Figure 3.16 Schematic diagrams showing parallel and perpendicular sample orientation to the beam geometry. Sample orientations are defined relative to the scattering vector (Q) of the goniometer. It also shows the direction of the c axis in the hexagonal structure.

Chapter 4

Results and discussions

4.1 X-ray fluorescence (XRF) results

The results of the XRF analysis for each sample are presented as ten individual spectrums of intensity (counts per second) versus energy from 0 to 36 keV. The peak pattern of the spectrums enable identification of the elemental content by matching the peak positions against a database using the search/match routine of the iQ+ software. Figures 4.1 and 4.2 show the typical spectrums obtained per sample analysis. Each spectrum has its own energy range that has specific sensitivities for specific grouping of elements. Elements are present on a number of the different energy spectrums depending on the electronic shell the fluorescence x-rays originated from. For example CuKA (copper K alpha) refers to the K-alpha line of copper, CuLA refers to the L line of copper as indicated in the figures. As a typical result Fig 4.1 shows the XRF results obtained from sample SE50207 with the beam respectively directed at the prominent brown stain, as well as off-stains position as indicated in Fig 2.3 using beam dimension approximately 1.5 mm circular. The on-stain position results are referenced by index 1 at the end of the sample reference, off-stain position is referenced by index 2. The spectrums show the presence a large quantity of Ca and P. The Ca and P originate from the hydroxylapatite of the bone material. The spectrums also show a small presence of Mn at the on-stain positions. The Mn on the on-stain position is indicative of MnO_2. Figure 4.2 shows the results from sample SK30121 with the beam directed at the on-stain and off-stain positions indicated in Fig 2.5. The spectrums show the presence of Ca and P but no Mn. Table 4.1 summarises the elements identified from the search/match procedures for the spectrums of Fig 4.1 including contributions originating from the mask shown in Fig 3.8 (c). The presence of the latter spectral lines on the various spectrums of the samples is ascribed to contributions from the mask. Sodium (Na) and chlorine (Cl) are contained in salts used

for daily cooking, these may be caused by human contact. Silicon (Si), Phosphorus (P) and calcium (Ca) are caused by the substrates, which are chert (SiO_2) and bone material ($Ca_5(PO_4)_3OH$). Tables 4.2 to 4.5 summarise the major (above 1%) and minor (below 1%) elemental concentrations for the various samples as determined from XRF. Mn concentration in many cases is below 1% but is listed with the major elements because it is the topic for this study. Minority elemental concentrations are only indicated in Table 4.2 only as they are present on most of the measurement patterns and subsequently subtracted. Major elements are arranged according to their peak intensities (concentrations). Minor elements are arranged according to their atomic numbers. In Tables 4.2 to 4.5 the column label 1 refers to regions of interest on the brown stains whereas label 2 refers to the regions of interest on the bone material without stains (off-stain position). In the case of the chert rock, index 1 refers to the substrate (chert rock), 2 to the live lichen (green stain) and index 3 refers to the brown stains on the surface of the rock. The XRF results are only qualitative, reason being that the samples were not smooth and flat enough to satisfy the calibration procedure of the instrument.

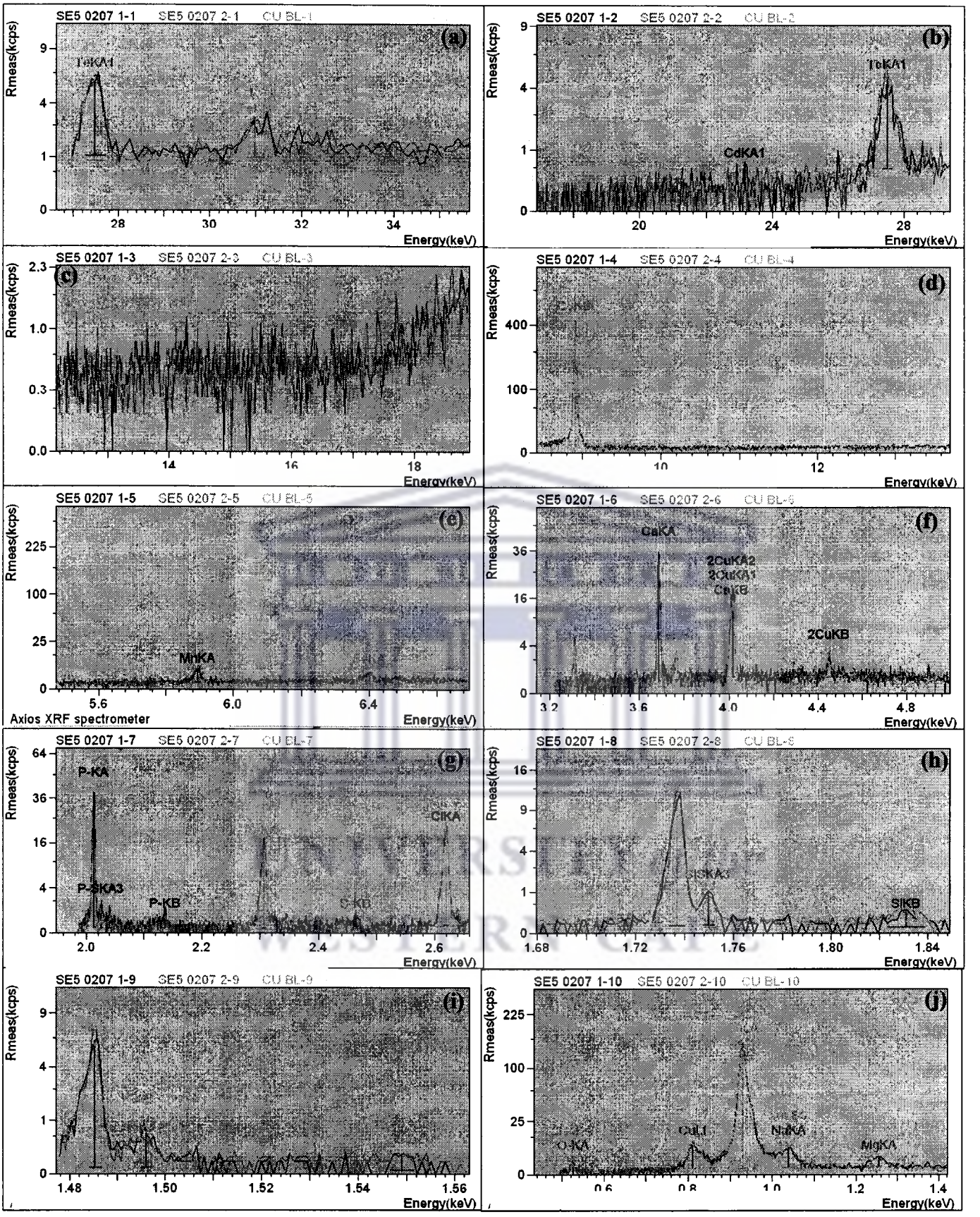

Figure 4.1 WDS XRF results of sample SE50207 masked to produce a beam of 1.5 mm that exposed only an on-stain position indicated in Fig 2.5. The different spectra (a) to (j) indicate different energy ranges covered by XRF configuration. (a) Is the first scan, (b) scan number 2, (c) scan number 3, (d) scan number 4, (e) scan number 5, (f) scan number 6, (g) scan number 7, (h) scan number 8, (i) scan number 9 and (j) scan number 10.

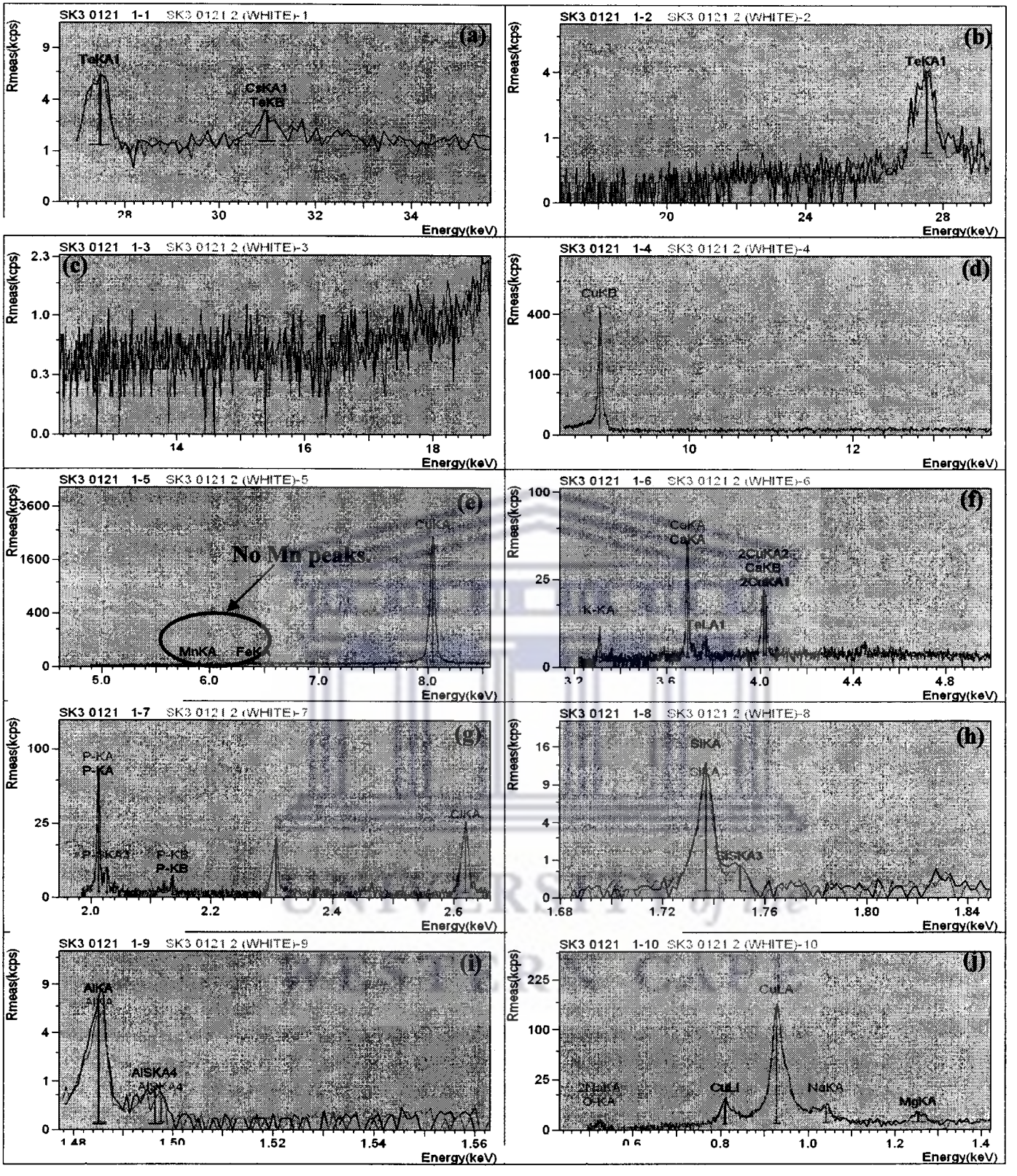

Figure 4.2 WDS XRF results of sample SK30121 masked to produce a beam of 1.5 mm that exposed only an off-stain position indicated in Fig 2.5. The different spectra (a) to (j) indicate different energy ranges covered by XRF configuration. (a) Is the first scan, (b) scan number 2, (c) scan number 3, (d) scan number 4, (e) scan number 5, (f) scan number 6, (g) scan number 7, (h) scan number 8, (i) scan number 9 and (j) scan number 10.

Stains on SE5 0207		Mask	
Elements	Conc (%)	Elements	Conc (%)
Na	1.2	Na	0.2
Si	0.9	Si	0.7
P	0.6	S	0.3
Cl	1.1	Cl	1.3
K	0.2	K	0.2
Ca	1.2	Cu	61.5
Mn	0.1	Te	0.3
Cu	61.1	Al	0.0
Te	0.3		

Table 4.1 Summary of the elemental analysis and their concentrations obtained from WDS XRF measurements of SE5 0207 and mask to reduce the beam size. The elements originating from the mask were present on all XRF analysis of this study.

Table 4.2

	SK1 0313		SK1 0414		SK2 0217		SK2 0419		SK3 0323		SK3 0121	
Major elements	**1**	**2**	**1**	**2**	**1**	**2**	**1**	**2**	**1**	**2**	**1**	**2**
	Ca	Ca	Ca	Ca	Ca	Ca	Ca	Ca	Ca	Ca	Ca	Ca
	P	P	P	P	P	P	P	P	P	P	P	P
	Salts	**Salts**	**Salts**	**Salts**	**Salts**	**Salts**	**Salts**	**Salts**	**Salts**	**Salts**	**Salts**	**Salts**
	Cl	Na	Cl	Cl	Na	Cl	Cl	Cl	Cl	Cl	Cl	Na
	Na	Cl	Na	Na	Cl		Na	Na			Na	Cl
	Mask	**Mask**	**Mask**	**Mask**	**Mask**	**Mask**	**Mask**	**Mask**	**Mask**	**Mask**	**Mask**	**Mask**
	Cu	Cu	Cu	Cu	Cu	Cu	Cu	Cu	Cu	Cu	Cu	Cu
	Stains						**Stains**					
	Mn		no Mn		no Mn		Mn		no Mn		no Mn	
Minor elements	O	O	O	O	O	O	O	O	O	O	O	O
	Al	Al	Al	Al	Al	Al	Al	Al	Al	Al	Al	Al
	K	S	K	K	K	S	S	S	K	K	Si	Si
	Te	K	Te	Te	Te	Si	K	K	Te	Te	K	K
		Te				K	Te	Te			Te	Te

Table 4.2 XRF elemental analysis of samples from Swartkrans cave. The column labeled 1 represents analysis on a brown stain (on-stains position), with labeled 2 representing analysis taken on the hydroxylapatite region without stains (off stain position).

Table 4.3

	KDA 0530		KDA 0227		KDB 0131		KDB 0434	
Major elements	**1**	**2**	**1**	**2**	**1**	**2**	**1**	**2**
	Ca	Ca	Ca	Ca	Ca	Ca	Ca	Ca
	P	P	P	P	P	P	P	P
	No Mn		No Mn		No Mn		No Mn	

Table 4.3 XRF elemental analysis of samples from Kromdraai cave.

Table 4.4

	ST4 0404		ST4 0202		SE5 0207		SE5 0510	
	1	**2**	**1**	**2**	**1**	**2**	**1**	**2**
Major elements	Ca	Ca	Ca	Ca	Ca	Ca	Ca	Ca
	P	P	P	P	P	P	P	P
					Stains			
	No Mn		No Mn		Mn		No Mn	

Table 4.4 XRF elemental analysis of samples from Sterkfontein cave.

Table 4.5

	Chert	Chert Lichen	chert Brown
	1	**2**	**3**
	Substrate	**Substrate**	**Substrate**
Major Elements	Si		Si
		Lichen	**Stains**
		Mn	Mn
			Fe

Table 4.5 XRF Results from the analysis of chert rock with lichen and brown stains on its surface.

4.1.1 XRF results discussions

Assessment of the XRF results reveals that all fossil samples show the presence of Ca and P on both the on-stain and off-stains positions. The presence of these elements is reminiscent of the hydroxylapatite substrate. Only some of the fossil samples show the presence of Mn from the on-stain positions not withstanding visible stains existing. Results from samples within the same member are also not consistent in revealing Mn. The reason why not all the stains give positive indication of Mn is that the stains thicknesses are substantially less than the penetration depth of the x-rays. Based on the absorption coefficients of x-rays by Mn, it is concluded that the MnO_2 are less than 6.5 μm in thickness. In this case Mn content is thus below the detection limit of XRF.

The XRF analysis of the chert rock shows the presence of Si signal from quartz. Results from the green spot (live lichen) show a strong presence of Mn but not Si. In the case of the brown stain the Mn signal is stronger than in green spot, but cannot be quantified. Si of the substrate is also observed. It is concluded from the presence of the Si signal that the x-ray beam penetrates the brown stains but not the green lichen. The lichen is either too thick for the incident beam to penetrate or the biological contents of the growing organisms absorb the incident beam. Similarly to the fossil sample analysis, it is concluded that the brown stains on chert is less than the penetration depth of the x-ray beam as the x-ray beam clearly sees the substrate material.

Analysis of the EDS results from samples KDA0530 and SK30121 did show the presence of manganese peaks whereas the WDS analysis did not show any manganese peaks. The EDS spectrums are shown in Fig 4.3 and 4.4. The reason for this might be the fact that EDS was done on a larger sampling area. The Mn deposits are not necessarily of uniform thickness over the stained regions, but rather concentrated in the crevices of the bone material where the thicknesses of the deposits are largest.

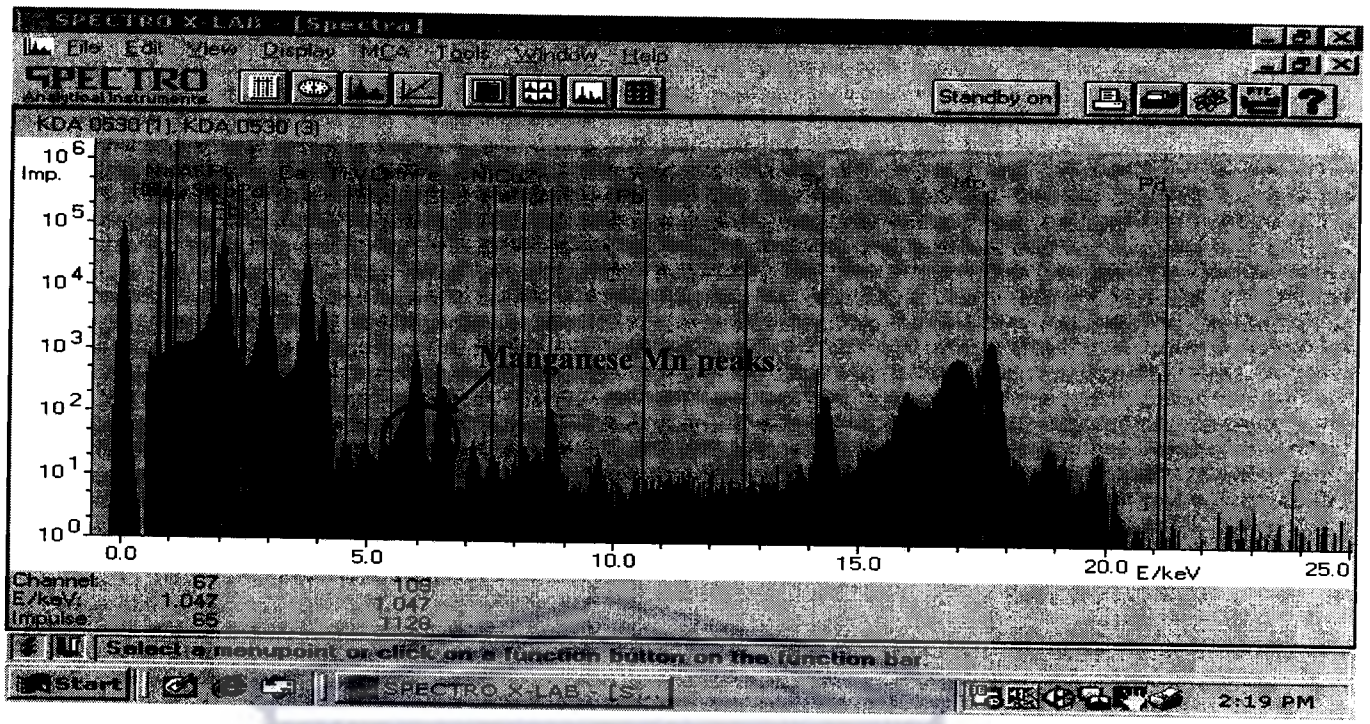

Figure 4.3 EDS XRF analysis of sample KDA 0530. Vertical lines indicate elements identified in this sample. Prominent Mn signals are obtained in this sample.

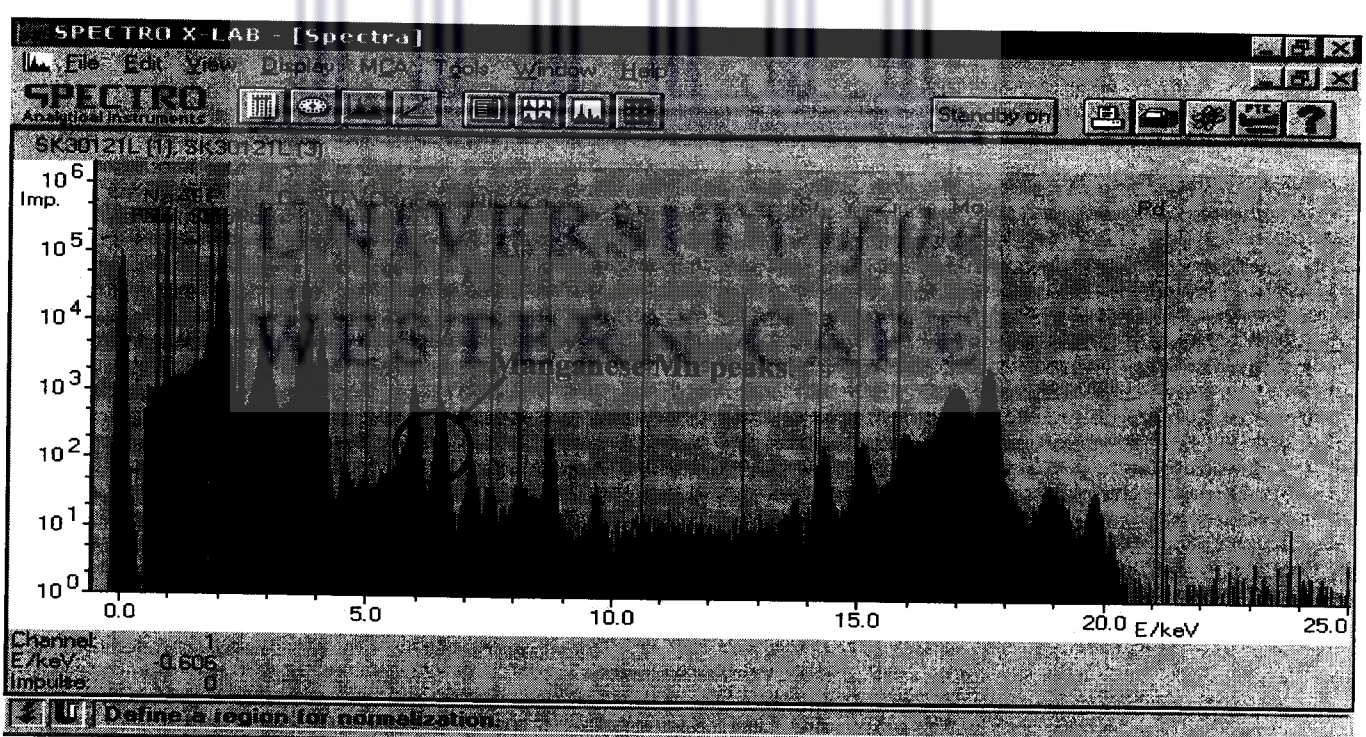

Figure 4.4 EDS XRF analysis of sample SK3 0121. Prominent signals for Mn are observed.

4.1.2 Conclusion of the XRF results

Only some samples show the presence of manganese. All samples show the presence of Ca and P from the fossilized bone material at both on-stain and off-stain positions. This means that the stains on the different samples have different thickness. Since some samples have more prominent visible stains than others but is not correlated by the XRF results, it is concluded that most stains are very thin compared to penetration depth of x-rays, rendering signals below the detection limit of 0.1 wt%.

4.2 X-ray diffraction results

The XRD results are indicated as intensity peaks in the x-ray spectrum versus either 1/d spacing or two-theta angle. Chemical phase identifications were done by search/match software procedures by matching the patterns (heights and peak positions) of the stains or samples against the International Center for Diffraction Data (ICDD) database. Labels L and S respectively refer to the orientation of the dendrites along the bones with reference to the x-ray beam geometry. Label L refers to the measurements taken with the longitudinal bone dendrites horizontal i.e. scattering vector (Q) normal to dendrites. Label S refer to the measurements taken with the bone dendrite directions vertical, i.e. scattering vector (Q) parallel to dendrites. The orientations are shown in Fig 4.5. Figures 4.6 to 4.9 show the XRD patterns for one sample from each cave as well as the analysis of the chert rock from Sterkfontein cave.

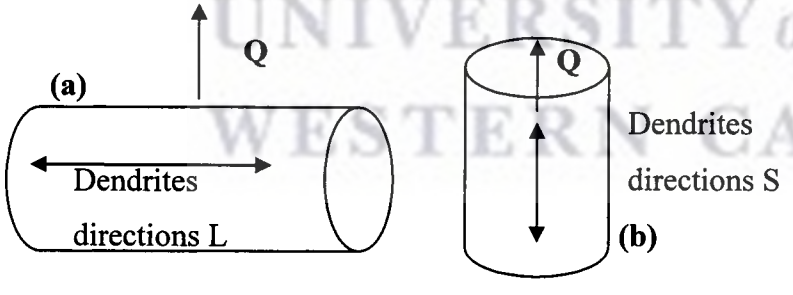

Figure 4.5 Schematic representation of the orientations of the bone samples, dendrites directions relative to the diffraction process scattering vector **Q:** (a) demonstrates the normal to the dendrite direction geometry; (b) demonstrates the parallel to the dendrite direction geometry.

None of the XRD results show the presence of MnO_2 for any of the samples. To assist the reader, a XRD analysis from a reference MnO_2 sample is shown in Fig 4.10, and included on each of the XRD patterns from the different sites as a guide to the eye to assist in the possible identification of MnO_2 on the fossil samples. In an attempt to get a specific reference pattern on the brown coating of the rocks from the Kromdraai caves the, brown stains (coatings) were chemically removed from a number of chert rock samples using hydrogen peroxide (30% H_2O_2) diluted in distilled water and depositing on filter paper. Approximately 1 gram of brown powder was accumulated and analysed with XRD. The results of the redeposited stain material is compared to the MnO_2 reference sample in Fig 4.11.

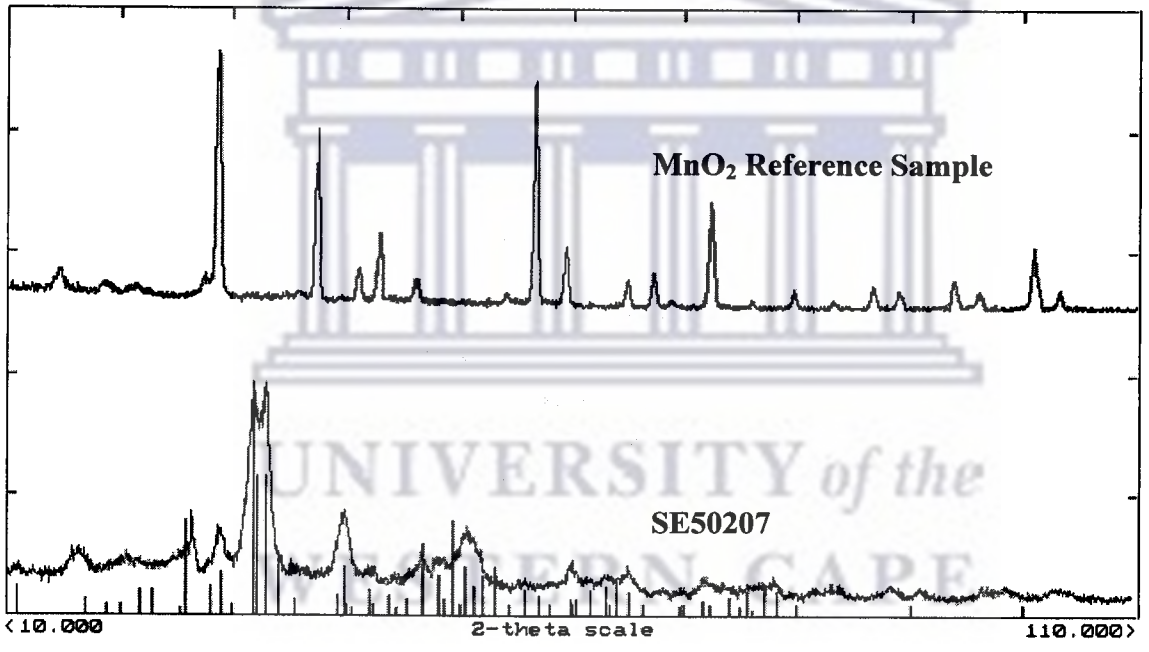

Figure 4.6 XRD pattern taken on sample SE50507 (Sterkfontein cave) as well as the pattern from a MnO_2 reference sample. The vertical lines represent the ICDD lines and intensities of hydroxylapatite.

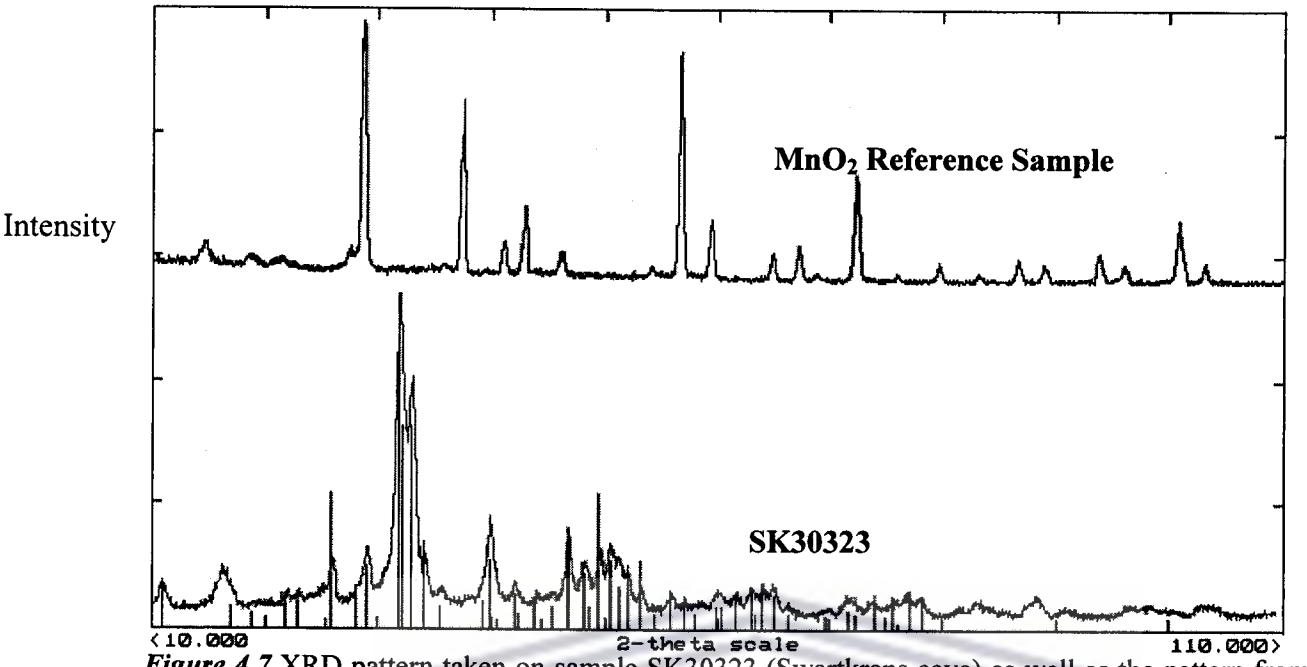

Figure 4.7 XRD pattern taken on sample SK30323 (Swartkrans cave) as well as the pattern from a MnO_2 reference sample. The vertical lines represent the ICDD lines and intensities of hydroxylapatite.

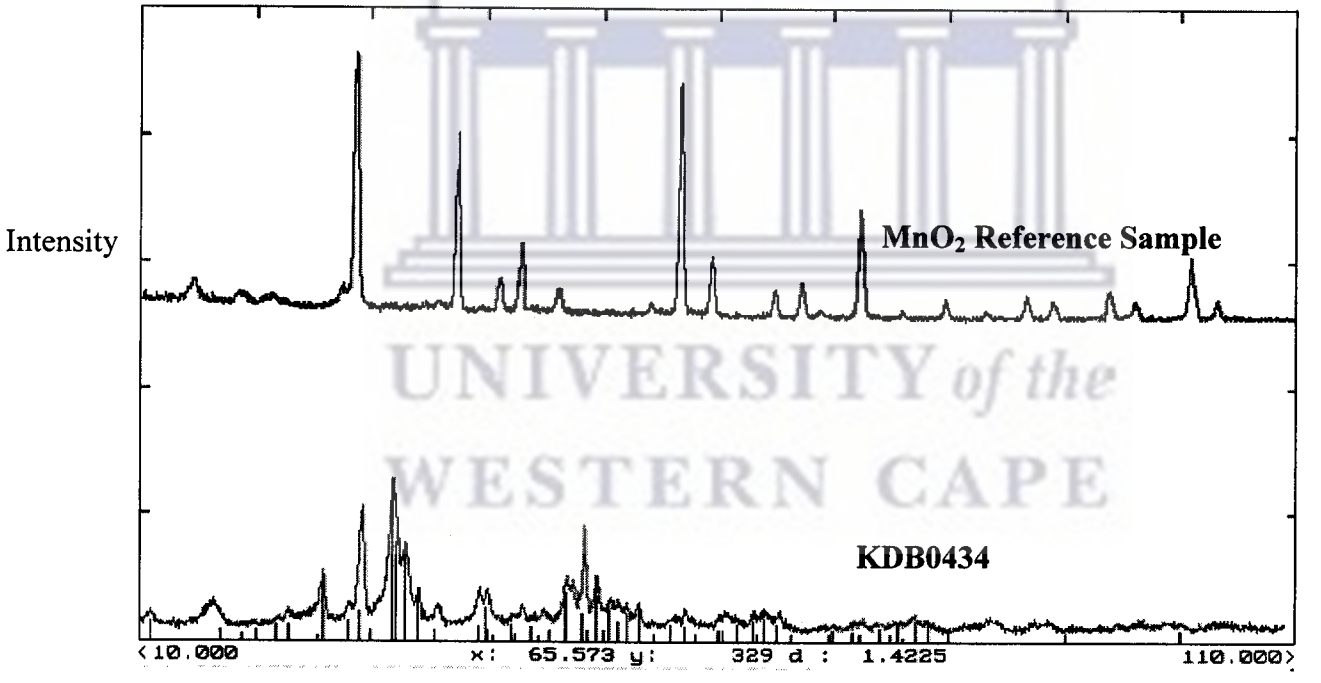

Figure 4.8 XRD pattern taken on sample KDB0434 (Kromdraai cave) as well as the pattern from a MnO_2 reference sample. The vertical lines represent the ICDD lines and intensities of hydroxylapatite.

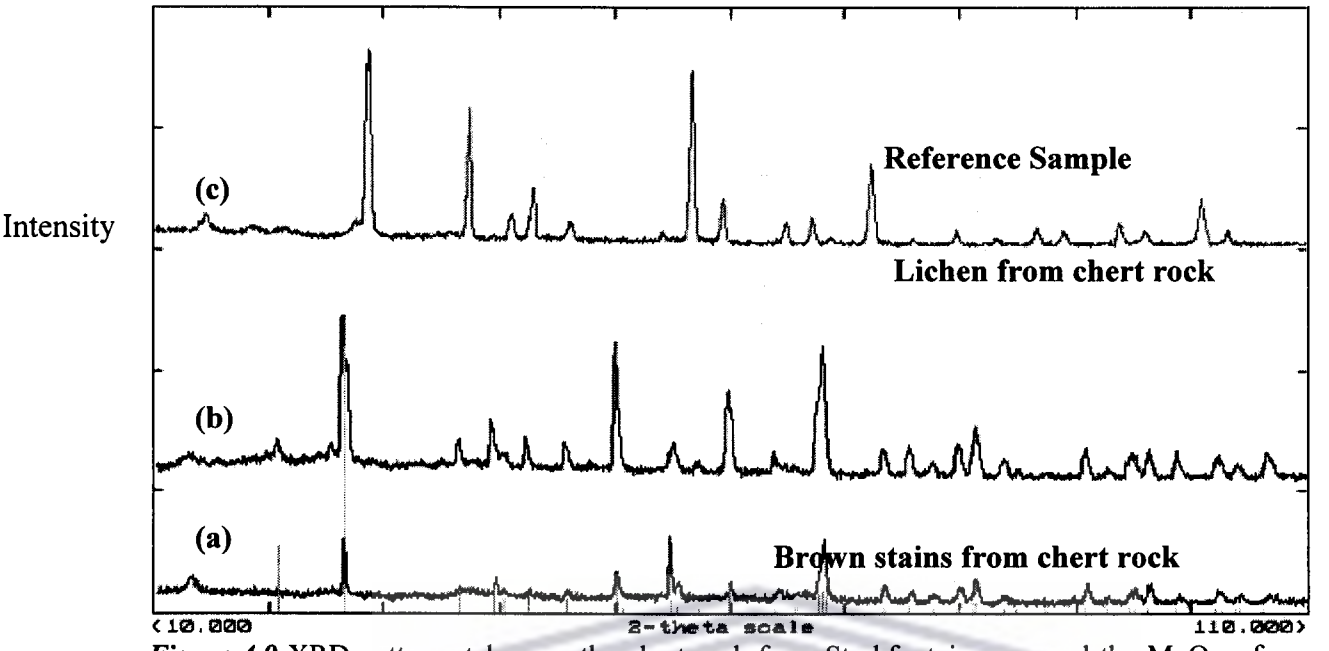

Figure 4.9 XRD patterns taken on the chert rock from Sterkfontein cave and the MnO_2 reference sample (pattern c). Pattern (a) was taken on a region of the chert rock that has extensive visible brown stains. Pattern (b) was taken on a region of the chert rock where prominent green lichen is growing.

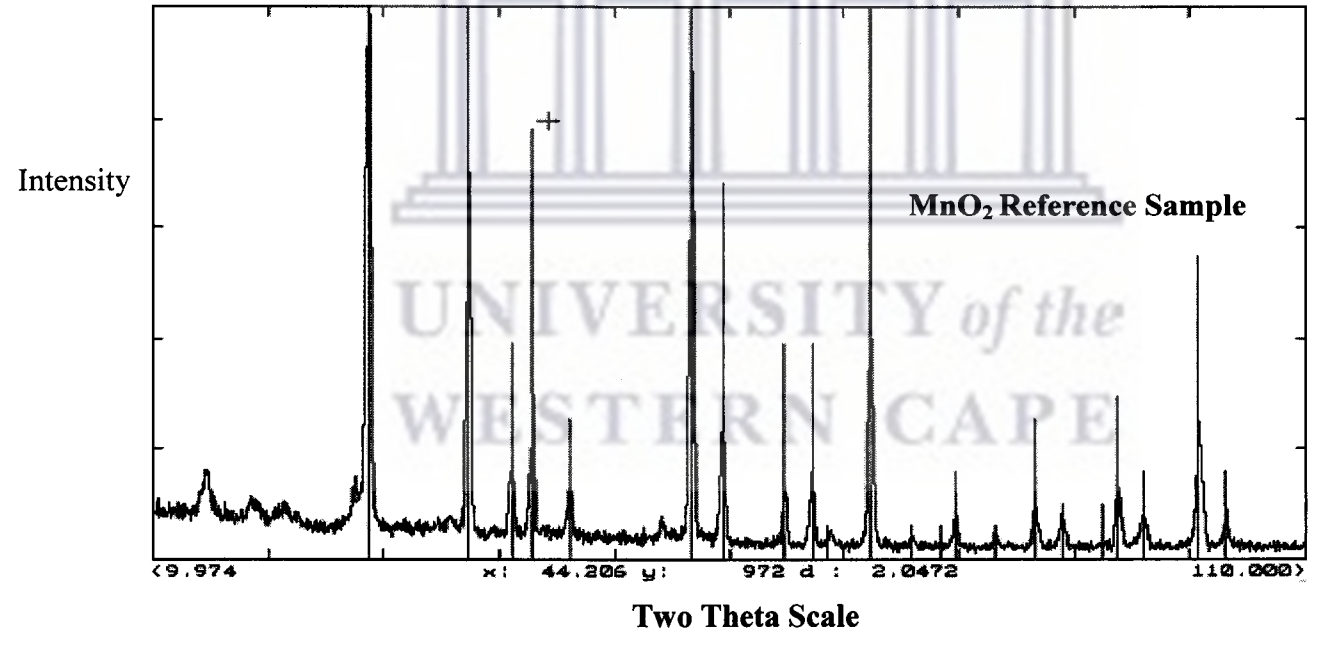

Figure 4.10 XRD pattern of MnO_2 "reference'' sample. The vertical lines represent manganese dioxide matching of the peaks with the ICDD database standard number. The vertical lines present the ICDD lines and intensities of quartz.

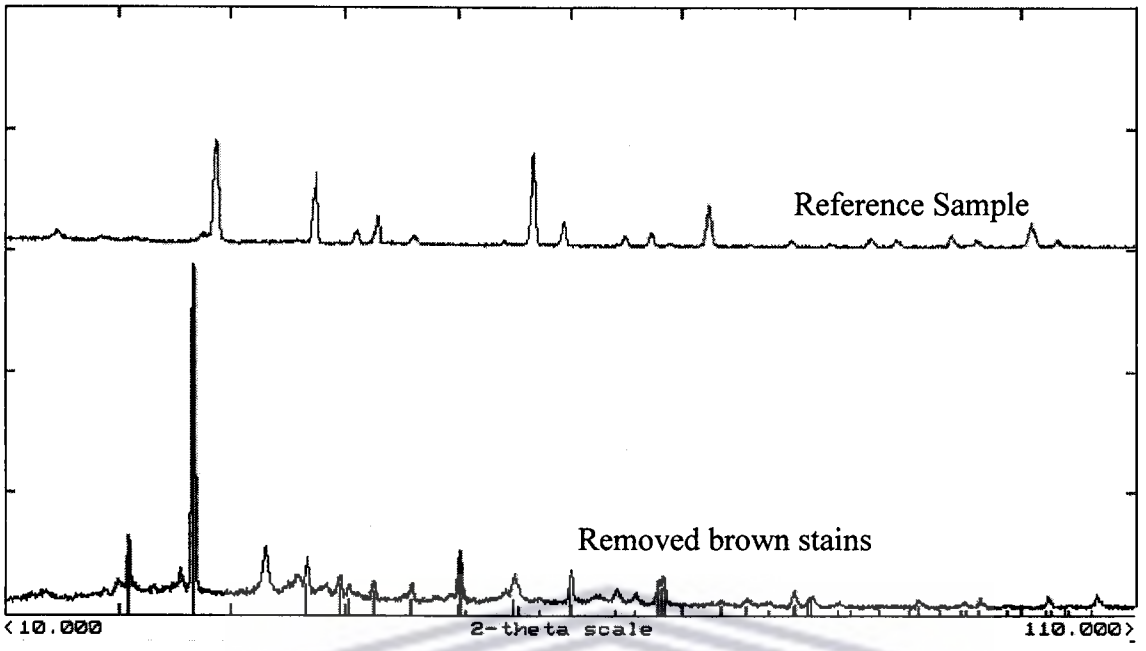

Figure 4.11 XRD patterns from the redeposited brown coatings dissolved from chert rock taken from Kromdraai cave and the MnO_2 reference sample. The redeposited sample corresponds to SiO_2. No correspondence between the redeposited material and the MnO_2 reference pattern was observed.

Conclusions of XRD chemical phase identification

None of the fossil samples, or chert rock, or redeposited stains with H_2O_2 showed the presence of MnO_2. Since XRF showed manganese peaks on fossil samples and chert rock, it is concluded that the MnO_2 layers are too thin to contribute at least 1 wt% to the probe volume, which is the detection limit of XRD.

4.2.1 XRD investigation of preferred orientation in fossil samples

Hydroxylapatite ($Ca_5(PO_4)_3(OH)$ has hexagonal crystal symmetry with a representation of the crystallite relevant orientations shown in Fig 4.12. Amongst others the structure contains two prismatic and basal plane orientations of interest. The prismatic planes are (100) and (310) and basal planes are (002) and its higher order (004). These crystallite orientations are relevant as qualitative indicators of preferred orientation in hydroxylapatite. As they are most sensitive to the occurrence of this phenomenon. The plane positions are identified by observing d_{hkl} (interplanar spacing in Å) values corresponding to the different peaks (100) (310), (002) and (004) on the XRD patterns and comparing their relative intensities against the powder diffraction database. One

sample each member was analysed for the presence of preferred orientation. A clear signal for a random sample was obtained from a powdered bone sample that gave a random orientation for the crystallites. The powdered sample has intensities that are in accordance with the ICDD, as shown in Fig 4.13. Figures 4.14 to 4.20 show the XRD patterns on sample from the caves. Each figure displays results for sample orientations normal to the dendrites (S) and parallel to the dendrites (L), as well as their comparisons to the reference powdered bone sample. The pattern for the powdered bone is shown on the top position of all figures, patterns for basal faces are the second ones from the top (S) and patterns for prismatic faces are given at the bottom (L) of the figures. The patterns for prismatic faces are referenced by the sample reference with a capital letter L at the end, patterns for basal faces are referenced by the sample name with capital letter S.

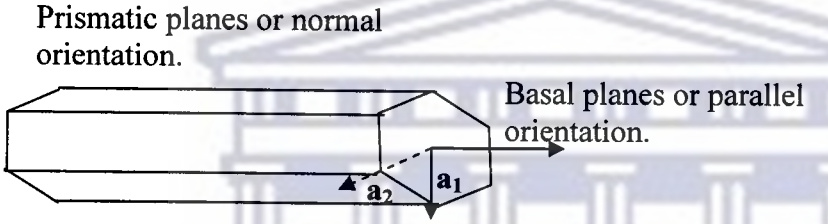

Figure 4.12 Schematic diagram of hexagonal crystal system structure showing the prismatic faces (a_1 and a_2) and basal face (c). Alphabets a_1, a_2 and c are axial lengths defining the plane.

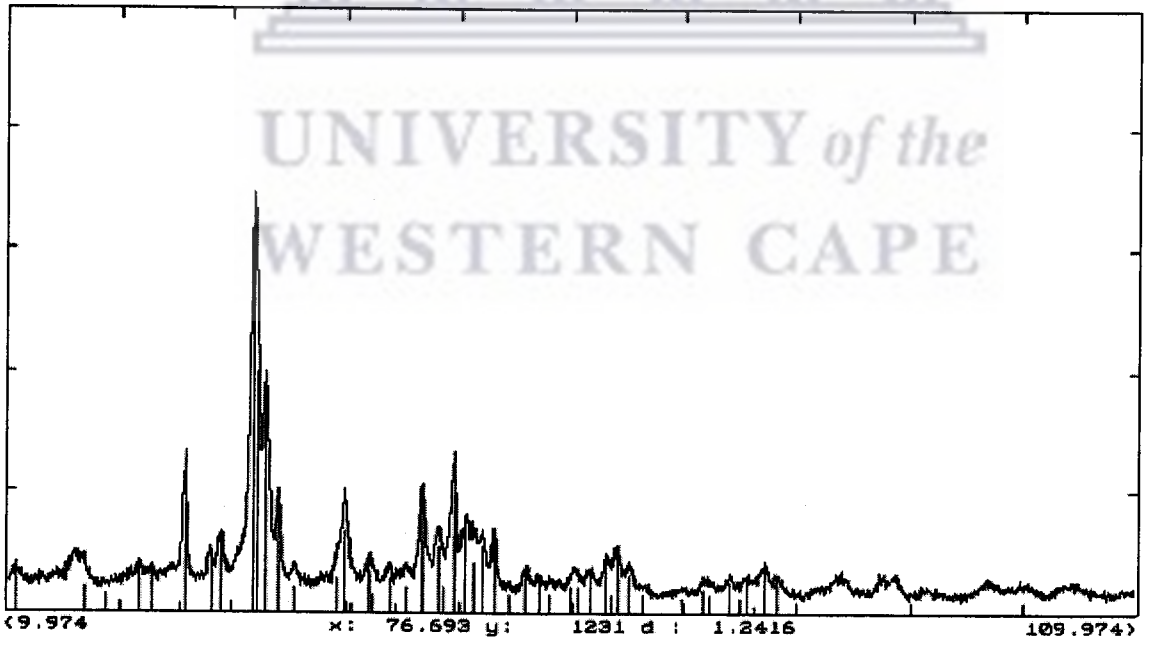

Figure 4.13 XRD pattern of a powdered bone sample from Kromdraai caves. Vertical lines represent hydroxylapatite. The peak positions and intensities are in accordance of intensities to the ICDD database values. This condition indicated that the crystallites have random orientations.

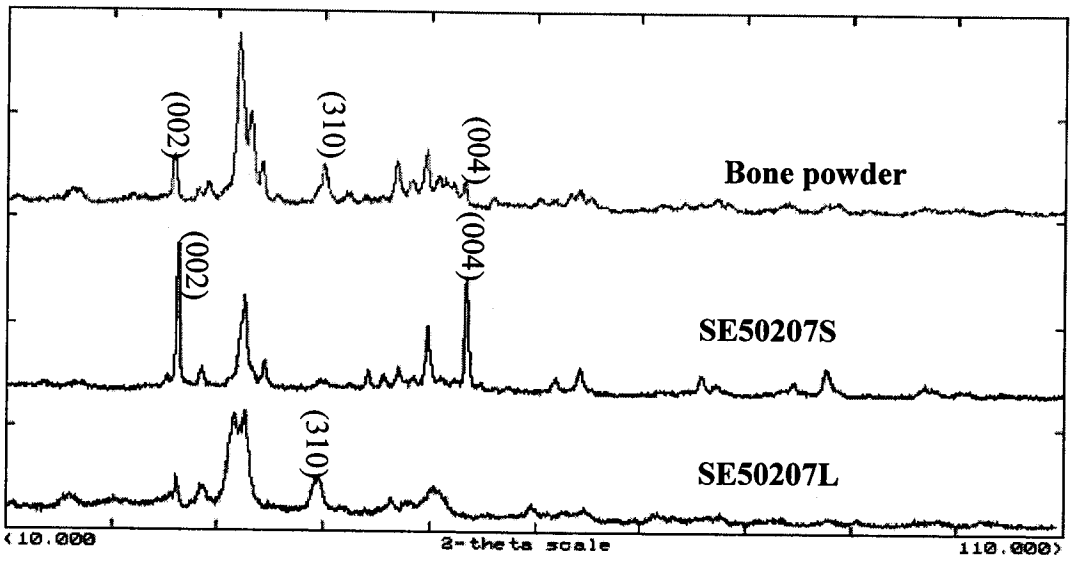

Figure 4.14 XRD patterns from sample SE50207 (Sterkfontein member 5) and the powdered sample. Pattern SE50207L refers to the scattering vector perpendicular to the dendrites direction with pattern SE50207S representing orientation with the scattering vector parallel to the dendrites direction.

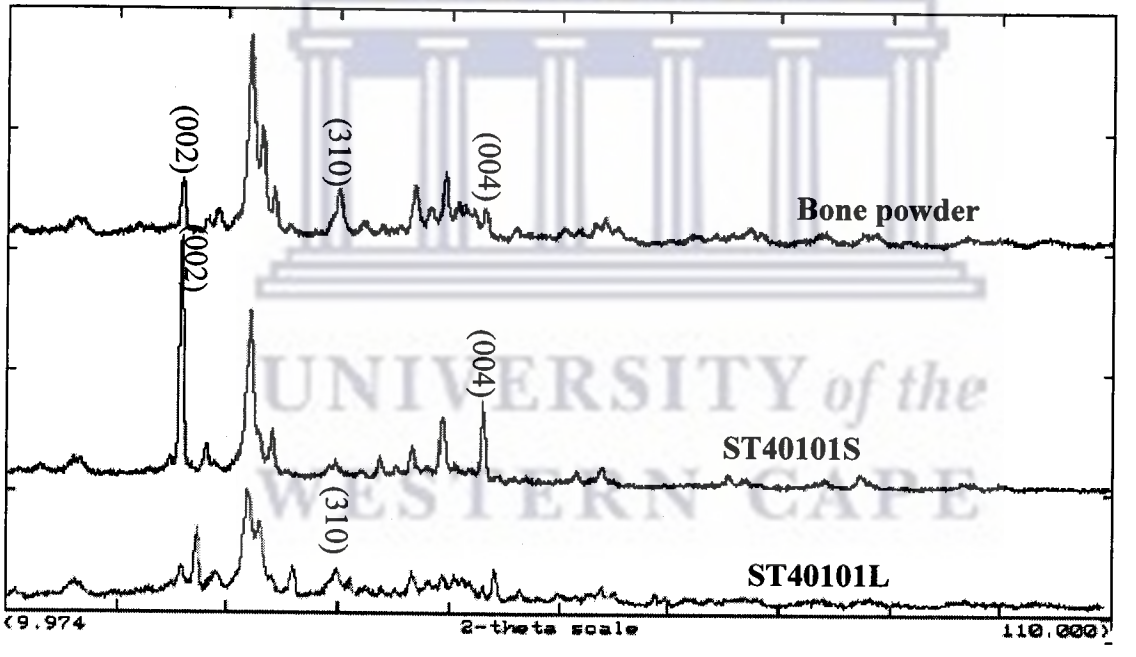

Figure 4.15 XRD patterns from sample ST40101 (Sterkfontein member 4) and the powdered sample. Pattern ST40101L refers to the scattering vector perpendicular to the dendrites direction with pattern ST40101S representing orientation with the scattering vector parallel to the dendrites direction.

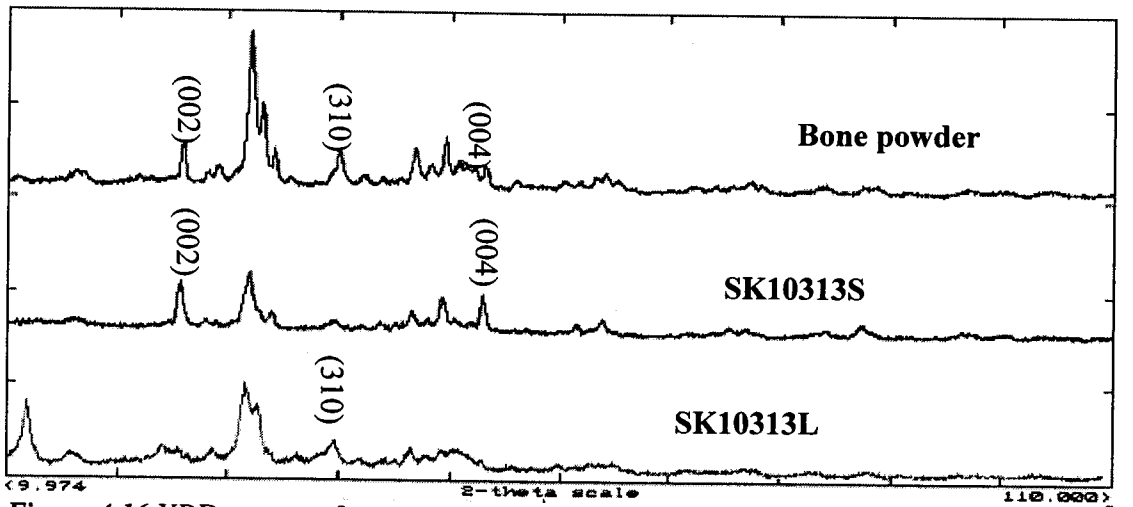

Figure 4.16 XRD patterns from sample SK10313 (Swartkrans member 1) and the powdered sample. Pattern SK10313L refers to the scattering vector perpendicular to the dendrites direction with pattern SK10313S representing orientation with the scattering vector parallel to the dendrites direction.

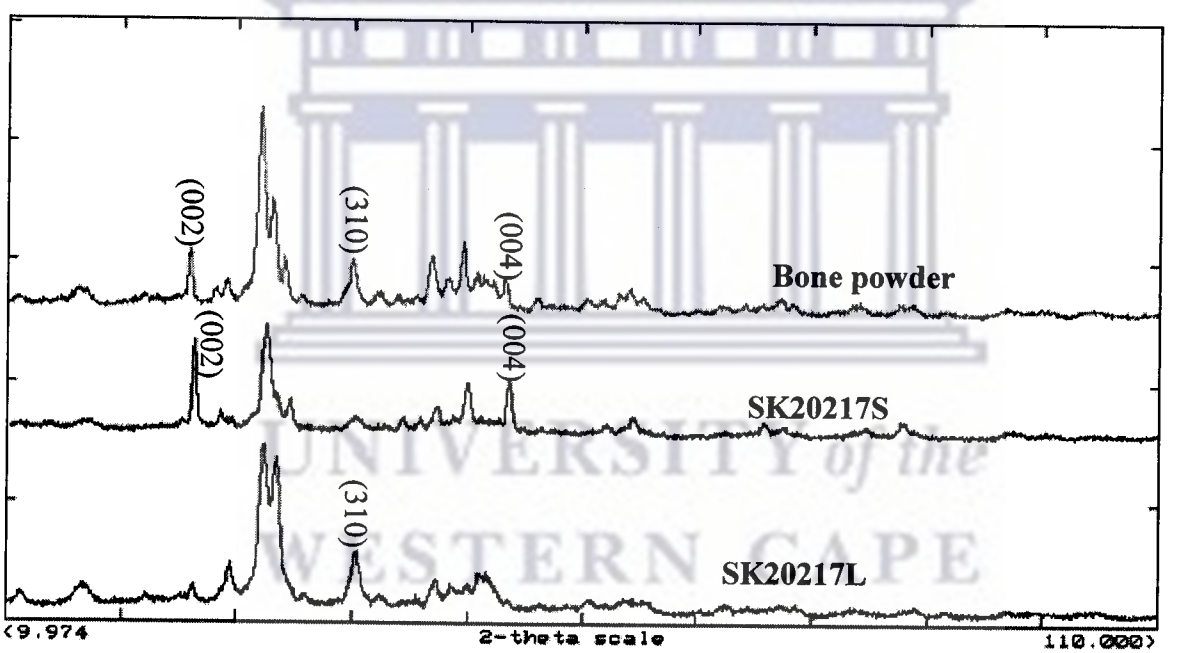

Figure 4.17 XRD patterns from sample SK20217 (Swartkrans member 2) and the powdered sample. Pattern SK20217L refers to the scattering vector perpendicular to the dendrites direction with pattern SK20217S representing orientation with the scattering vector parallel to the dendrites direction.

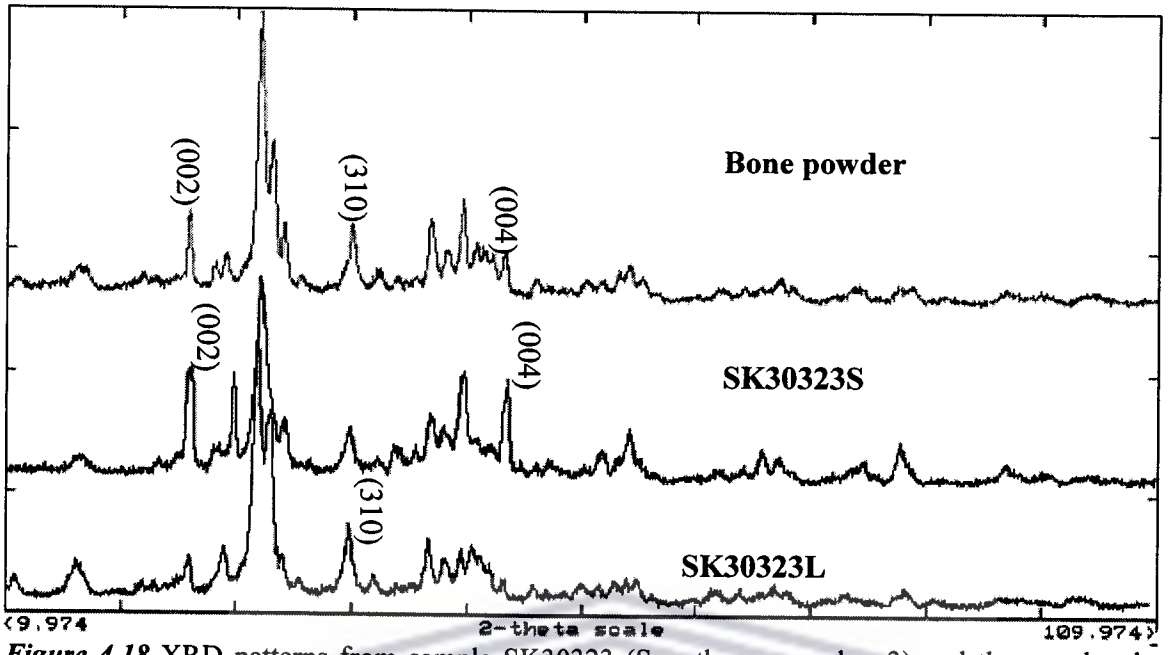

Figure 4.18 XRD patterns from sample SK30323 (Swartkrans member 3) and the powdered sample. Pattern SK30323L refers to the scattering vector perpendicular to the dendrites direction with pattern SK30323S representing orientation with the scattering vector parallel to the dendrites direction.

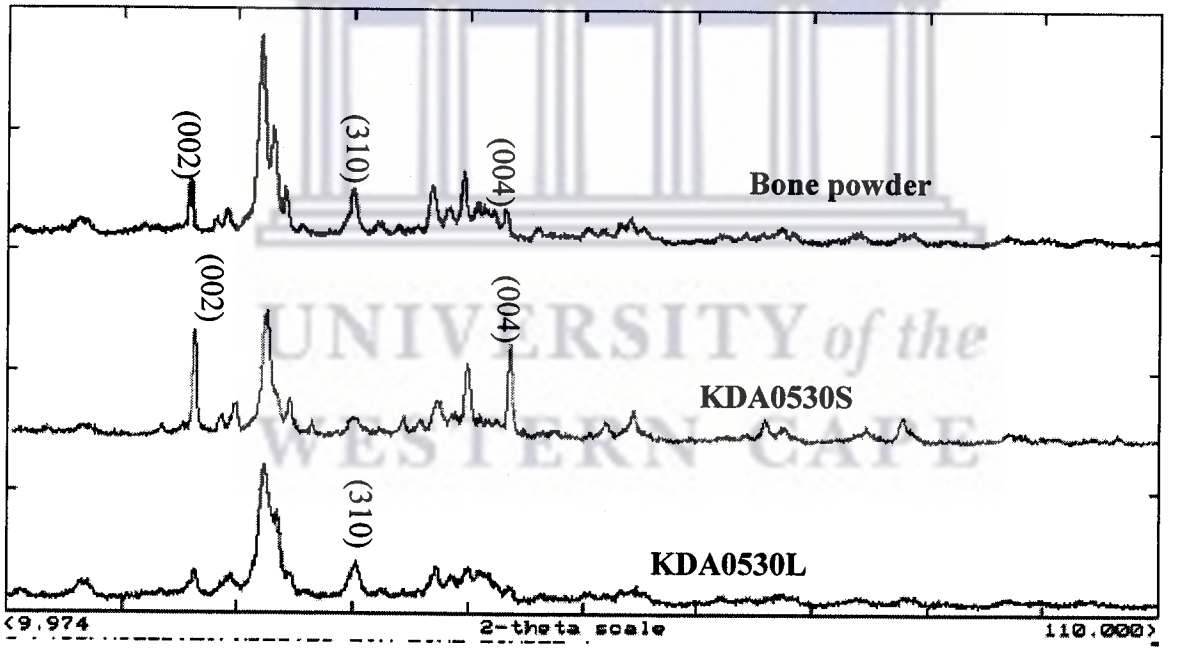

Figure 4.19 XRD patterns from sample KDA0530 (Kromdraai member A) and the powdered sample. Pattern KDA0530L refers to the scattering vector perpendicular to the dendrites direction with pattern KDA0530S representing orientation with the scattering vector parallel to the dendrites direction.

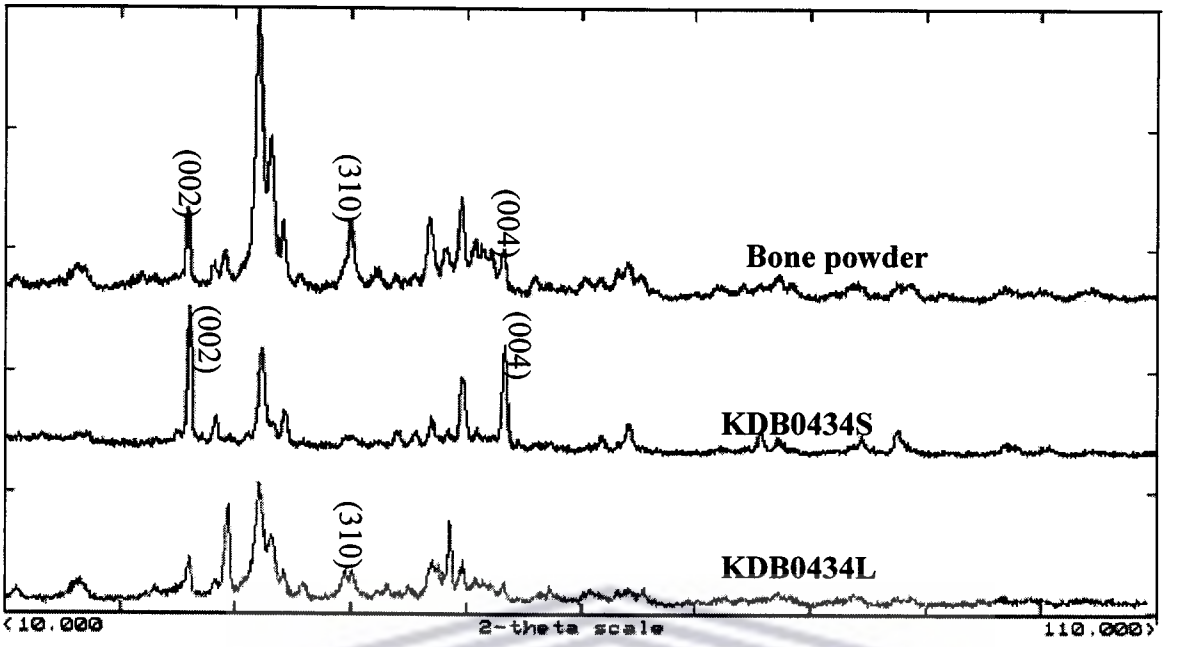

Figure 4.20 XRD patterns from sample KDB0434 (Kromdraai member B) and the powdered sample. Pattern KDB0434L refers to the scattering vector perpendicular to the dendrites direction with pattern KDB0434S representing orientation with the scattering vector parallel to the dendrites direction.

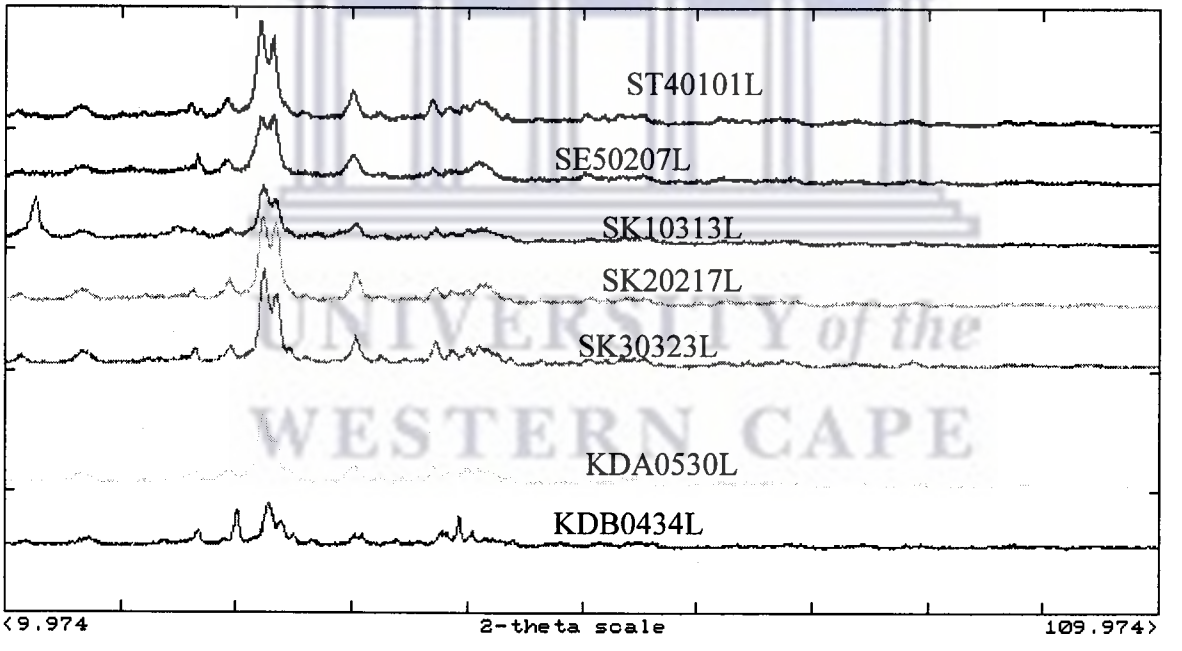

Figure 4.21 XRD patterns showing comparison of intensities from the prismatic planes (L) for the fossilized bone samples from all the caves.

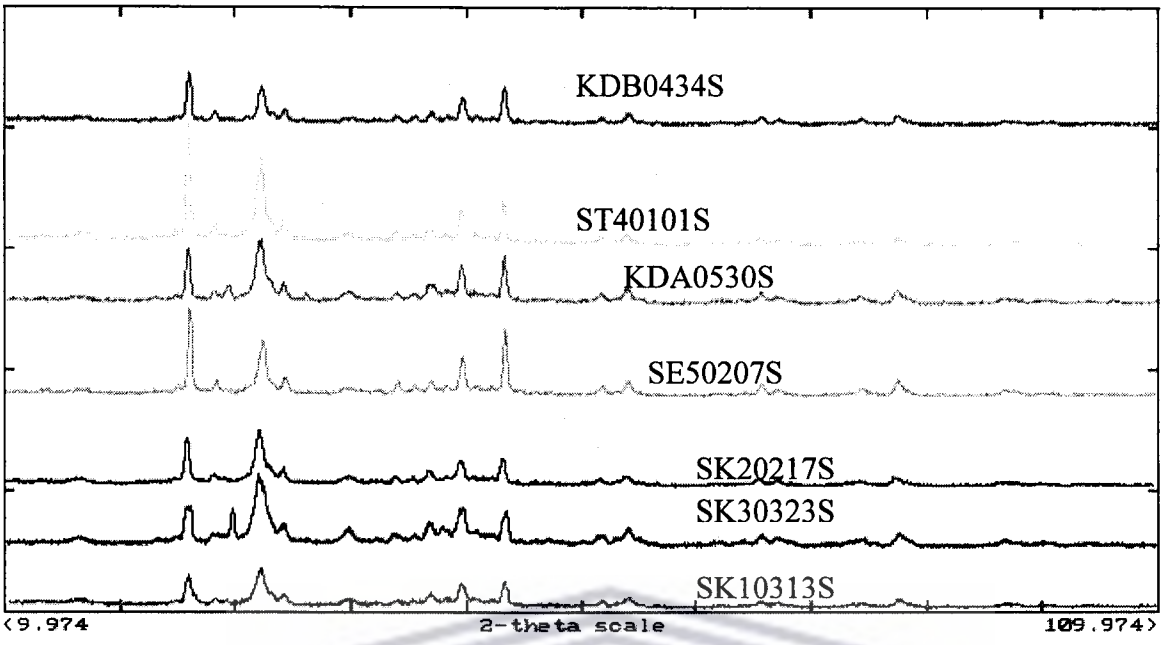

Figure 4.22 XRD patterns showing comparison of intensities taken on the orientation with the scattering vector parallel to the dendrite directions, these include one sample from each member.

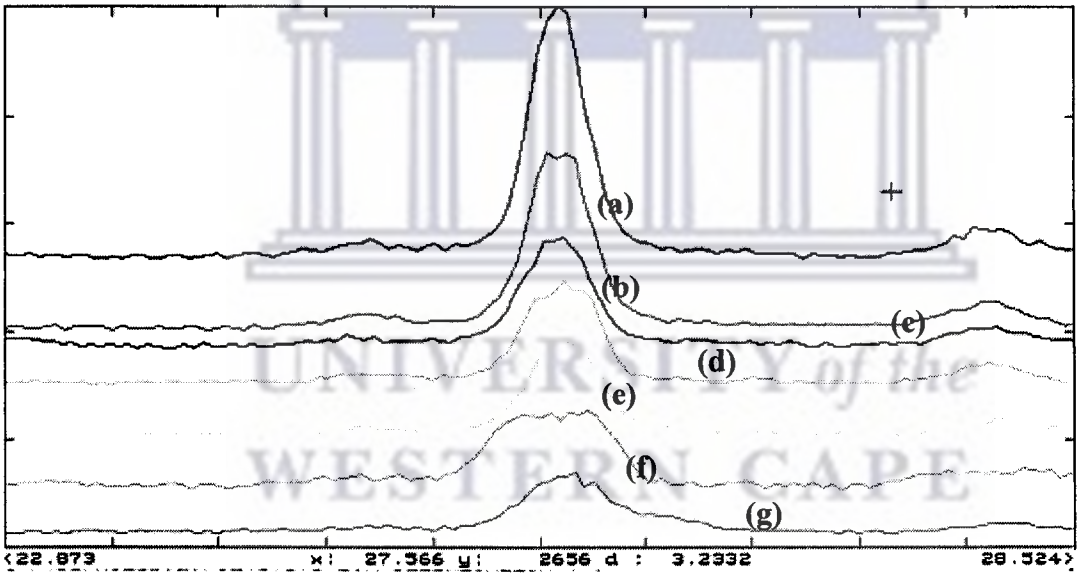

Figure 4.23 XRD patterns of (002) peaks of different samples from different members. (a) ST40101S, (b) SE50207S, (c) KDA0530S, (d) KDB0434S, (e) SK20217S, (f) SK30323S and (g) SK10313S.

The above XRD pattern represents comparisons of the intensities from the (002) peaks, for all seven members of this study. The same pattern was analysed for (004) and (310) planes, we felt is not necessary to include all the patterns because they are arranged in the

same manner as (002) peaks. The intensities from the (100) peaks were generally very weak and left out for analysis. Sample ST40101 has intense and sharper peaks as its surface is flat across the whole illuminated area. Samples from the Swartkrans cave members have wider and flatter peaks because of their irregular surfaces deteriorating the diffraction pattern quality due to multiple surface scattering. The intensities of different peaks were extracted from the peaks and plotted against age of samples to search for possible trends. The plots are shown in Figs 4.24 to 4.29, the integrated peak intensities with corresponding age and samples names are summarised in Tables 4.8 and 4.9. Figures 4.24 to 4.26 plot the intensities for the different peaks in normal orientation to the dendrites direction geometry (L) for each cave members, whereas Figs 4.27 to 4.29 shows that for the parallel orientation (S) versus age (million years).

Sample Name	Age(M years)	Inte I (002)	Inte I (004)	Inte I (310)	Uncertainty
ST40101L	2.3	7	5	63	0.2
SE50207L	1.8	31		87	
SK10313L	1.7	7	2	54	0.15
SK20217L	1.5	9	3	73	
SK30323L	1	20	0	60	
KDA0530L	1.65	25	5	46	
KDB0434L	1.95	22	1	35	
ST4 Age Range	2.1	to	2.5		
KDA Age Range	1.5	to	1.8		

Table 4.8 Table showing comparison from the (002), (004) and (310) Bragg peaks as function of intensities and age for the samples from different members for the L orientation (perpendicular to Q). The samples represent all caves.

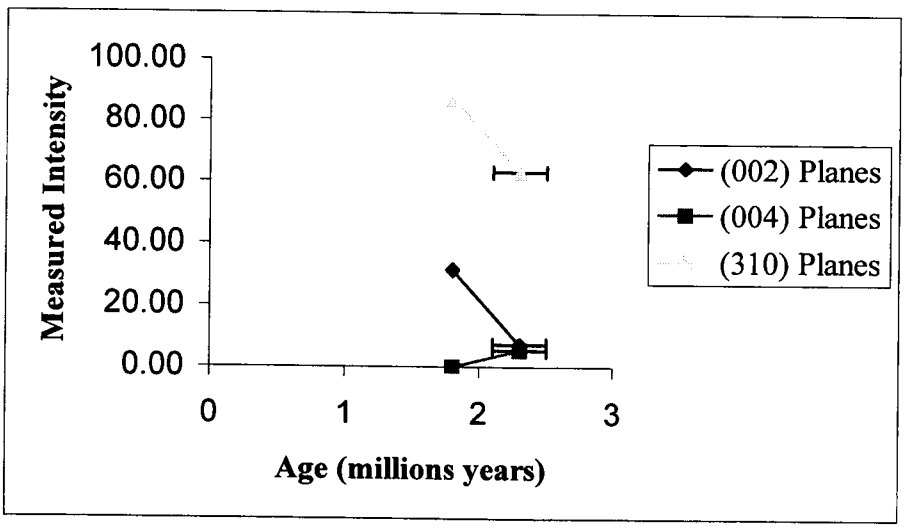

Figure 4.24 Plots of (002), (004) and (310) integrated intensities from the normal orientation measurements of Sterkfontein cave members versus estimated age (million years) of the fossilised bones. The error bars indicate the age range i.e. age can be at any point along the bars.

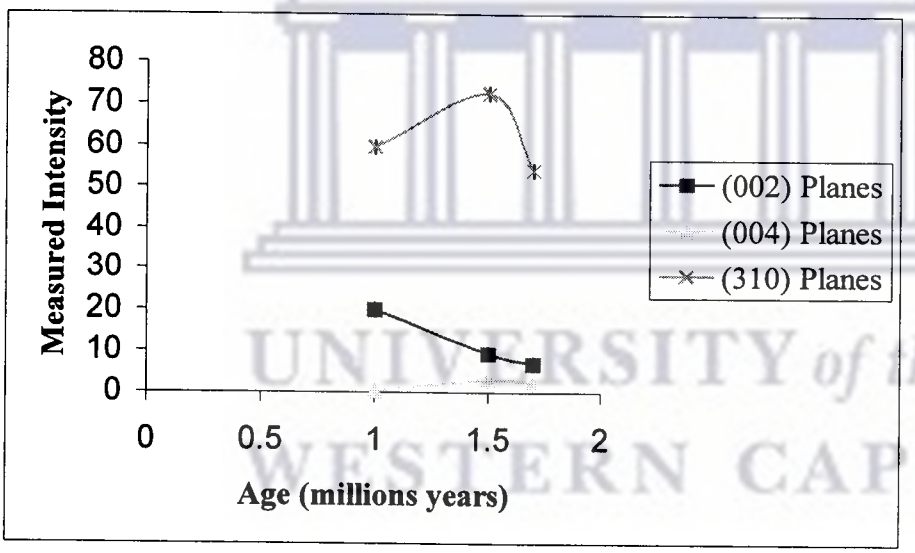

Figure 4.25 Plots of (002), (004) and (310) integrated intensities from the normal orientation measurements of Swartkrans cave members versus estimated age (million years) of the fossilised bones.

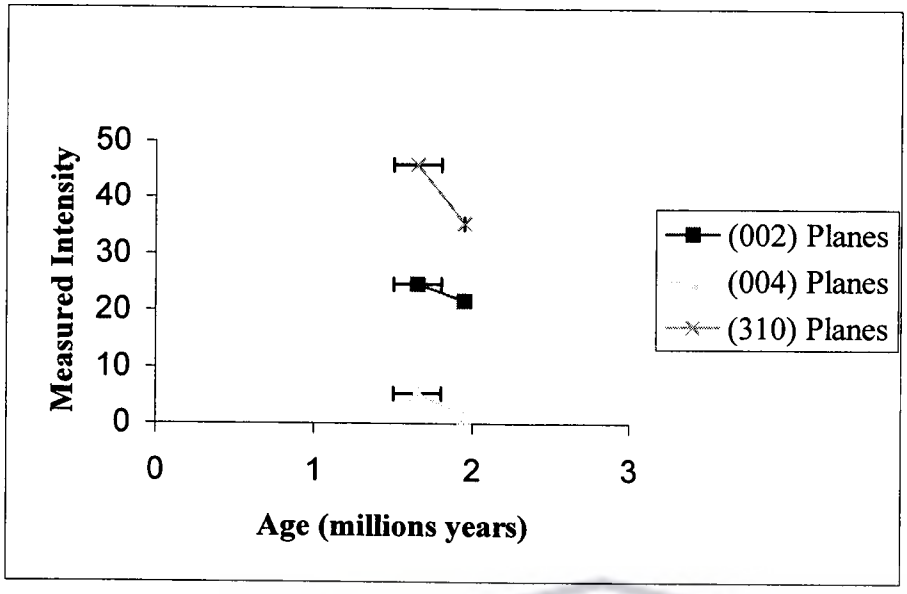

Figure 4.26 Plots of (002), (004) and (310) integrated intensities from the normal orientation measurements of Kromdraai cave members versus estimated age (million years) of the fossilised bones.

Sample Name	Age(M years)	Inte I (002)	Inte I (004)	Inte I (310)	Uncertainty
ST40101S	2.3	119	58	18	0.2
SE50207S	1.8	111	94	22	
SK10313S	1.7	51	32	21	
SK20217S	1.5	61	35	22	
SK30323S	1	88	53	39	
KDA0530S	1.65	79	60	27	0.15
KDB0434S	1.95	64	53	14	
ST4 Age Range	2.1	to	2.5		
KDA Age Range	1.5	to	1.8		

Table 4.9 Table showing comparisons of integrated intensities and age from the different sample from different members. The samples represent all caves. This table includes sample parallel orientation measurements.

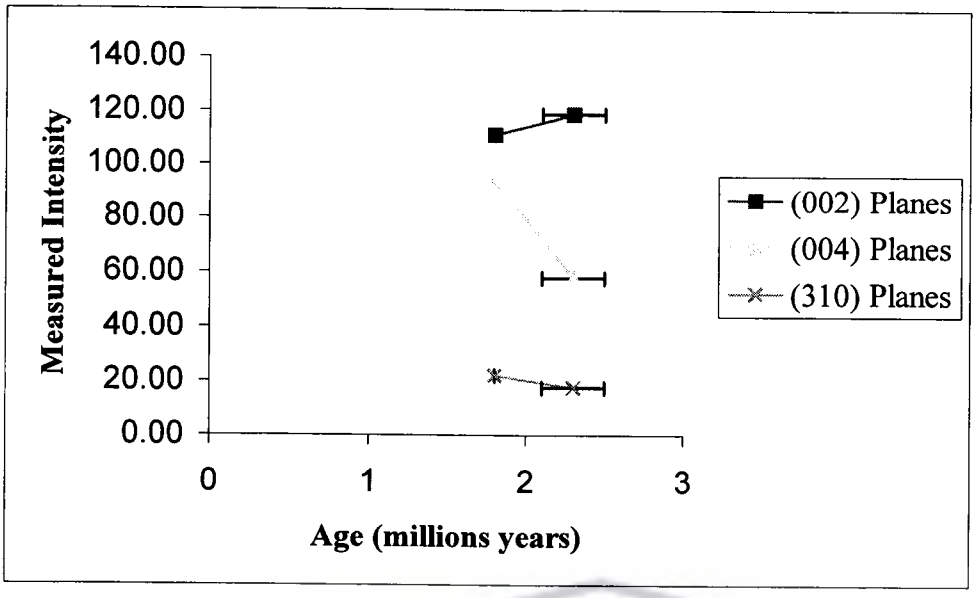

Figure 4.27 Plots of (002), (004) and (310) integrated intensities from parallel orientation measurements of Sterkfontein cave members versus estimated age (million years) of the fossilised bones.

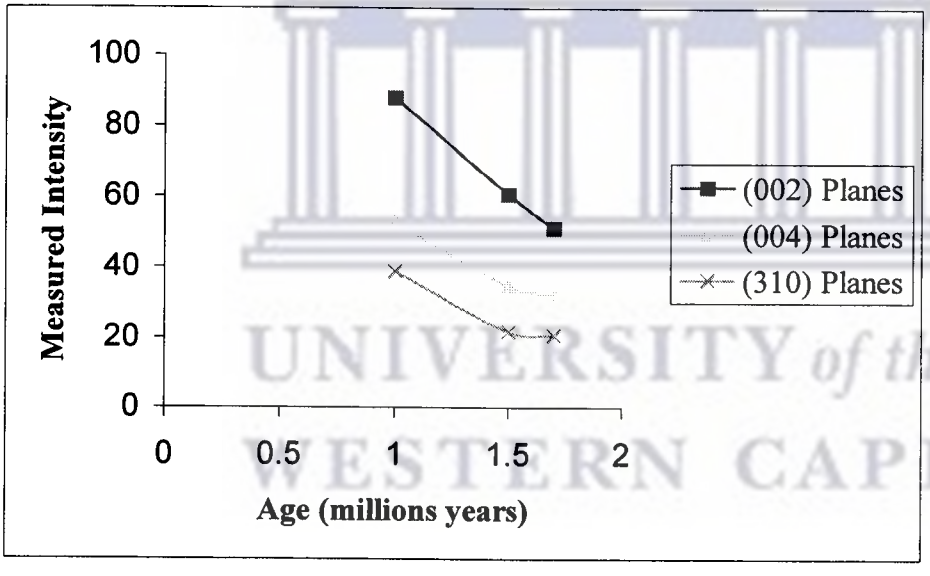

Figure 4.28 Plots of (002), (004) and (310) integrated intensities from parallel orientation measurements of Swartkrans cave members versus estimated age (million years) of the fossilised bones.

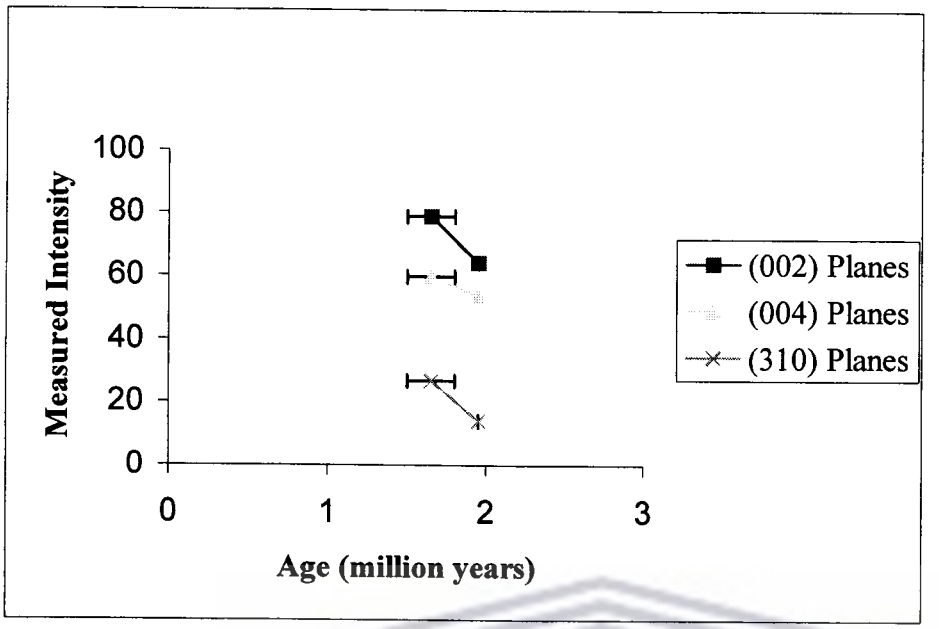

Figure 4.29 Plots of (002), (004) and (310) integrated intensities from parallel orientation measurements of Kromdraai cave members versus estimated age (million years) of the fossilised bones.

4.2.2 X-ray diffraction discussions on preferred orientation

Preferred orientation in the crystallite orientations is observed in all seven members from all three caves with the XRD results showing differences between the basal and prismatic planes as shown in Figs 4.14 to 4.20. The normal orientation measurements showed enhanced intensities for the (310) planes compared to the parallel orientation whereas the parallel orientation measurements showed enhanced intensities for (002) and (004) planes compared to normal orientation. The reason for this being that these planes lay along distinct directions within the bone samples. In plotting measured intensities versus age (million years) for different orientations and different members of the caves, some trends were noticed.

These results are only an indication of possible trends. For a quantitative analysis it is essential that all sample surfaces are smooth and flat to limit any possible artifice effects due to multiple scattering. Furthermore, all sampling should be identical.

Conclusion on XRD preferred orientation

In all the fossilized bone samples preferred orientation of the crystallite orientations are observed. The hexagonal c-axis of the hydroxylapatite is aligned along the bone axes with the prismatic planes normal to the bone axes.

4.3 Scanning Electron Microscope (SEM) results

Observation of Mn from the fossilized bone samples proved difficult in general. The procedure adopted was to do EDX analysis over areas sufficiently large, typically a few mm^2 in size, until Mn was observed. By systematically reducing the analysis area and zooming into areas where Mn signals were present, localized spots of 10x100 μm^2 could be isolated in same cases. The SEM results are presented as images and EDX spectral analysis of either areas or spots. The measurement parameters applicable to each SEM and EDX analyses are shown in the comment at the bottom of each SEM image i.e. magnification and resolution.

Figure 4.30 shows spot analyses where Mn was observed in Sterkfontein sample (ST40404). The morphology of the SEM images does not reveal any prior indication of the Mn rich regions. Successful spot analyses over regions of 100x100 μm^2 were also in Sterkfontein sample (ST40202) as shown in Figs 4.40 and 4.41. These spots seem to be Fe and not Mn. In Swartkrans samples SK10313, Fig 4.37, SK20419, Fig 4.38 and SK30121, Fig 4.39, the sizes of the area analyses could not be reduced to identify isolated Mn rich areas. No samples originating from Kromdraai were analysed by SEM.

Analysis of the chert rock proved easier in that the brown stains clearly showed up as Mn containing as shown in Figs 4.32 to 4.36. No Mn was identified from the analysis of the green spots (live lichen).

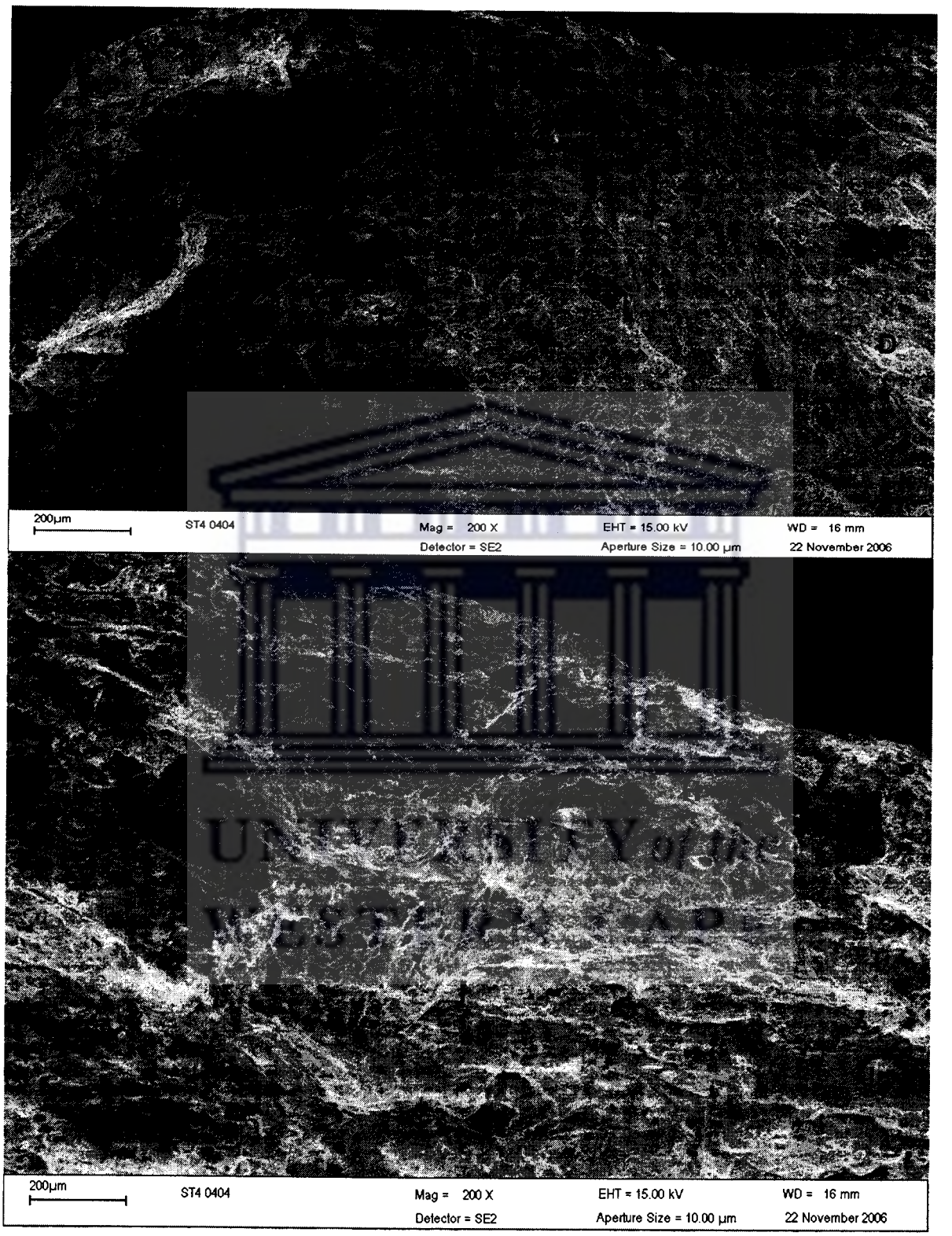

Figure 4.30 SEM images of Sterkfontein sample (ST40404). Spot analyses were taken at points by A to J. The magnification and resolution are shown under the images.

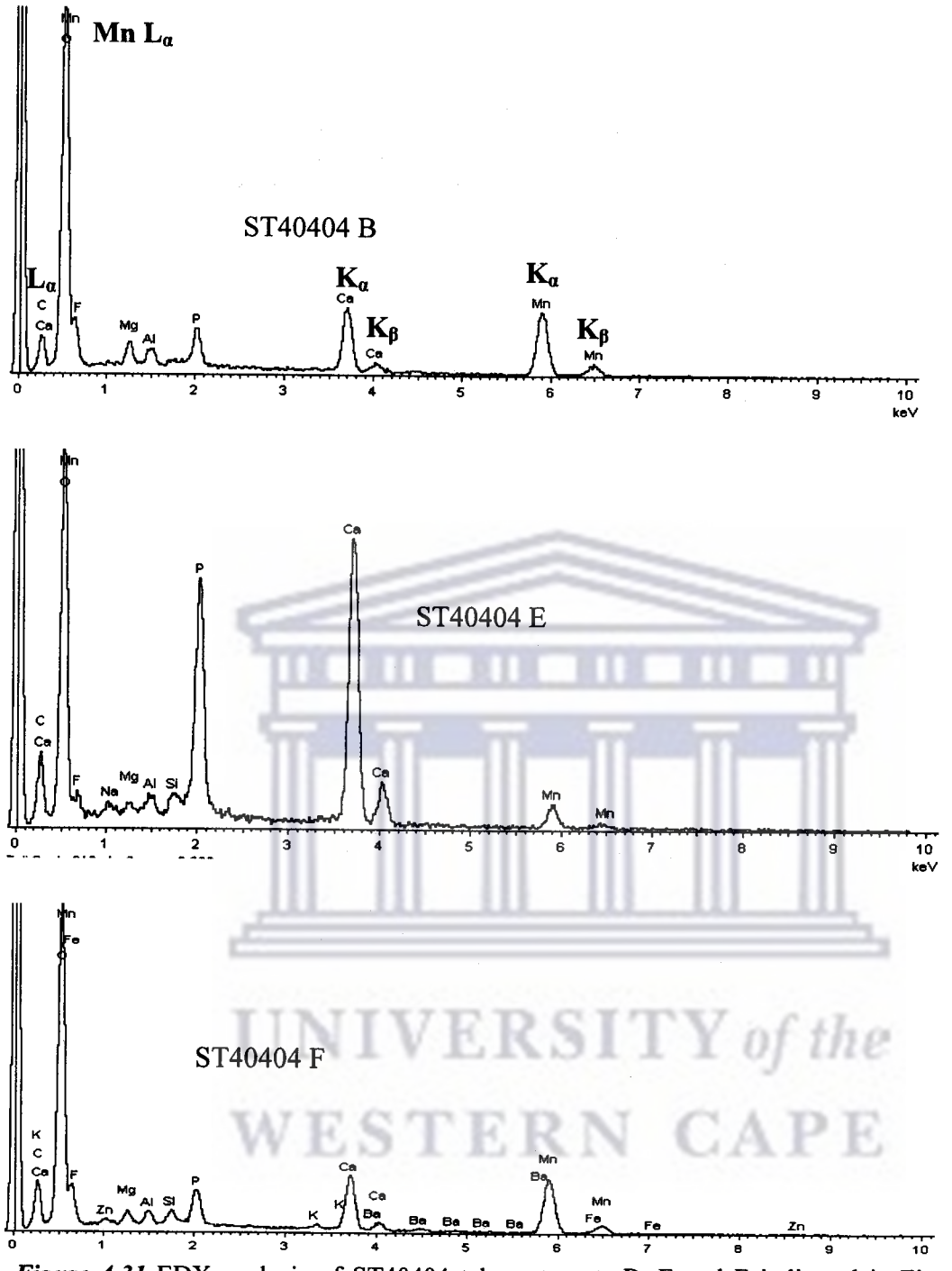

Figure 4.31 EDX analysis of ST40404 taken at spots B, E and F indicated in Fig 4.30 that corresponded to brown stains.

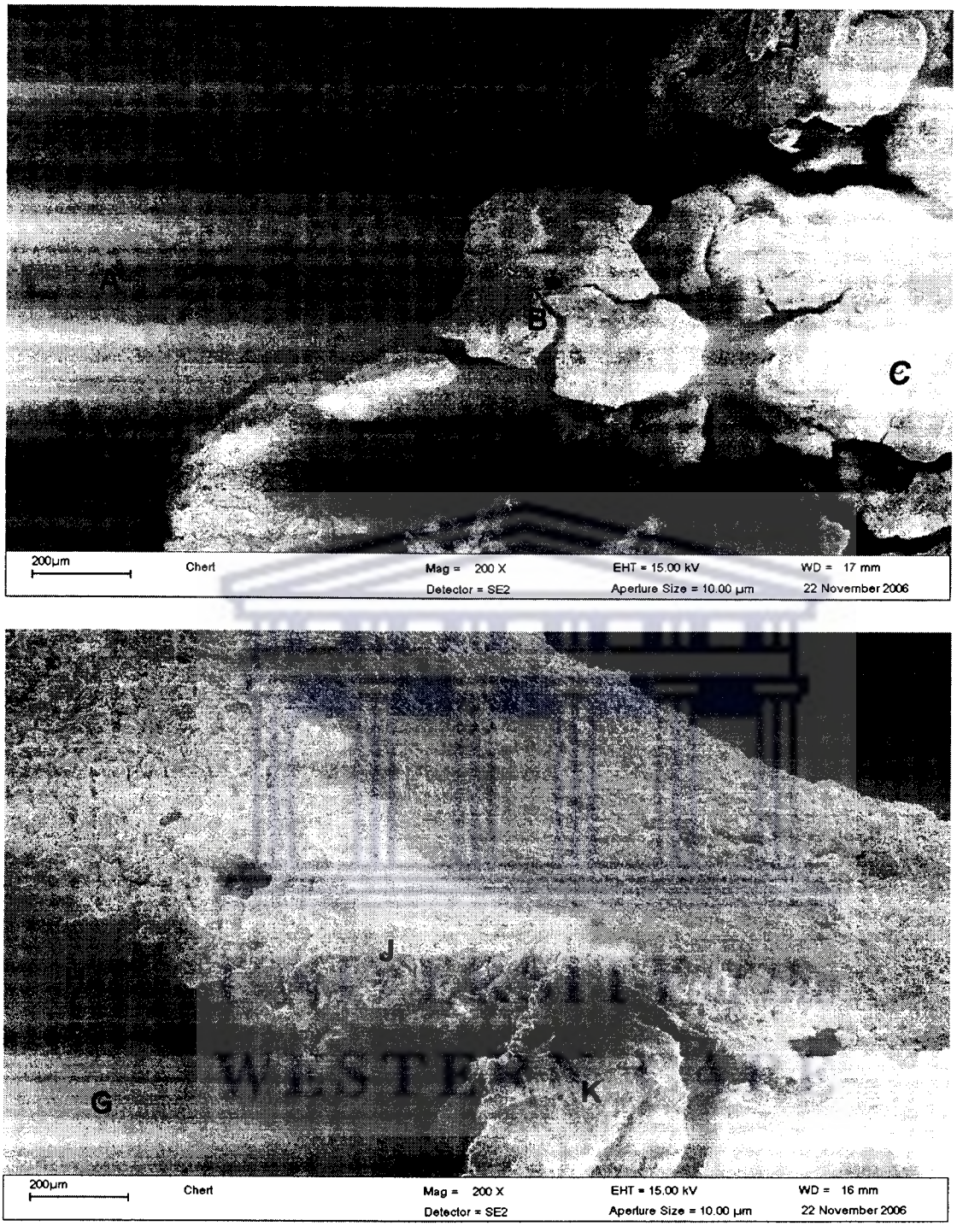

Figure 4.32 SEM images from chert rock. Spots B and C were taken at positions on the live lichen whereas the other positions correspond to the brown stains.

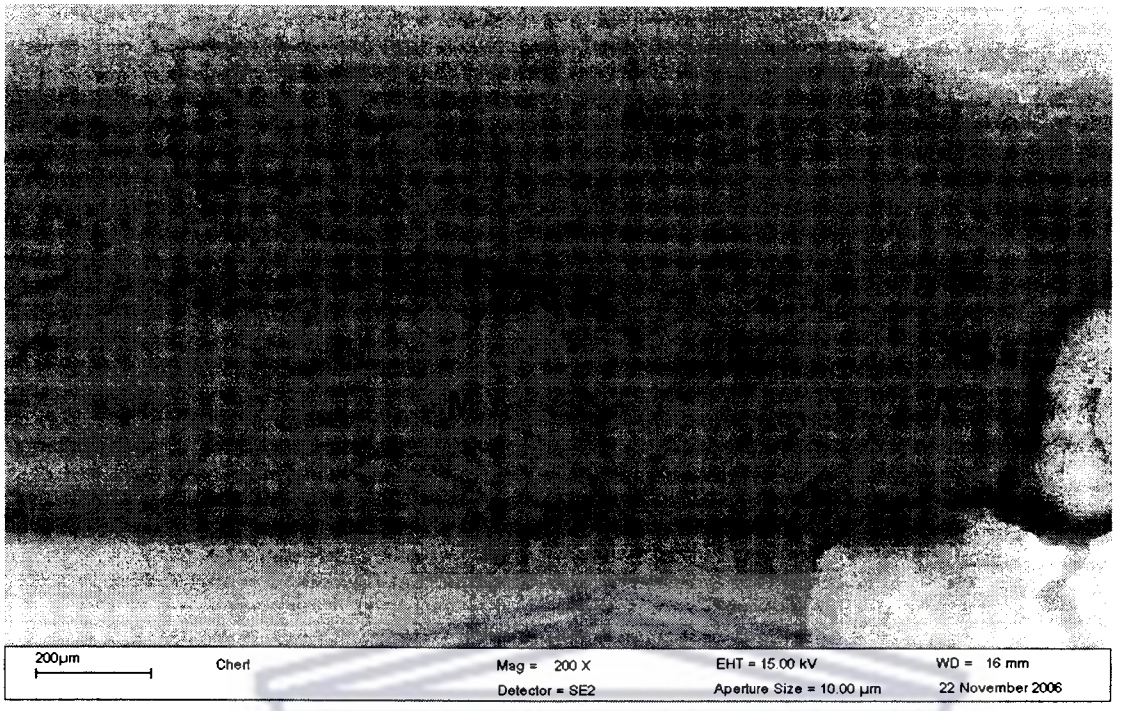

Figure 4.33 Image from chert rock showing spots L, M and N corresponding to brown stains.

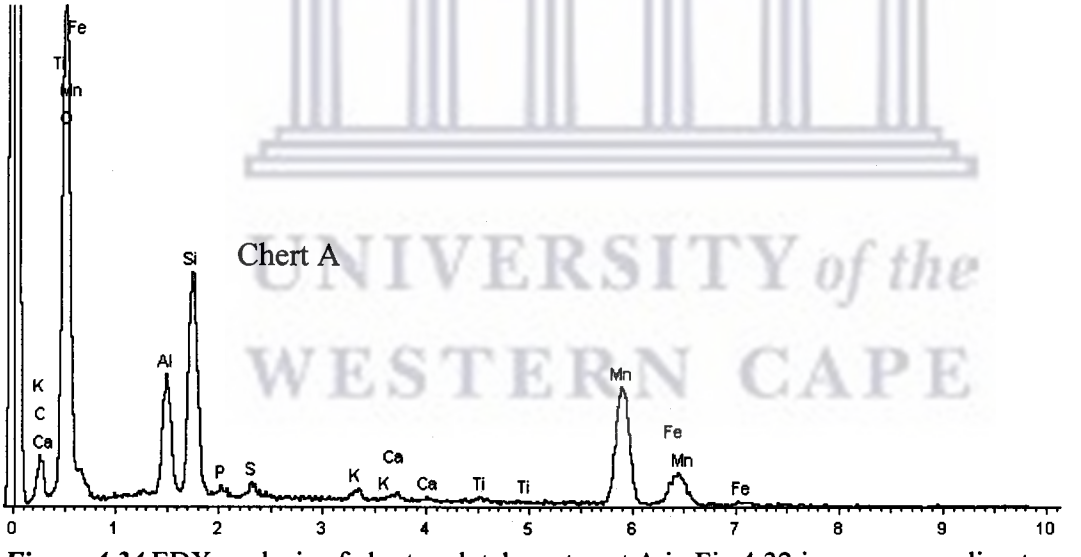

Figure 4.34 EDX analysis of chert rock taken at spot A in Fig 4.32 i.e. corresponding to a brown stain.

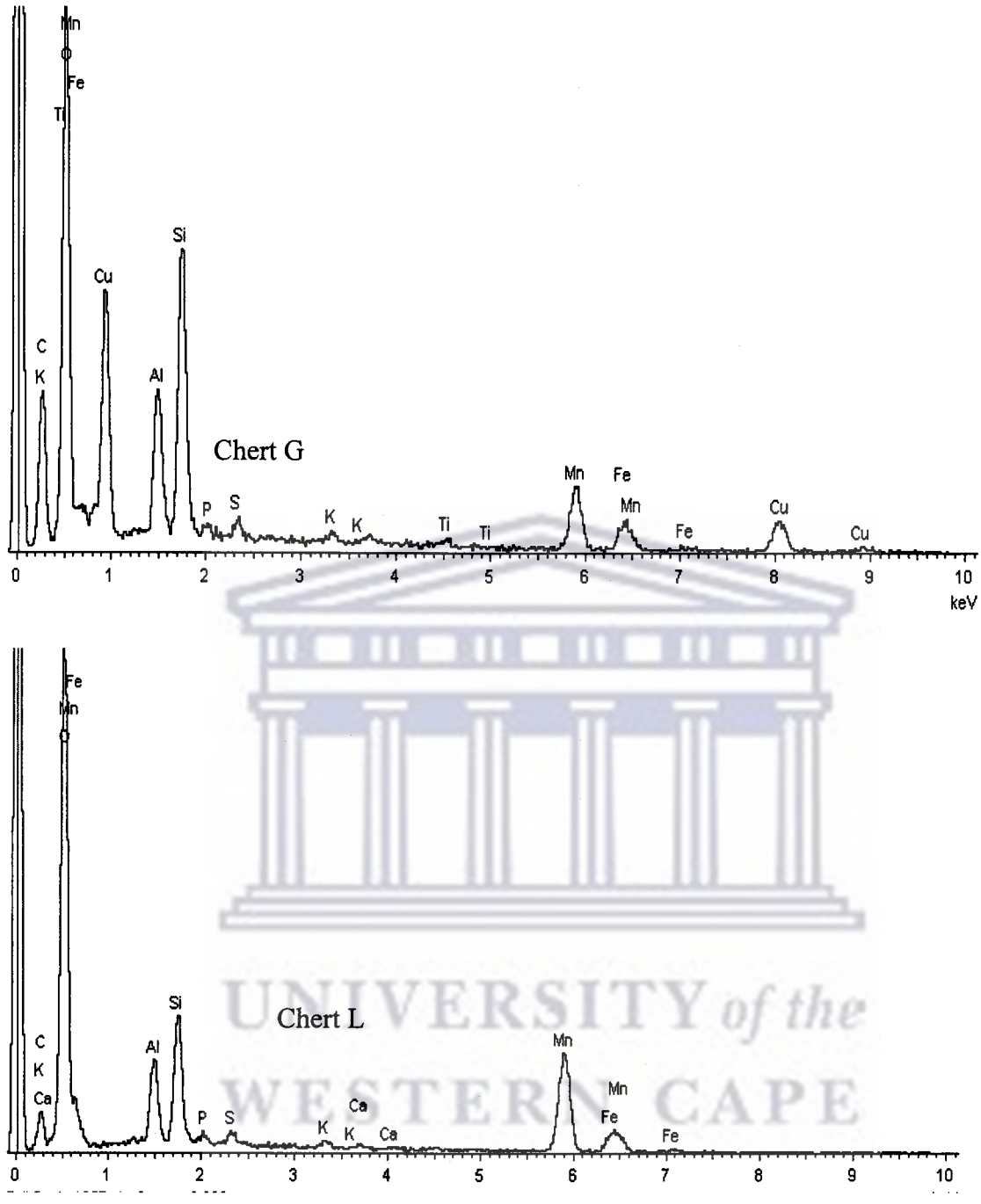

Figure 4.35 EDX analyses taken at spots G and L indicated in Figs 4.32 and 4.33. Both locations correspond to prominent brown stains.

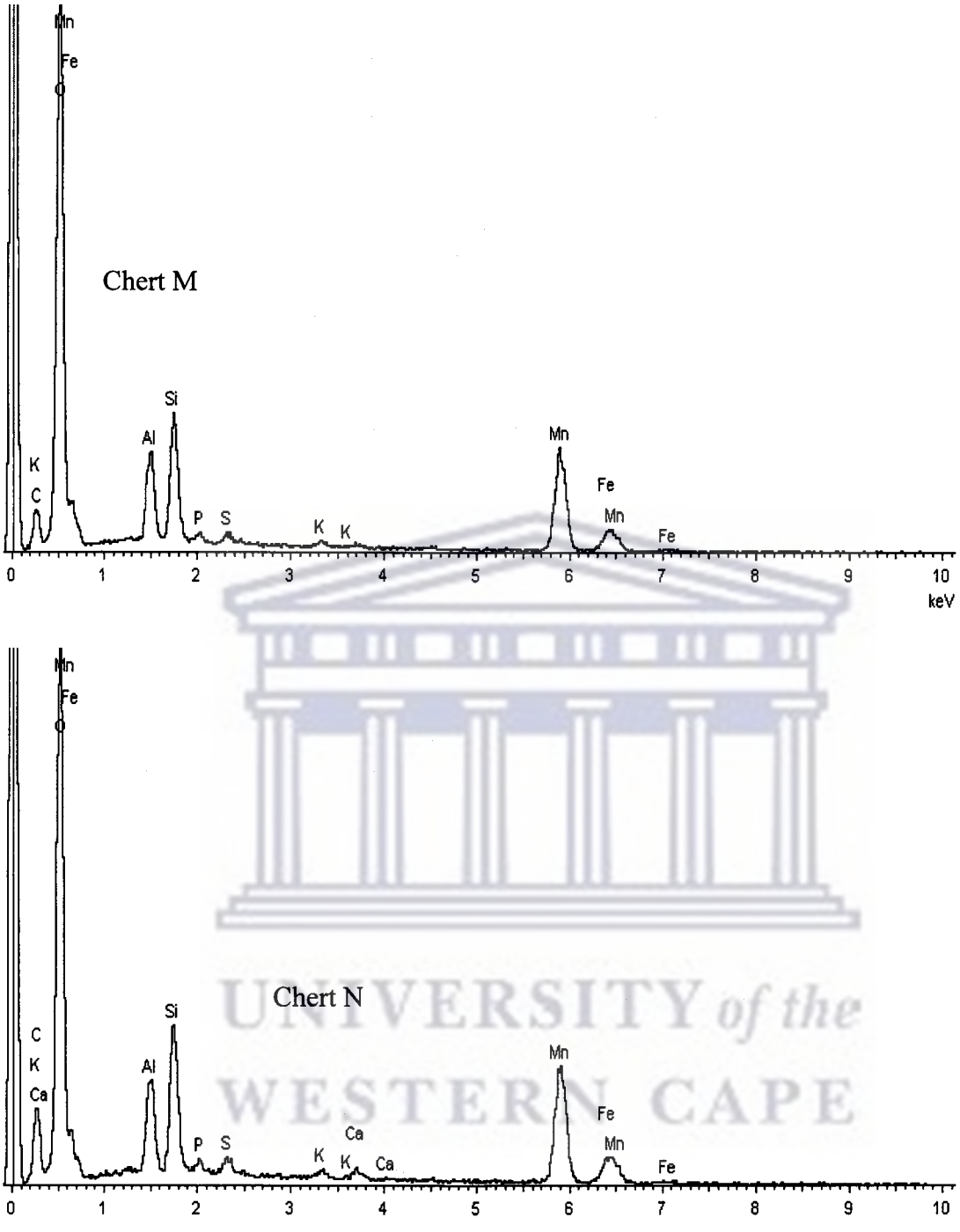

Figure 4.36 EDX analyses taken at spots M and N indicated in Fig 4.33. Both locations correspond to prominent brown stains.

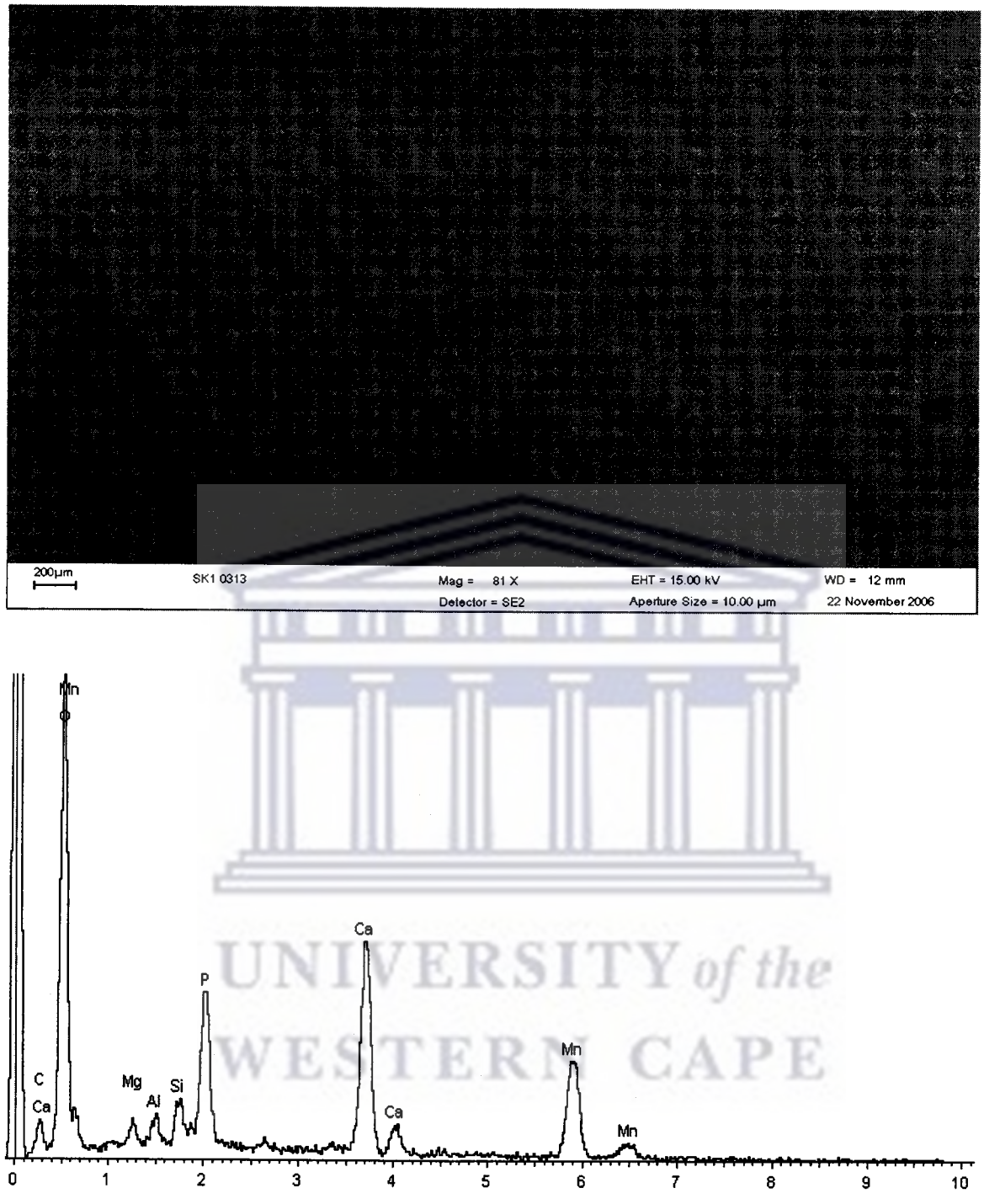

Figure 4.37 This figure shows the SEM images of sample SK10313 and the EDX result obtained from an area analysis of entire SEM image.

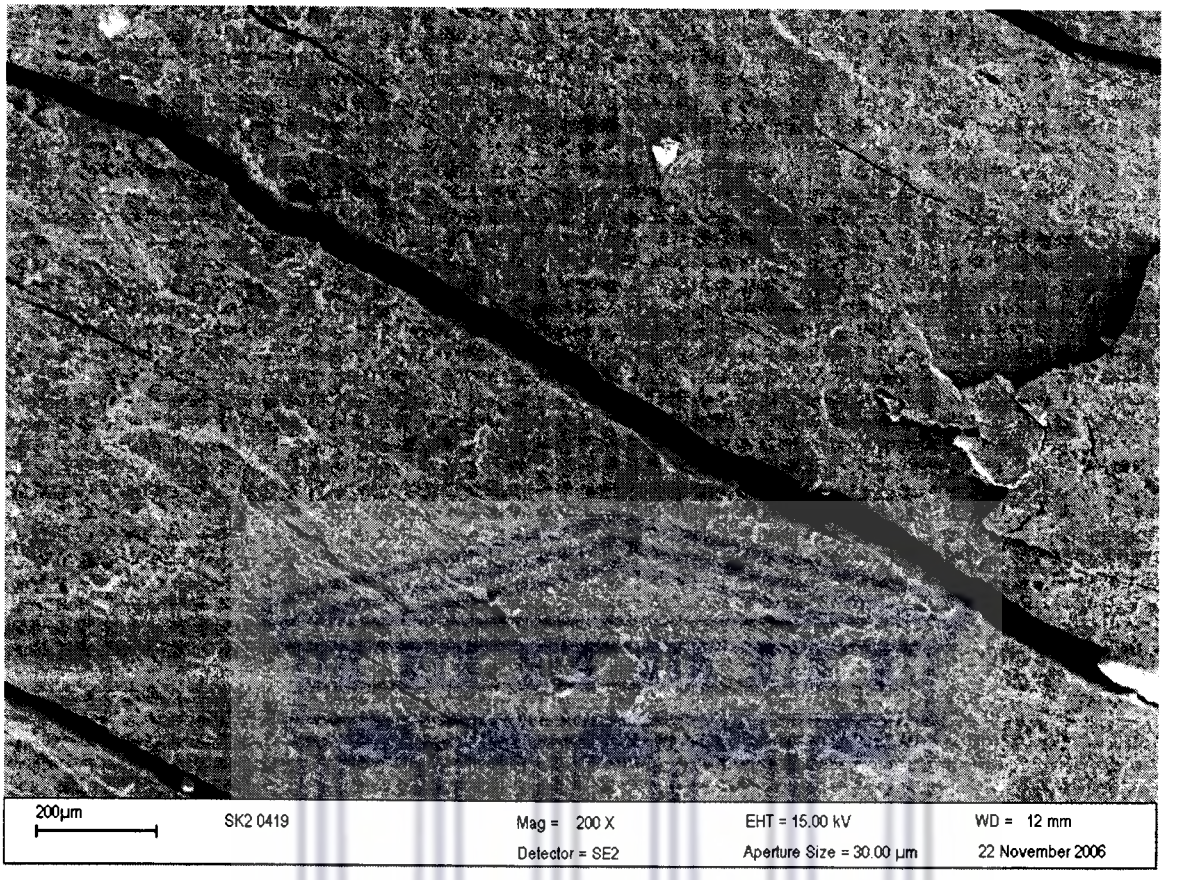

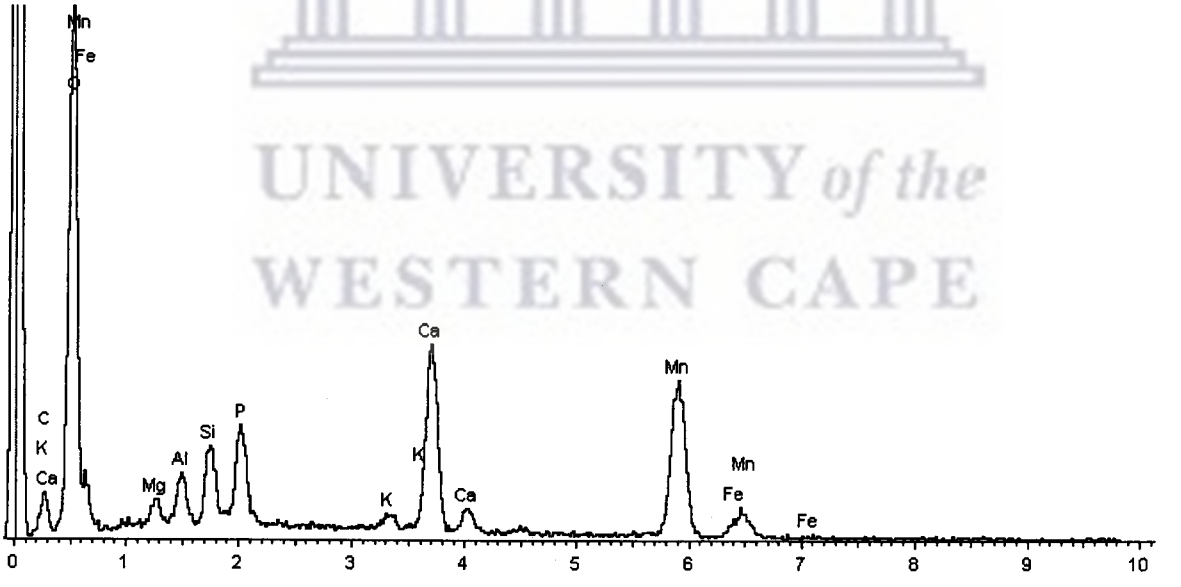

Figure 4.38 This figure shows the SEM image of sample SK20419 and the EDX results obtained from an area analysis of the entire image.

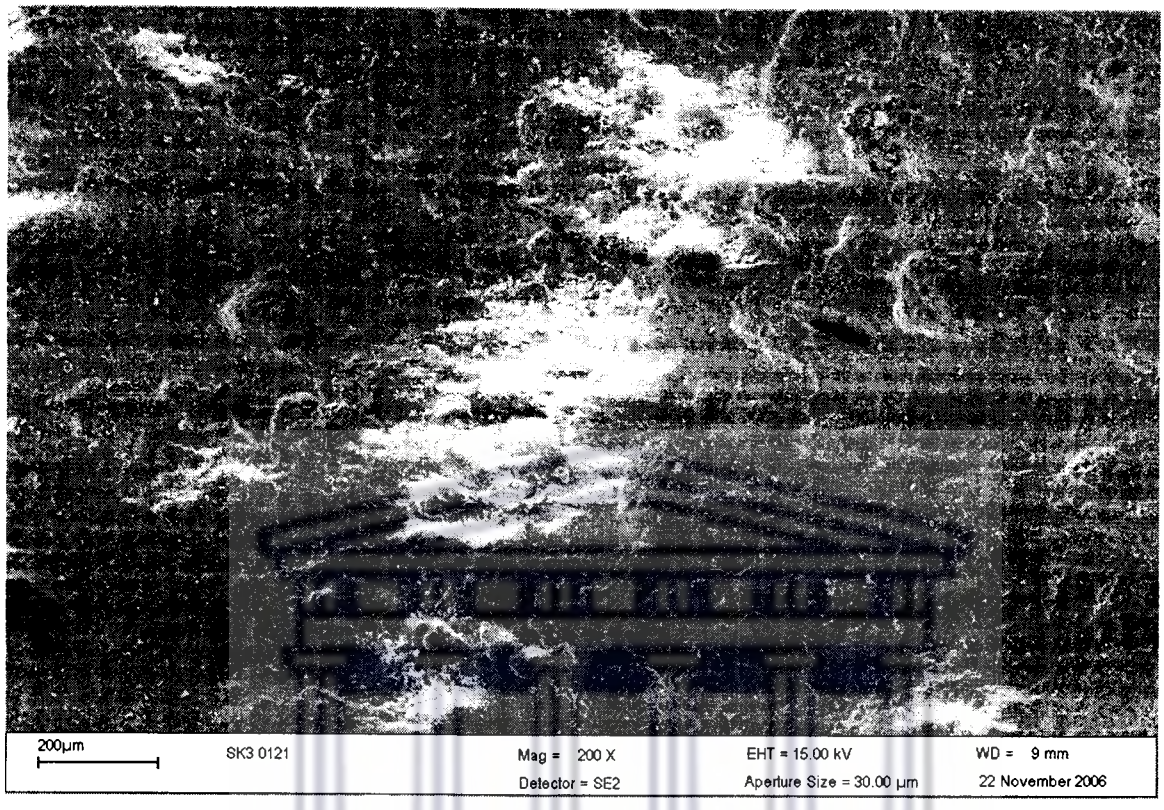

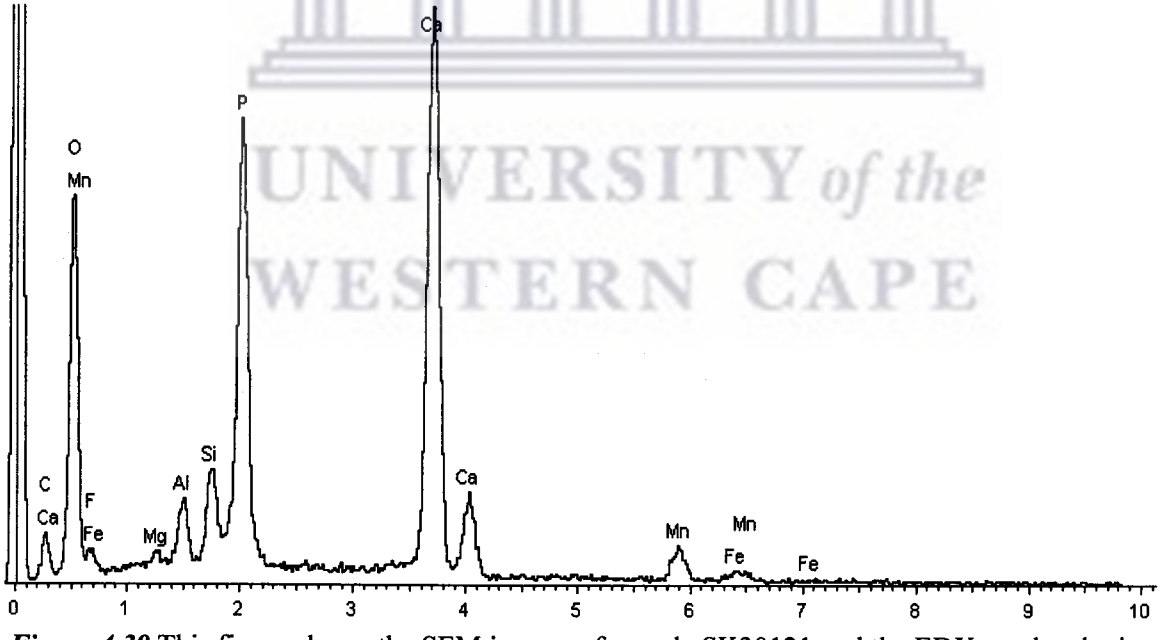

Figure 4.39 This figure shows the SEM images of sample SK30121 and the EDX results obtained from an area analysis of the entire SEM image.

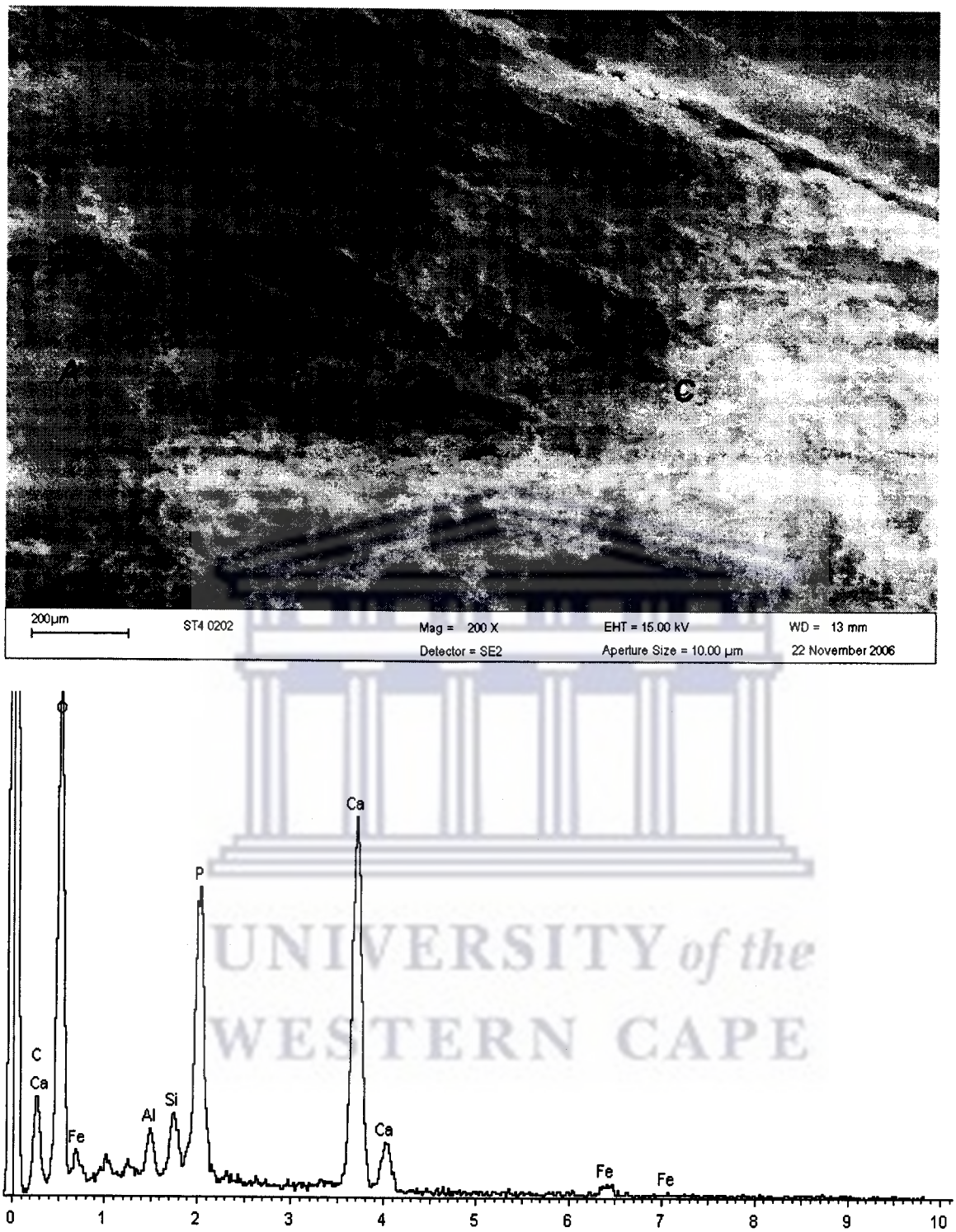

Figure 4.40 A SEM image taken from sample ST40202and spot locations where EDX analyses were done. The EDX analysis at spot A is shown.

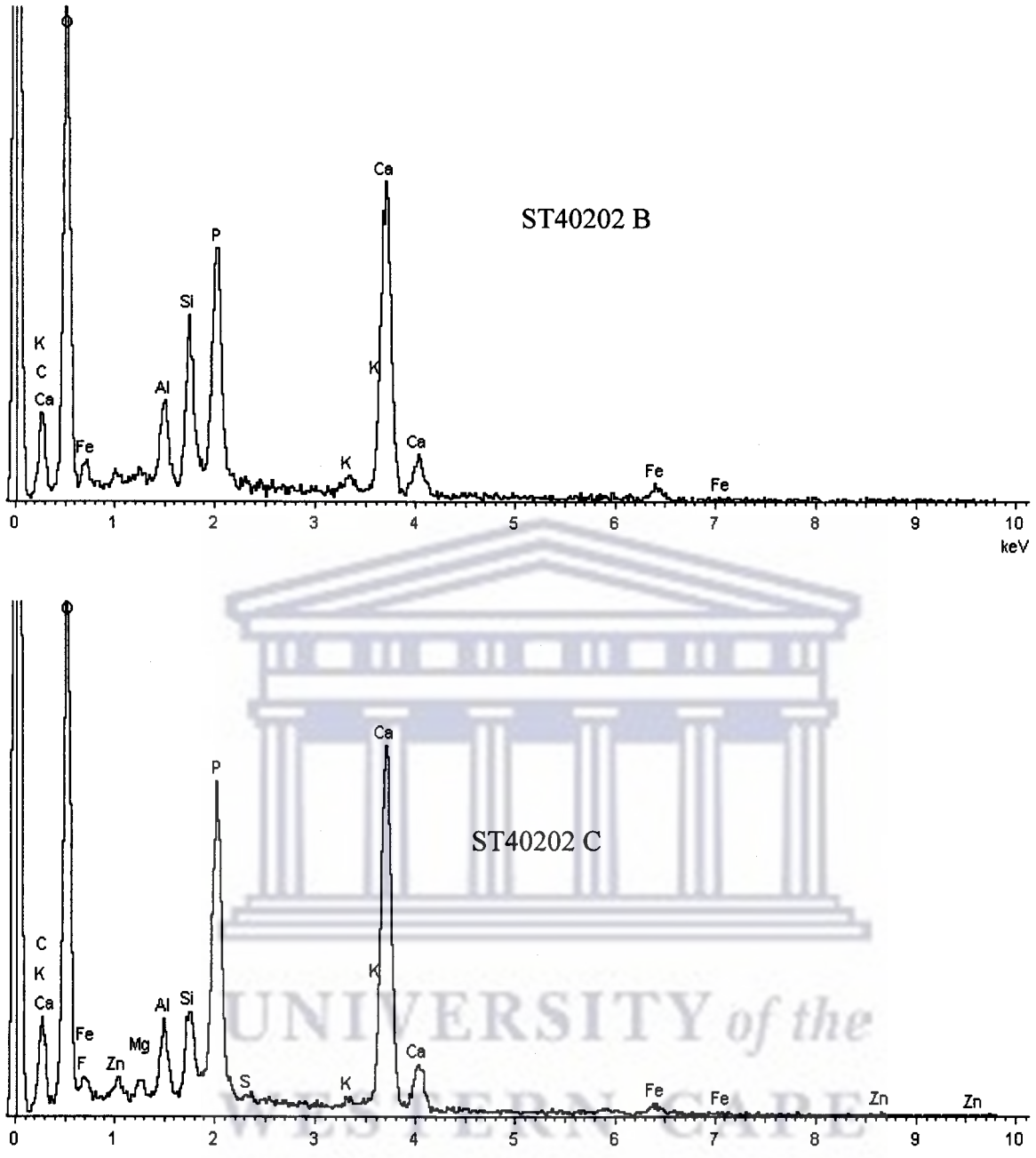

Figure 4.41 EDX results of Sterkfontein sample of fossil bone (ST40202) taken from spots B and C showed in Fig 4.40.

4.3.1 SEM results discussions

The SEM results showed that manganese content in the fossils is very localized and not necessarily distributed over the surface areas of the entire brown stains. It was not found in the most parts of the sample unless specific positions of high Mn were searched for. It is postulated that manganese is detected mostly in the grooves or crevices. Sterkfontein

sample ST40202 has less visible stains compared to any other analysed fossil bone samples. Its SEM analysis shows the spots to be Fe containing instead of Mn. Analysis of the live lichen does not reveal the presence of manganese.

4.3.2 Conclusion on the SEM Results

The presence of Mn in the fossilized bone samples does not seem to cover the complete areas of the brown stains, but rather localized to the grooves and crevices. The highest prevalence of Mn seems to exist in the samples originating from Sterkfontein as they have localized spot areas of high Mn existence, whereas in the samples from Swartkrans the Mn is spread over larger areas as Mn is only observed in the latter in area analyses and not spot analyses.. This conclusion cannot be fully verified for all three caves as no samples from Kromdraai caves were analysed by SEM/EDX. The strong Mn signals in the chert rock could be related to the deeper crevices of the rock morphology. No Mn signals were observed from the green lichen spot on the chert rock.

Chapter 5

Conclusions and recommendations

5.1 Conclusions

The aim of this study was to investigate stains existing on fossil surfaces, but only qualitative results were obtained. There are many factors that contributed to this, such as thickness of the stains, manganese content and flatness of the sample surfaces. Three measurement techniques were used i.e. SEM, XRF and XRD but none of them gave quantitative results due to the above mentioned factors. In the XRD measurements some of the expected chemicals were detected (Si, P and Ca), but only XRF and SEM showed some manganese signals. The results showed that these stains contain very small manganese contents. Based on these observations it is therefore concluded that the thickness of these MnO_2 stains is less than the penetration depth of the x-rays used, the XRD analyses as the substrates are clearly identified. The MnO_2 content in the illuminated area is below the 1detection limit of the technique. The existence of preferred orientation of the crystallite orientations of the hydroxylapatite are 1wt% detection in the fossilized bone samples.

5.2 Recommendations

Based on the above conclusions it is therefore recommended that complementary measurements techniques be used for continuation of the study. The measurement techniques that should be used need to have less penetration depth compared to the techniques utilised. Some techniques proposed are X-ray Photoelectron Spectroscopy (XPS) and Time of Flight Secondary Ion Mass Spectrometry (TOF-SIMS) at the CSIR Pretoria. The other technique that can be used is SEM dual system, which is the combination of the SEM and Focus Ion Beam (FIB), a new instrument at NECSA.

For quantitative preferred orientation analysis, samples needs to be prepared with flat surfaces, or alternative methods such as neutrons diffraction used that is not influenced by the surface roughness.

References

[Ara2004] Arakawa-Kobayashi S. et al., "Identification of crystalline material found in the thallus of the lichen, Myelochroa leucotyliza" Journal of Structural Biology **146**: 393-400; (2004).

[Baf2002] Baffi C. et al., "Comparison of different analytical procedures in the determination of trace elements in lichens" Chemosphere **48** :299-306; (2002).

[Ber2004] Bergamaschi L., et al., "Determination of baseline elements composition of lichens using samples from high elevations" Chemosphere **55**:933-939; (2004).

[Bra1981] Brain C.K., "The Hunters or the Hunted" University of Chicago Press (1981).

[Bro1947] Broom R., Discovery of a new skull of the South-African apeman, Pleasianthropus, Nature **159**: 672; (1947).

[Bun1982] Bunge H.J., Texture Analysis in Material Science, (1982).

[Cha1986] Chapman S.K., Working with Electron Microscope, Lodge mark Press (1986).

[Cla1999] Clark B.M. et al., "Analysis of lichen thin sections by PIXE and STIM using proton microprobe" Nuclear Instruments and Methods in Physics Research B **150**: 248-253; (1999).

[Cla1998] Clarke R.J., First ever discovery of a well-preserved skull and associated skeleton of Australopithecus, S. Afr.J.Sci.**944**: 60-463; (1998).

[Cuk2005] E.M Cukrowska, T.S McCarthy, S. Pole, L. Backwell and C. Steininger "The chemical removal of manganese dioxide coatings from fossil bones from the Cradle of Humankind, South African Journal of Science **101**, January/February 2005

[Cul1978] Cullity B.D. , "Elements of X-Ray Diffraction, Second Edition", (1978).

[Ege2005] Egerton R.F., Physical Principles of Electron Microscopy (2005).

[Eug1978] Eugene P. Bertin, "Introduction to X-Ray Spectromic Analysis", Plenum Press, New York;(1978)

[Gui1963] Guinier A., X-ray Diffraction, Freeman (1963).

[Hau2005] Hauck M. and Spribille T., "The significance of precipitation and substrate chemistry for epiphytic lichen diversity in spruce-fir forests of the Salish\ Mountains, northwestern Montana" Flora **200**: 547-562; (2005).

[Hey2006] Heyman J.A.W et al."Site-specific 3D imaging of cells and tissues with a dual beam microscope", Journal of structural Biology **155**: 63-73; (2006).

[Joh1976] Johari O.M., Scanning Electron Microscopy, April 5-9 by (1976).

[Jen1996] Introduction to X-ray Powder Diffractometry, Ron Jenkins, Robert L. Snyder (1996).

[Kan1972] Kanaya K, Okayama, S Penetration and energy-loss theory of electrons in solid targets. J Phys D App Phys **5:** 43-58; (1972).

[Las2002] László Sass, Éva Hideg, Imre Vass, Kozi Asada., "Desiccation and rehydration in the lichen Cladonia convolute monitored by laser scanning microscopy" Proceedings of the 7th Hungarian Congress on Plant Physiology, S6-P08; (2002).

[Mar2005] Hauck M. et al., "Uptake and toxicity of manganese in epiphytic cyanolichens" Environmental and Experimental Botany xxx (2005) xxx-xxx.

[Nie1978] Nieboer E., D.H.S Richardson, F.D Tomassini Bryologist Mineral uptake and release by lichens, , vol **81**:226-246;(1978).

[Pra2001] Sandrine Prat, John Francis Thackeray, Position des lignes temporales sur le cranium de <<Mrs>> Ples (A. africanus): une attribution sexuelle est-elle possible, ;(2001).

[Sie1967] Siegbahn K. et al, Nova Acta Regiae Soc.Sci., Ser. IV, Vol. **20**: 1981 Nobel Prize in Physics;(1967).

[Tha2005] Thackeray J.F, Sénégas F. and Laden G., "Manganese dioxide staining on hominid crania from Sterkfontein and Swartkrans: possible associations with lichen" South African Journal of Science **101**, January/February 2005.

[Uch2006] Uchic M. D. et al.3D microstructural characterization of nickel superalloys via serial-sectioning using a dual beam FIB-SEM, Script Materialia **55:** 23-28; (2006).

[Vic2001] Vickermal John C. and Briggs D. TOF-SIMS: Surface Analysis by Mass Spectroscopy; (2001).

[www01]http://www.discoveryouself.co.za/sterkfontein/source/content/visitor_info_map.htm taken on 07/07/06.

[www02] http://www.nfi.org.za/palaeo/mrsples.htm taken on 15/03/06.

[www03] http://www.nfi.org.za/palaeo/millennium_sudial.htm taken on 15/03/06.

[www04] http://helios.bto.ed.ac.uk/bto/microbes/lichen.htm taken on 25/05/06.

[www05] http://mgd.nacse.org/hyperSQL/lichenland/html/biology/meeting.html taken on 30/05/06.

[www06] http://dictionary.reference.com/browse/vascular%20tissue taken on 15/09/06.

[www07] http://dictionary.reference.com/browse/xylem taken on 15/09/06.

[www08] http://dictionary.reference.com/browse/phloem taken on 15/09/06.

[www09] http://wwwuser.gwdg.de/~botanik/vegetation/spribille/ taken 20/05/06.

[www10] http://mineral.galleries.com/minerals/carbonat/dolomite/dolomite.htm taken on 10/03/06.

[www11] http:www.mostateparks.com/onondaga/cavesformed.htm taken on 05/10/06.

[www12] http://mse.iastate.edu/microscope/whatsem.html taken on 10/10/06.

[www13] http://en.wikipedia.org/wiki/scanning_electron_microscope taken on 15/10/06.

[www14] http://www.unl.edu/CMRA/fem/em.html taken on 10/10/06.

[www15] http:// ion.asu.edu/descript_easyxrf.htm taken on 10/08/06.